UAB
Universitat Autònoma de Barcelona

Immune dynamics in Diffuse Large B cell Lymphoma affecting the Central Nervous System

Carlota Pagès Geli

UAB
Universitat Autònoma
de Barcelona

PhD in Medicine

Department of Medicine

Immune dynamics in Diffuse Large B cell Lymphoma affecting the Central Nervous System

Doctoral thesis presented by

Carlota Pagès Geli

to qualify for the degree of

Doctor

Supervisor

Dr Marta Crespo Maull

Tutor

Dr Pere Barba Suñol

Barcelona, 2024

List of abbreviations

A

ABC	Activated B-cell like
ADCC	Antibody-dependent cellular cytotoxicity
ADCP	Antibody-dependent cellular phagocytosis
APC	Antigen-presenting cell
ASCT	Autologous stem cell transplantation

B

ß2M	Beta-2-microglobulin
BBB	Blood-brain barrier
BCR	B-cell receptor
BLI	Bioluminescence imaging
BsAb	Bispecific antibody

C

CAR	Chimeric antigen receptor
CAR-T	Chimeric antigen receptor T-cell
CFSE	Carboxyfluorescein succinimidyl ester
cHL	Classical Hodgkin lymphoma
CHOP	Cyclophosphamide, doxorubicin, vincristine, prednisone
CIITA	Class II transactivator
CNA	Copy number alteration
CNS	Central nervous system
CNS-IPI	CNS international prognostic index
CNV	Copy number variants
COO	Cell of origin

CI	Confidence interval
CR	Complete remission
CSF	Cerebrospinal fluid
CSR	Class switch recombination
CT	Computed tomography
ctDNA	Circulating tumor DNA

D

DC	Dendritic cell
DEG	Differentially expressed gene
DLBCL	Diffuse large B-cell lymphoma

E

ECOG	Eastern cooperative oncology group

F

Fab	Fragment antigen-binding
Fc	Fragment crystallizable
FC	Fold change
FcR	Fc receptor
FcγR	Fc-gamma receptor
FDA	Food and drug administration
FDR	False discovery rate
FFPE	Formalin-fixed paraffin-embedded

G

GC	Germinal center

GCB	Germinal center B-cell like
GM-CSF	Granulocyte-macrophage colony-stimulating factor
GO	Gene Ontology
GOBP	Gene Ontology Biological Process
GSEA	Gene set enrichment analysis

H

HD-MTX	High-dose methotrexate
HSC	Hematopoietic stem cell

I

IC	Immunocompetent
Ig	Immunoglobulin
IgH	Immunoglobulin heavy chain
IgL	Immunoglobulin light chain
IHC	Immunohistochemistry
IPI	International prognostic index
ITAM	Immunoreceptor tyrosine-based activation motif
ITIM	Immunoreceptor tyrosine-based inhibitory motifs
IT-MTX	Intrathecal methotrexate

K

KO	Knockout
KPS	Karnofsky performance status

L

LDH	Lactate dehydrogenase

LILRB1 Leukocyte immunoglobulin-like receptor B1

LPS Linear Predictor Score

M

mAb Monoclonal antibody

M-CSF Macrophage colony-stimulating factor

MFI Mean fluorescence intensity

MHC Major histocompatibility complex

MHC I MHC class I

MHC II MHC class II

MMD Macrophage/microglia-depleted

MRI Magnetic resonance imaging

MSigDB Molecular Signatures Database

N

NES Normalized enrichment score

NGS Next generation sequencing

NHL Non-Hodgkin lymphoma

NK Natural killer

O

ORR Overall response rate

OS Overall survival

P

p P-value

Padj Adjusted p-value

PCA	Principal component analysis
PCNSL	Primary central nervous system lymphoma
PD-1	Programmed cell death protein 1
PD-L1	Programmed cell death ligand 1
PD-L2	Programmed cell death ligand 2

R

RBC	Red blood cell
R-CHOP	Rituximab, cyclophosphamide, doxorubicin, vincristine, prednisone
R-IPI	Revised international prognostic index
RNA-seq	RNA sequencing
R/R	Relapsed/refractory

S

scFv	Single-chain fragment variable
SCNSL	Secondary central nervous system lymphoma
SEM	Standard error of the mean
SD	Standard derivation
SG	StayGold
SIRPα	Signal regulatory protein alpha
SHM	Somatic hypermutation

T

TAM	Tumor-associated macrophage
TCR	T-cell receptor
TGF-β	Transforming growth factor-beta
TIL	Tumor-infiltrating lymphocyte
TLR	Toll-like receptor

TME	Tumor microenvironment

V

VLA4	Very late antigen 4

W

WHO	World Health Organization
WT	Wild-type

TABLE OF CONTENTS

Abstract

Primary central nervous system lymphoma (PCNSL) is an aggressive extranodal diffuse large B-cell lymphoma (DLBCL) that affects the central nervous system (CNS), which includes the brain, eyes, leptomeningeal compartments and/or the spinal cord. It characterized by unique genetic alterations that contribute to its pathogenesis and supported by the brain immunosuppressive microenvironment. Notably, PCNSL patients frequently exhibit MHC class I downregulation and PD-L1 overexpression, both of which impair T cell recognition. It is well established that cancer cells downregulating MHC I are more vulnerable to macrophage recognition and cytotoxic activity. Furthermore, macrophages express PD-1 and SIRPα, and blocking these pathways can enhance their anti-tumor function. Since macrophages are the most common immune cell infiltrating in the CNS in PCNSL, we hypothesize these could act as effector cells against PCNSL with downregulated MHC I. The objective of this study is to investigate the role of macrophages in the pathogenesis of PCNSL and in response to anti-PD-1 therapy, with a focus on their potential anti-tumor role in CNS lymphoma cases that employ T cell evasion mechanisms. To explore this, we developed a syngeneic mouse model of PCNSL, in which we depleted both systemic macrophages and brain-resident microglia, while simultaneously downregulating MHC I expression in cancer cells, impairing T cell function. Our findings reveal that MHC I-negative PCNSL tumors exhibit a highly aggressive phenotype and respond exclusively to macrophage-mediated activity. This was demonstrated by the reduced treatment response observed in immunocompetent mice and the complete lack of response in macrophage-depleted mice, compared to wild-type CNS lymphoma. Additionally, blocking the PD-1/PD-L1 and/or CD47/SIRPα pathways was insufficient to trigger a robust macrophage-mediated anti-tumor response, underscoring the need for novel macrophage-targeted therapies to effectively combat MHC I-negative lymphomas.

To achieve this goal, we established a high-throughput system to identify monoclonal antibodies that enhance macrophage activity against B-cell lymphoma cells. Through this approach, we identified several novel antigens as promising therapeutic targets in both mouse and human systems. Blocking these antigens—either individually or in combination—significantly enhanced macrophage activity against lymphoma cells *in vitro*,

with a particularly strong effect against MHC I-negative cells. Building on these findings, we developed a rapid platform to generate and evaluate bispecific antibodies, providing new therapeutic strategies that stimulate macrophage-mediated cytotoxicity against lymphoma cells. Among the bispecifics tested, WTa2d1xCD38, composed of a low-affinity SIRPα decoy protein and an anti-CD38 binding arm, emerged as the most promising candidate. This bispecific demonstrated potent macrophage-mediated cytotoxicity against lymphoma cells and low red blood cell toxicity, showing significant efficacy in both *in vitro* and *in vivo* models of aggressive B-cell lymphoma.

In aggressive DLBCL, CNS relapse is a serious clinical event. While clinical scores like the CNS-IPI are used to predict CNS relapse at diagnosis in high-risk patients, their precision remains limited. Therefore, we conducted a comprehensive analysis of the immune, genomic, transcriptomic, and epigenomic profiles of systemic DLBCL tumors to identify key features associated with CNS relapse at diagnosis. We found that DLBCL tumors with CNS tropism already exhibit distinguishing characteristics at diagnosis compared to those that relapse systemically or do not relapse. We have identified the *PIM1* mutation as a predictor of CNS relapse at diagnosis. Furthermore, our results highlight the upregulation of genes associated with cell migration and proliferation, including *ITGA4*, *CCR6*, *BTLA*, and *IL7R*, which have previously been linked to B cell infiltration into the CNS. Additionally, CpG hypomethylation in migration-related genes further underscores their potential for invasiveness. These findings provide valuable insights for identifying high-risk patients for CNS relapse at diagnosis, thereby enhancing the accuracy of prophylactic treatments.

Resum

El limfoma primari del sistema nerviós central (LPSNC) és un limfoma difús de cèl·lules B grans (LDCBG) extranodal que afecta el cervell, els ulls, les meninges i/o la medul·la espinal. Es desenvolupa en un microambient cerebral amb poca activitat immunitària. A més, un alt percentatge de pacients amb LPSNC presenten alteracions genètiques que els permeten evitar el reconeixement i l'atac del sistema immunitari, com els limfòcits T citotòxics, mitjançant la disminució de l'expressió de MHC I i l'augment de l'expressió de PD-L1. Aquests factors fan que aquest tipus de càncer sigui altament agressiu i que les opcions terapèutiques siguin limitades.

Les cèl·lules tumorals amb manca d'HLA I són més vulnerables al reconeixement i a l'activitat citotòxica dels macròfags. Aquests macròfags expressen les proteïnes PD-1 i SIRPα, la qual cosa inhibeix la seva funció citotòxica en interaccionar amb PD-L1 i CD47, respectivament, expressats a les cèl·lules tumorals. El bloqueig d'aquestes vies pot potenciar la seva activitat antitumoral. Atès que els macròfags són el tipus cel·lular immunitari més abundant al sistema nerviós central (SNC), podrien constituir una estratègia immunoterapèutica prometedora, especialment en aquells casos amb una forta evasió de les cèl·lules T. L'objectiu d'aquest estudi és analitzar el paper dels macròfags i de les cèl·lules T en el desenvolupament del LPSNC, així com l'impacte de l'evasió immunitària i la resposta a les immunoteràpies. Per dur a terme aquest estudi, hem desenvolupat un model de ratolí amb LPSNC en què hem eliminat tant els macròfags sistèmics com la micròglia resident al cervell, alhora que hem delecionat MHC I a les cèl·lules tumorals, inhibint l'activitat de les cèl·lules T. Els resultats obtinguts han demostrat que el LPSNC amb deleció de MHC I presenta un fenotip altament agressiu en comparació amb els tumors sense la mutació. A més, mostren una resposta més baixa al tractament en ratolins immunocompetents i una resposta totalment deficient en ratolins sense macròfags. Això evidencia que els LPSNC amb manca d'expressió de MHC I depenen exclusivament de l'activitat antitumoral dels macròfags. Tot i així, en aquest context, el bloqueig de les vies PD-1/PD-L1 i/o CD47/SIRPα no resulta suficient per erradicar el tumor, posant de manifest la necessitat de noves teràpies dirigides als macròfags per combatre eficaçment els limfomes negatius per MHC I. Per assolir aquest objectiu, hem establert un sistema per identificar anticossos monoclonals que potenciïn l'activitat dels macròfags contra cèl·lules de limfoma de cèl·lules B. Mitjançant aquest

mètode, hem identificat diversos antígens que, en bloquejar-los, ja sigui individualment o en combinació, es potencia l'activitat dels macròfags contra les cèl·lules de limfoma *in vitro*, amb un efecte més pronunciat contra les cèl·lules negatives per MHC I. A partir dels resultats obtinguts, hem desenvolupat una plataforma per generar i avaluar anticossos biespecífics. D'entre els anticossos biespecífics provats, el WTa2d1xCD38, compost per una proteïna SIRPα de baixa afinitat i un braç d'unió anti-CD38, és el candidat terapèutic més prometedor, ja que presenta una potent citotoxicitat regulada pels macròfags contra les cèl·lules de limfoma i una baixa toxicitat.

En el LDCBG, la recaiguda en el sistema nerviós central (SNC) és un esdeveniment clínic greu. Tot i que s'utilitzen sistemes clínics, com el CNS-IPI, per predir la recaiguda al SNC en el moment del diagnòstic, aquest mètode encara no és completament precís. Per identificar biomarcadors que puguin millorar la identificació del risc elevat de recaiguda al SNC, hem estudiat retrospectivament els perfils immunològics, genòmics, transcriptòmics i epigenòmics dels tumors sistèmics de DLBCL amb tropisme al SNC en el moment del diagnòstic. A través d'aquest anàlisi, hem observat que aquests tumors ja presenten característiques distintives en el diagnòstic en comparació amb aquells que recauen de manera sistèmica o no recauen. Hem identificat la mutació de *PIM1* com un predictor de la recaiguda al SNC en el moment del diagnòstic. A més, els nostres resultats destaquen l'elevada expressió de gens associats amb la migració i la proliferació cel·lular, com *ITGA4*, *CCR6*, *BTLA* i *IL7R*, els quals han estat prèviament relacionats amb la infiltració de cèl·lules B al SNC. A més, la hipometilació de CpG en gens relacionats amb la migració reforça el seu potencial invasiu. Aquests resultats proporcionen informació valuosa per identificar pacients d'alt risc per a la recaiguda al SNC en el moment del diagnòstic, millorant així la precisió dels tractaments profilàctics.

1. Introduction

1.1. Hematopoiesis

Hematopoiesis is a complex, tightly regulated process through which hematopoietic stem cells (HSCs) generate the diverse array of blood cells required for maintaining physiological function (Figure 1). This process predominantly occurs in the bone marrow, though during embryonic development it also takes place in extramedullary sites such as the yolk sac, liver, and spleen[1].

HSCs are characterized by their capacity for both self-renewal and differentiation. These stem cells reside in a specialized microenvironment within the bone marrow, known as the hematopoietic niche, which provides critical signals that regulate their proliferation and lineage commitment[2]. HSCs differentiate into two primary progenitor populations: common myeloid progenitors (CMPs) and common lymphoid progenitors (CLPs)[3].

CMPs further differentiate into various myeloid lineage cells, including erythrocytes, platelets, granulocytes, and monocytes. The differentiation of CMPs into erythrocytes, a process called erythropoiesis, involves multiple intermediate stages, including proerythroblasts and erythroblasts[4]. Thrombopoiesis, the process of platelet formation, involves the differentiation of CMPs into megakaryocytes, which then fragment to release platelets into the bloodstream[5].

Two processes that lead to the formation of granulocytes and monocytes, respectively, also originate from CMPs. Granulopoiesis involves the development of granulocyte progenitors into myeloblasts, promyelocytes, myelocytes, metamyelocytes, and finally, mature granulocytes such as neutrophils, eosinophils, and basophils[6]. Similarly, monopoiesis progresses from myeloid progenitors through stages including monoblasts and promonocytes to produce mature monocytes[7]. After being released into the bloodstream, monocytes circulate throughout the body until they encounter specific signals or migrate into tissues, where they differentiate into macrophages[8].

On the other hand, CLPs give rise to the lymphoid lineage, which includes T cells, B cells, and natural killer (NK) cells. Lymphopoiesis begins with the differentiation of CLPs into lymphoid progenitors that migrate to primary lymphoid organs such as the thymus and bone marrow. In the thymus, precursor T cells undergo selection and maturation, while

B cells mature in the bone marrow[9]. NK cells also differentiate in lymphoid organs but do not require thymic selection[10].

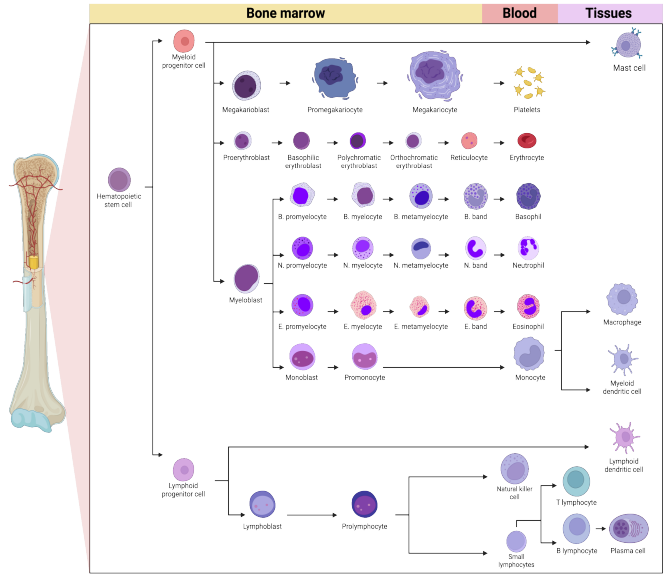

Figure 1 | Hematopoiesis. Differentiation of hematopoietic stem cells into the various lineages of blood cells, including myeloid and lymphoid lineages. Image adapted from Biorender.com.

1.1.1. B cell development

B cell development is a highly regulated process that begins in the bone marrow and culminates in the production of functionally mature B cells, which are essential for the adaptive immune response. B cells are responsible for producing different types of specialized immunoglobulins (Ig), also known as antibodies, that play a key role in identifying and neutralizing pathogens and abnormal cells, including cancer cells.

CLPs first mature into pro-B cells in the bone marrow, where they initiate rearrangement of immunoglobulin heavy chain (IgH) gene segments, essential for the formation of the pre-B cell receptor (pre-BCR). After that, they progress to the pre-B cells stage, where they rearrange the immunoglobulin light chain (IgL) genes. This completes the formation of the fully functional B-cell receptor (BCR)[11]. These immature B cells then proceed through further maturation stages, including a negative selection process that takes place in the bone marrow to ensure self-tolerance. Cells that bind strongly to self-antigens are

eliminated by apoptosis to prevent autoimmunity, while those that survive migrate to peripheral or secondary lymphoid tissues, such as the spleen and lymph nodes, and continue their maturation process[12,13].

1.1.2. Germinal Center Reaction

B cells then enter the germinal center (GC) to undergo further maturation (Figure 2). The GC is a specialized microenvironment within secondary lymphoid tissues where B cells move between two compartments within the GC: the dark zone and the light zone, and they generate high-affinity antibodies[14].

In the dark zone, B cells undergo somatic hypermutation (SHM) and class switch recombination (CSR). SHM introduces mutations into the variable regions of Ig genes to increase BCR affinity for antigens. CSR enables antibodies to gain different effector functions while retaining their specificity[15]. This zone is characterized by intense proliferation and significant genomic instability, managed by BCL6, a key regulator that suppresses apoptosis and regulates DNA damage checkpoints to facilitate SHM and CSR without inducing cell death or cycle arrest.

In the light zone, B cells test their antibody affinity through interactions with antigen-presenting cells (APCs), mainly follicular dendritic cells (FDCs). In this zone, BCL6 expression decreases, leading to reduced proliferation[16]. Only high-affinity B cell clones are selected and successfully exit the GC, differentiating into memory B cells or plasma cells that secrete antibodies. Most cells that are not selected typically undergo apoptosis; however, some cells are rescued, often through MYC, and may re-enter the dark zone for additional rounds of SHM and selection. MYC, which is crucial for the selection process and the cyclic reentry of B cells, controls the formation and maintenance of the germinal center[17]. This integrated process ensures the generation of functional B cells capable of producing high-affinity antibodies while maintaining tolerance to self-antigens.

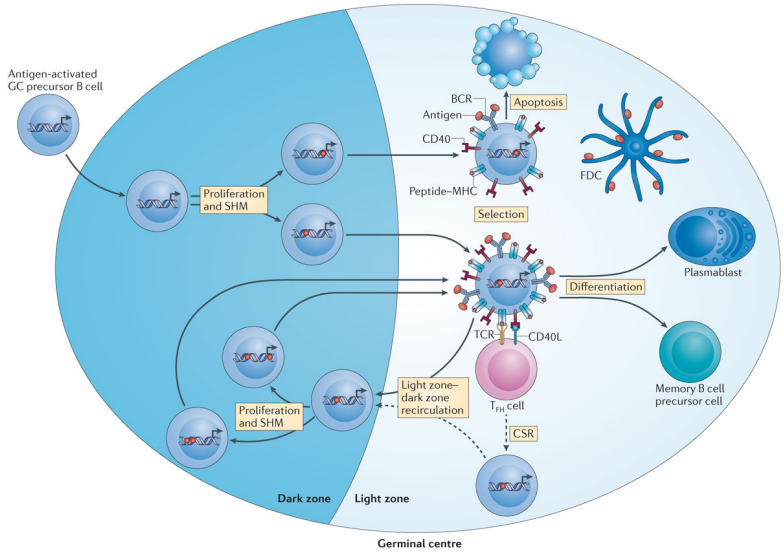

Figure 2 | Germinal center reaction. From De Silva N. and Klein U. Nat. Rev. Immunol. 2015.

1.1.3. B-cell receptor

The BCR is responsible for recognizing specific antigens, thereby initiating a series of intracellular signaling events that lead to the activation, proliferation, differentiation, and eventual antibody production by B cells[18]. Structurally, the BCR is composed of two primary components: the membrane-anchored complex and the Igα/Igβ heterodimer, also known as CD79A/CD79B. The membrane-anchored complex, which has a characteristic Y-shaped structure, is composed of two functional regions: the Fab (Fragment antigen-binding) or variable region and the Fc (Fragment crystallizable) or constant region. The Fab regions consists of two IgL and two IgH that together form the antigen-binding site, which are highly specific and can vary to bind different antigens (Figure 3). The BCR can exist in different isotypes, including IgD, IgM, IgA, IgG, or IgE, which trigger different immune responses. When not anchored in the membrane, the BCR can act as a soluble Ig or antibody. Immunoglobulins can bind to single or multiple circulating antigens (forming immune complexes), or membrane antigens expressed in pathogens or cells, thereby antibody-coating or tagging targets for further elimination.

The CD79A and CD79B proteins contain cytoplasmic tails with immunoreceptor tyrosine-based activation motifs (ITAMs), which trigger several signaling pathways, related to B-cell survival and proliferation, initiated upon antigen binding[19].

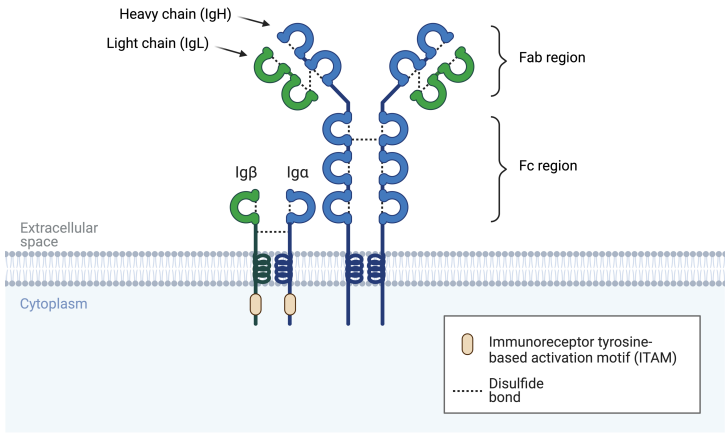

Figure 3 | BCR structure. Image adapted from Biorender.com

1.2. Cellular immune response

The immune system consists of two main components: the innate and adaptive immune systems. The innate immune system delivers a rapid, non-specific response through key players such as macrophages, neutrophils, and NK cells, acting as the first line of defense against pathogens. In contrast, the adaptive immune system develops a highly specific and long-lasting response, mediated by B and T lymphocytes, which recognize distinct antigens and develop immunological memory. This allows for more effective and quicker responses upon re-exposure to the same antigen. MHC class I (MHC I) molecules, which are expressed on the surface of almost all cells, present endogenous antigens to CD8+ cytotoxic T cells, facilitating the detection of infected or abnormal cells. On the other hand, MHC class II (MHC II) molecules are predominantly expressed on antigen-presenting cells (APCs) such as macrophages, dendritic cells, and B cells, where they present exogenous antigens to CD4+ helper T cells, initiating the adaptive immune response. This section will focus specifically on the type and role of macrophages and T cells in the immune response.

1.2.1. Macrophages

Macrophages are highly specialized APCs that arise from monocytes upon stimulation with granulocyte-macrophage colony-stimulating factor (GM-CSF). These cells play a central role in immune defense by eliminating pathogens, apoptotic cells, and cellular debris through phagocytosis, thereby maintaining tissue homeostasis. Upon internalizing and processing antigens, macrophages present these antigens on their surface via MHC molecules to activate T cells. This antigen presentation is critical for the priming, activation, and differentiation of T cells, thereby coordinating adaptive immune responses[20].

Macrophage activation is a balance between "eat-me" signals, like externalized phosphatidylserine or calreticulin, which promote phagocytosis, and "don't eat me" signals, such as CD47, which inhibit it, regulating the clearance of target cells.

Recent research has identified various macrophage subsets with specialized roles, reflecting their functional plasticity. Macrophages without any defined functional state

(M0) can be polarized into distinct functional states known as M1 and M2 macrophages[21]. M1 macrophages, also known as classically activated macrophages, are typically characterized by their production of pro-inflammatory cytokines and their ability to effectively initiate an immune response, but they can also contribute to chronic inflammation and tissue damage. These secrete cytokines and chemokines like TNFα to recruit additional immune cells, amplifying the immune response and promoting a strong pro-inflammatory response. In contrast, M2 macrophages secrete anti-inflammatory cytokines, such as IL-10 to induce anti-inflammatory responses and tissue repair[22]. These express high levels of CD163, CD204 and CD206[23]. The balance between these cytokine signals is crucial for maintaining immune homeostasis and preventing excessive or chronic inflammation[24].

In the context of cancer, tumor-associated macrophages (TAMs) can significantly impact tumor progression. TAMs can either promote or inhibit tumor growth depending on their polarization state and the microenvironment. Generally, M1 enhance antitumor immunity and M2 TAMs contribute to tumor progression and the development of an immunosuppressive tumor microenvironment (TME) that promotes tumor progression, angiogenesis, metastasis and immunotherapy resistance[25,26].

Macrophages can also be categorized based on their tissue localization, each specialized for distinct functions. For example, microglia, the resident macrophages of the central nervous system, are essential for maintaining neural homeostasis and responding to neuronal injury[27].

1.2.1.1. FcRs and antibody-directed mechanisms

Macrophages and other cells express Fc receptors (FcRs), a class of immunoreceptors that specifically recognize and bind to the constant Fc region of Ig antibodies. Although there exist several types of FcRs, only the Fc-gamma receptors (FcγRs) will be further described.

FcγRs specifically recognize IgG antibodies. Different types of FcγRs can be distinguished based on their role in the immune response. FcγRI (CD64) is a high affinity receptor that triggers phagocytosis and facilitates the presentation of antigens to T cells

through MHC molecules, thus bridging innate and adaptive immune responses[28]. FcγRII (CD32) exists in several isoforms with varying affinities for IgG. Depending on the isoform and cellular context, FcγRII can either activate or inhibit immune responses. Activating forms of FcγRII contribute to an antibody-dependent cellular phagocytosis (ADCP)[29] mechanism, which specifically promotes phagocytosis to coated or opsonized cells. FcγRIII (CD16) is expressed on NK cells and binds to IgG antibodies with lower affinity compared to FcγRI. This receptor is involved in antibody-dependent cellular cytotoxicity (ADCC), which promotes the release of cytotoxic granules to eliminate the coated cell[30]. In the context of cancer, ADCP and ADCC play an important role in targeting and eliminating tumor cells that are marked by immunotherapeutic antibodies[31].

1.2.2. T cells

T cells originate in the bone marrow and mature in the thymus, where they undergo a critical education process to distinguish between the body's own cells and foreign or abnormal cells. This process is facilitated by the T-cell receptor (TCR), which recognizes antigens presented by MHC molecules. The binding of the TCR to an antigen-MHC complex triggers intracellular signaling that activates the T cell, leading to its proliferation and specific immune functions. Full T cell activation also requires costimulatory signals, such as the interaction between CD28 on T cells and B7 molecules (CD80/CD86) on APCs, which enhance TCR signaling and promote cytokine production and survival.

There are two main types of T cells with specialized roles in the immune response. CD8+ cytotoxic T cells recognize foreign antigens presented by MHC class I molecules on infected or abnormal cells, including cancer cells expressing neoantigens (Figure 4). Upon activation, CD8+ T cells release perforin and granzymes to induce apoptosis in the target cell. CD4+ helper T cells, on the other hand, recognize antigens presented by MHC class II molecules on APCs, such as macrophages, dendritic cells, and B cells (Figure 4). Activated CD4+ T cells secrete cytokines that coordinate the activity of other immune cells, including CD8+ T cells and B cells, thereby orchestrating the overall immune response.

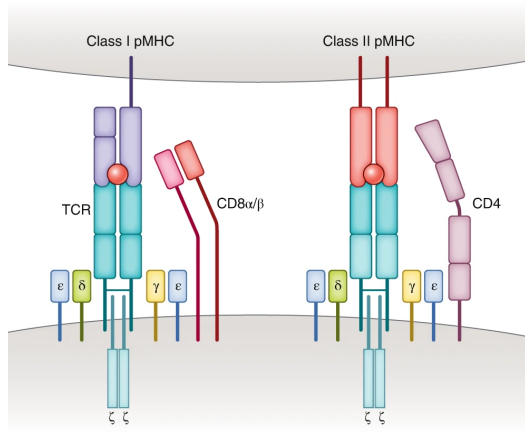

Figure 4 | Interaction between MHC molecules and T cells. From Joglekar A.V. and Li G. Nat. Methods. 2021.

1.3. Immune evasion in cancer

Tumor cells can evade the immune system through various mechanisms, including the suppression of antigen recognition, overexpression of immune-inhibitory molecules, and the induction of T cell exhaustion, among others. The TME, composed of various cells such as TAMs, dendritic cells, and/or stromal cells, plays a pivotal role in either promoting tumor destruction or facilitating immune evasion, regulated by a balance of co-stimulatory and inhibitory signals[32]. Here, we will focus on the key mechanisms and the expression of immune checkpoints that drive immune escape, resulting in the dysfunction of T cells and macrophages in cancer.

1.3.1. Antigen presentation mechanisms

A key strategy for immune evasion in tumoral cells is the downregulation of MHC molecules to evade T cell recognition and cytotoxicity. The most common genetic alterations involve mutations in genes located within the HLA region on the short arm of chromosome 6 (6p21.3), including mutations in the HLA genes (*HLA-A*, *HLA-B*, and *HLA-C*), as well as in the *TAP1*, *TAP2*, and *Tapasin* genes—critical for peptide loading—

leading to the loss of MHC I protein expression on the surface of tumor cells[33,34]. Additionally, mutations in the *B2M* gene, located on chromosome 15 (15q21-q22), which encodes beta-2 microglobulin (ß2M)—a protein essential for the assembly and stable expression and function of MHC I—can also lead to MHC I loss[35]. These mutations enable tumors to escape from tumor specific cytotoxic CD8+ T lymphocyte response.

MHC II downregulation is observed in some hematological tumors, where malignant cells themselves are professional APCs. The most common alterations involve the *CIITA* gene, which encodes the class II transactivator (CIITA), a master regulatory transcription factor crucial for the expression of MHC II molecules[33]. These mutations confer tumor cells the ability to evade recognition from CD4+ T cells[34].

Importantly, the infiltration of T lymphocytes into the tumor microenvironment, referred to as tumor-infiltrating lymphocytes (TILs), is heavily dependent on the expression of MHC molecules on tumor cells. Studies have shown that some cancers with low MHC I expression contain significantly fewer TILs compared to those with high expression[36,37]. Consequently, MHC I loss is strongly linked to poor clinical outcomes, unfavorable prognosis, and resistance to T-cell-based therapies in many cancers.

1.3.2. Immune checkpoints

Another crucial mechanism by which cancer cells evade immune detection involves the expression of immune checkpoints, often referred to as "don't eat me" signals. Immune checkpoints are inhibitory pathways that regulate immune cell activation and function, maintaining immune responses and preventing autoimmunity. However, in the context of cancer, malignant cells frequently overexpress these checkpoints, which hampers the ability of the immune system to recognize and eliminate them effectively. High expression of immune checkpoints is often associated with poor prognosis, as it allows tumors to evade immune surveillance, leading to increased tumor growth and resistance to immunotherapy[38].

The programmed cell death protein 1 (PD-1) receptor is the most widely studied immunecheckpoint in T cells. PD-1 is a monomeric type I transmembrane receptor

characterized by intracellular immunoreceptor tyrosine-based inhibitory motifs (ITIMs). It interacts with its ligands, programmed cell death 1 ligand 1 (PD-L1, also known as B7-H1 or CD274) and programmed cell death 1 ligand 2 (PD-L2, also referred to as B7-DC or CD273). PD-L1, encoded by the *CD274* gene, is constitutively expressed on a broad range of hematopoietic cells, including macrophages, dendritic cells, B cells, and T cells, as well as on some non-hematopoietic cells; while PD-L2, which is encoded by *PDCD1LG2* gene, is much more restricted in macrophages and dendritic cells[39]. Engagement of PD-1 with PD-L1/2 results in the inhibition of TCR/CD28-mediated T cell activation. In many cancers, tumor cells overexpress PD-L1 and PD-L2, thereby evading immune surveillance and cytotoxicity by T cells[40].

Moreover, PD-1 tends to be overexpressed on dysfunctional and exhausted T cells, due to persistent antigen exposure and chronic stimulation. In tumors, the increase of exhausted T cells (both CD8+ and CD4+) results in reduced proliferation, cytokine production, and cytotoxic activity, thereby facilitating T cell evasion and resistance to T-cell mediated therapies[41,42].

Beyond PD-1, other immune checkpoints like CTLA-4, TIM-3, and LAG-3 also play critical roles in regulating T cell activity[43].

Gordon et al. recently described that PD-1 can also be highly expressed on macrophages, and its expression correlates negatively with the phagocytic potency against tumor cells[44]. Nonetheless, the most well-known and extensively studied immune checkpoint pathway involving macrophages is the CD47/SIRPα pathway. CD47 is an immunoglobulin-like protein found on the surface of many normal cells. Its primary ligand, signal regulatory protein alpha (SIRPα), is a transmembrane protein predominantly expressed on macrophages. When CD47 binds to SIRPα, it triggers tyrosine phosphorylation of the ITIM domains on SIRPα[45]. This interaction sends a "don't eat me" signal to macrophages, effectively inhibiting phagocytosis and allowing cells to evade immune destruction[46]. In some malignancies, tumor cells highly express CD47 to avoid macrophage-mediated destruction; and is associated with poor prognosis[47].

1.4. Immunotherapy in cancer

Cancer immunotherapy has transformed cancer treatment by promoting the immune system to recognize and destroy cancer cells. Unlike traditional regimens like chemotherapy and radiation, which target tumors directly, immunotherapy specifically targets interactions between cancer cells and immune cells, providing a highly specialized immune response against tumoral cells. In this section, the most used immunotherapies that promote T cell and macrophage-directed activation will be described.

1.4.1. Therapeutic antibodies

Monoclonal antibodies (mAb) are laboratory-engineered molecules designed to bind specifically to certain proteins or antigens on the surface of cells. In cancer treatment, antibodies are commonly used to target tumor-specific antigens or proteins overexpressed on malignant cells, marking them for destruction through various immune mechanisms. Additionally, antibodies can target immune effector cells to enhance the immune response by stimulating cell activity or blocking inhibitory signals.

Firstly, antibodies may directly induce direct cell death of tumor cells through apoptosis[48]. Secondly, antibodies can opsonize tumoral cells and trigger their elimination by antibody Fc-dependent mechanisms including ADCC and ADCP. By ADCP, tumor antigens can also be processed and presented to CD4+ and CD8+ T cells, thereby initiating a broader antitumor adaptive immune response. This mechanism facilitates priming the immune system to recognize and attack tumor cells more effectively in the future[49]. Moreover, the binding of the antibody can activate the complement system, leading to the formation of a membrane attack complex that results in the lysis of the cancer cells[31].

Rituximab, which targets the CD20 antigen found on both normal and malignant B lymphocytes, was the first monoclonal antibody with this mechanism of action approved by the U.S. Food and Drug Administration (FDA) in 1997 for the treatment of B-cell non-Hodgkin lymphoma (NHL)[50].

Finally, and importantly, antibodies can act as immune checkpoint inhibitors, designed to block immune checkpoint pathways. This blockade can be achieved through different

methods that include using antibodies that directly target the checkpoint receptor, antibodies that block its ligand, or recombinant proteins that interfere with these pathways[51].

The interaction between PD-1 and PD-L1 plays a key role in immunosuppression, and it is well established that blocking this interaction between effector cells and tumor cells can enhance immune responses, enabling the elimination of tumor cells[52,53]. Nivolumab and pembrolizumab, two well-known anti-PD-1 mAbs, have demonstrated promising results in numerous clinical trials in hematologic and solid tumors, both as monotherapies and in combination with chemotherapy, radiotherapy, and other immunotherapies[54,55] .

1.4.1.1. Macrophage-activating antibodies

In addition to T-cell checkpoint inhibitors, there is growing interest in targeting immune checkpoints on macrophages[56]. Part of this thesis specifically explores macrophage-directed therapies, reflecting an increasing focus on understanding and enhancing the role of macrophages in the anti-tumoral response. Inhibitors of the CD47/SIRPα pathway are among the most extensively studied in this field. Magrolimab, a humanized monoclonal antibody that targets CD47 and disrupts its inhibitory signal, allows macrophages to recognize and phagocytose the cancer cells[57,58]. Further studies suggest that it may also attract macrophages to tumor sites and promote their polarization toward an anti-tumor M1 phenotype[25]. When combined with other therapies, magrolimab has demonstrated significant efficacy in clinical trials, leading to high overall response rates (ORR) and durable complete remissions (CR) in solid tumors. Moreover, preclinical studies have also shown that anti-CD47 antibodies can significantly enhance the response to anti-PD-L1 treatment, delaying tumor growth in some cancer types[59]. However, in hematological malignancies, there have been some discrepancies regarding its efficacy, with variable response rates observed across different studies. These inconsistencies suggest that the effectiveness of macrophage checkpoint inhibitors like magrolimab may be context-dependent, possibly influenced by the tumor microenvironment or disease subtype. Additionally, CD47 is highly expressed on red blood cells (RBCs), raising

concerns about off-target toxicity, particularly anemia due to unintended red blood cell clearance[60].

1.4.1.2. Bispecific antibodies

Bispecific antibodies (bsAb) have gained major interest in the past decade due to their unique ability to target distinct signaling pathways simultaneously, thereby maximizing therapeutic efficacy while minimizing toxicity. The most common mechanism of action for bsAbs involves bridging two cell types (in-trans binding), such as T cells and tumor cells, bringing them into close proximity to induce a direct cytotoxic effect while bypassing the need for MHC binding. Alternatively, bsAbs can also achieve dual inhibition of receptors on the same target cell (in-cis binding), particularly in cases where multiple signaling pathways drive disease phenotypes (Figure 5). By blocking both pathways, bsAbs can more effectively disrupt critical signals, enhancing therapeutic outcomes. In some cases, FcγR-mediated action is required, enabling bsAbs to facilitate ADCC by NK cells and ADCP by macrophages.

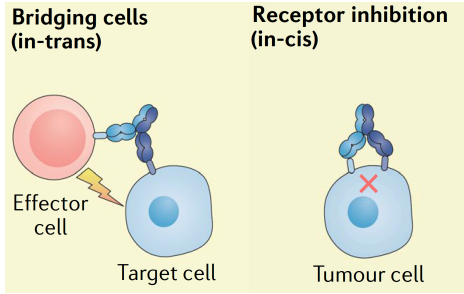

Figure 5 | Bispecific binding conformations. From Labrijn A.F. Nat. Rev. Drug. Discov. 2019.

1.4.2. Strategies for tumors with MHC I loss

MHC I expression on tumor cells should be a prerequisite for successful anti-PD-1/PD-L1 therapy. This is based on the commonly accepted key roles of cytotoxic T cell infiltration in tumor eradication and the function of PD-1/PD-L1 blockade in activating these cells[61]. However, as described before, many tumors frequently downregulate MHC I, leading to resistance against these therapies. In such cases, macrophages would play a

pivotal role in the immune response. A mechanism involving macrophages and MHC I centers on the leukocyte immunoglobulin-like receptor B1 (LILRB1). LILRB1 is an inhibitory receptor present on macrophages and other immune cells, composed of extracellular Ig-like regions, and transmembrane and intracellular regions containing ITIMs. LILRB1 binds to MHC I molecules transmitting a negative signal which suppresses the phagocytic capacity of macrophages (Figure 6). Essentially, it serves as a "don't eat me" signal, allowing cancer cells that express MHC I to evade macrophage-mediated destruction. Thus, while the loss or downregulation of MHC I helps tumors evade CD8+ T cell-mediated destruction, it also reduces inhibitory signaling through LILRB1. This reduction makes tumor cells more vulnerable to macrophage-mediated phagocytosis, especially when additional immune checkpoints, such as CD47, are blocked[62,63].

Classical Hodgkin lymphoma (cHL) is a type of hematological malignancy characterized by the overexpression of PD-L1 and PD-L2, along with the downregulation of MHC I, which lead to high levels of T cell evasion. Interestingly, cHL respons well to Nivolumab, and it is approved for relapsed/refractory (R/R) patients[64]. Reinke et al., demonstrated that a single dose of anti-PD-1 rapidly eliminated neoplastic cells from patients[65]. However, the analysis of the tumoral TCR repertoire and cytotoxic gene expression revealed no rise in intratumoral $CD8^+$ T cells or in the expression of T-cell and cytotoxicity-related genes following treatment. The observed eradication of malignant cells may be unlikely to be due to an adaptive cytotoxic T-cell response. These findings suggest that other immune cells, such as macrophages, could be responsible for the observed anti-tumoral response, given the role of macrophages against MHC I-negative tumors and the fact that PD-1 blockade is known to restore macrophage phagocytosis[66,67]. Understanding this balance is crucial for developing therapies that enhance macrophage activity against tumors, particularly in cases where tumors have downregulated MHC I to avoid T cell detection.

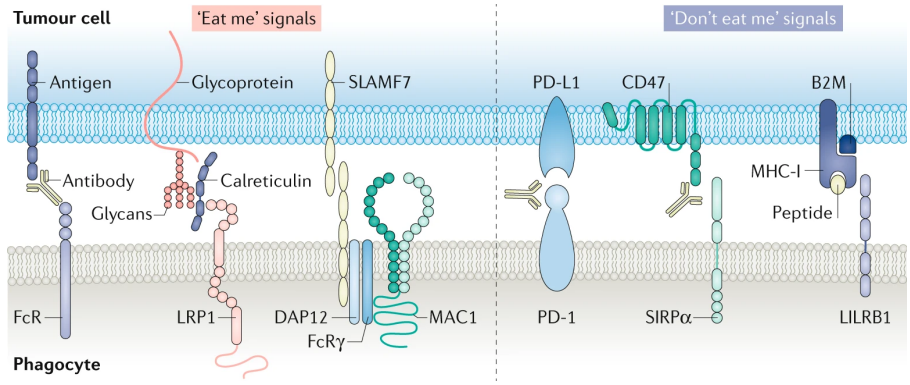

Figure 6 | Activating and inhibitory signals in macrophages. From Feng M. Nat. Rev. Cancer. 2019.

1.5. B-cell lymphoid neoplasms

Non-Hodgkin lymphomas are a diverse group of hematologic malignancies that originate in the lymphatic system, primarily arising from lymphocytes. NHLs encompasses a broad range of lymphomas with varied histological and clinical characteristics; and a significant majority—approximately 85%—are classified as B-cell neoplasms[68]. B-cell lymphomas are characterized by the abnormal proliferation of B lymphocytes, which can accumulate in lymph nodes, bone marrow, spleen, or other organs, leading to disease progression. These lymphomas vary in clinical behavior, genetic and molecular features, and their interactions with the immune microenvironment, which plays a crucial role in pathogenesis and progression[69]. The five-year overall survival rate for NHL depends on the specific subtype and stage at diagnosis, with rates ranging from 60% to 90% for many B cell lymphomas. However, more aggressive forms can have poorer outcomes. In the U.S., NHL accounts for about 4% of all cancers, with an annual incidence of around 80,000 new cases[70]. Globally, the incidence of NHL has been increasing, partly due to factors such as an aging population, immune suppression, and environmental exposures[70].

1.5.1. Classification

According to the World Health Organization (WHO) classification system, B-cell lymphomas are categorized into precursor B cell neoplasms and mature B cell neoplasms. Precursor B cell neoplasms include acute lymphoblastic leukemia/lymphoma, which arises from early B cell progenitors and are characterized by the rapid proliferation of immature B cells. Mature B cell neoplasms are further divided into indolent and aggressive types based on their clinical behavior and growth patterns[71]. Indolent B cell lymphomas generally exhibit slow progression and a less aggressive clinical course. This group includes follicular lymphoma, characterized by its follicle-like growth pattern; marginal zone lymphoma, which includes extranodal marginal zone lymphoma, nodal marginal zone lymphoma, and splenic marginal zone lymphoma; and lymphoplasmacytic lymphoma. In contrast, aggressive B cell lymphomas are marked by rapid growth and a tendency to present with more advanced disease at diagnosis[72]. This category includes diffuse large B cell lymphoma (DLBCL), the most common type of aggressive B cell lymphoma, Burkitt lymphoma, and primary mediastinal large B cell lymphoma.

1.5.2. Genetic and molecular pathogenesis

The broad range of B-cell lymphoid neoplasms arises from B cells that are blocked at different stages of differentiation within GCs, where the processes of SHM and CSR predispose them to genomic alterations[73]. These mutations often affect genes regulating cell cycle control, apoptosis, and DNA repair mechanisms, increasing the risk of oncogenic events. The specific mutations and the stage of B cell differentiation during which they occur determine the development of different lymphoma types (Figure 7). These lymphomas can often be distinguished based on their unique transcriptomic and mutational profiles, which reflect their cell of origin and the specific genetic alterations they harbor[74,75].

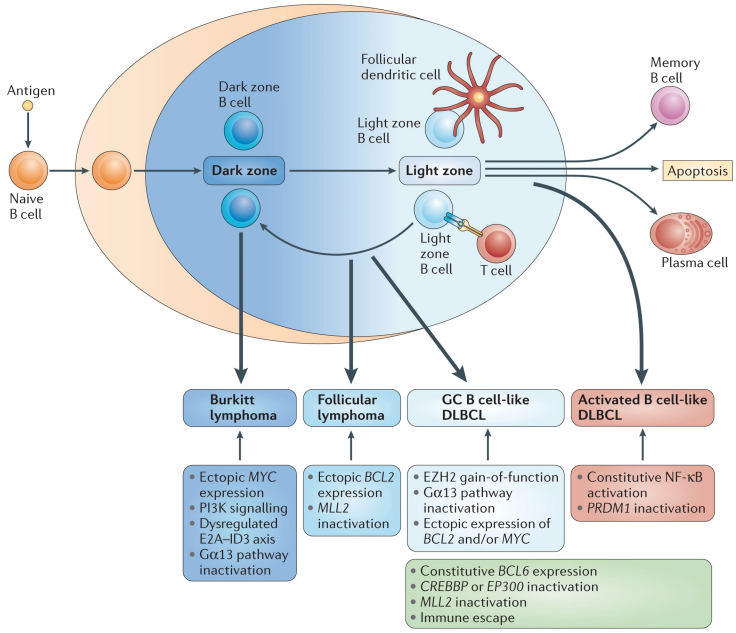

Figure 7 | Origin of GC-derived lymphomas and main oncogenic pathways. From Basso K. and Dalla-Favera R. Nat. Rev. Immunol. 2015.

1.6. Diffuse large B cell lymphoma

DLBCL is a heterogeneous and aggressive form of B-cell non-Hodgkin lymphoma, as classified in the 5th edition of the WHO Classification of Hematologic Tumors (WHO-HAEM5)[76]. It is the most common lymphoid malignancy in adults, accounting for approximately 80% of all aggressive lymphomas and around 35% of all NHL cases. DLBCL is characterized by the rapid proliferation of large, abnormal B cells that can arise in various lymphoid tissues or extranodal sites[77]. The median age at diagnosis is 70 years, with a higher prevalence observed in males (55%). The heterogeneity of DLBCL is reflected not only in its clinical presentations and sites of involvement but also in its genetic and molecular profiles[78].

1.6.1. Diagnosis and risk factors

Clinical scoring systems, such as the International Prognostic Index (IPI), are essential for risk stratification and guiding therapeutic decisions in patients with DLBCL. The IPI assigns one point for each negative prognostic factor: age over 60 years, elevated serum lactate dehydrogenase (LDH) levels, advanced disease stage (Ann Arbor stage III/IV), an Eastern Cooperative Oncology Group (ECOG) performance status of 2 or higher, and involvement of more than one extranodal site. Based on these scores, patients are classified into four risk categories: low (0-1 points), low-intermediate (2 points), high-intermediate (3 points), and high (4-5 points) risk[79].

The IPI score helps predict 5-year overall survival rates ranging from 73% in the low-risk group to 26% in the high-risk group. However, patients with R/R DLBCL face a significantly poorer prognosis, with an ORR of only 26%, a CR rate of 7%, and a median overall survival (OS) of just 6 months[80]. These statistics reveal the need for ongoing research to identify new markers to anticipate relapse and novel therapeutic strategies to improve outcomes for high-risk and R/R DLBCL patients.

The Revised International Prognostic Index (R-IPI) further refines this model by accounting for the improved outcomes achieved with modern immunochemotherapy, such as rituximab-based regimens. The R-IPI identifies three risk groups: very good (0 points), good (1-2 points), and poor (3-5 points), allowing for more precise prognostication and therapeutic planning in the current treatment landscape.

1.6.2. Genetic and molecular pathogenesis

DLBCL cells arise from the malignant transformation of mature B cells during the GC reaction[81]. Key mechanisms include chromosomal translocations involving *MYC, BCL2*, and *BCL6*, and aberrant SHM of *IG* genes and other proto-oncogenes[75,82]. Biologically, DLBCL can be classified into two main subgroups based on the cell of origin (COO) of the tumor: germinal center B-cell-like (GCB) and activated B-cell-like (ABC), with an intermediate unclassifiable phenotype. GCB-DLBCL typically originates in the GC light zone, while ABC-DLBCL exhibits a signature of mitogenically activated cells with increased NF-$\varkappa$B activity and alterations in BCR components[83].

Studies by Chapuy and Schmitz have further detailed the genetic heterogeneity of DLBCL, clustering it into more specific subgroups[84,85] (Figure 8).

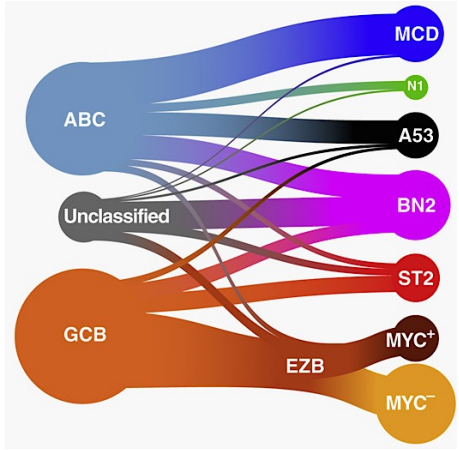

Figure 8 | Genetic subtypes of DLBCL. From Wright G.W. Cancer Cell. 2020.

Chapuy identified five genetic subgroups: the MCD subgroup, characterized by co-occurrence of *MYD88*^{L265P} and *CD79B* mutations, frequently observed in primary central nervous system lymphoma (PCNSL) and testicular lymphoma, both extranodal lymphomas in immune-privileged sites[86,87]; the BN2 subgroup, defined by *BCL6* fusions and *NOTCH2* mutations; the N1 subgroup, marked by *NOTCH1* mutations; the EZB subgroup, which includes mutations in *EZH2* and *BCL2*, often associated with the GCB subtype; and the ST2 subgroup, characterized by mutations in genes such as *SGK1* and *TET2*.

Similarly, Schmitz classified DLBCL into four genetic clusters: the C1 cluster, which includes mutations in *BCL6*, *NOTCH2*, and *B2M*, along with mechanisms of immune evasion; the C2 cluster, featuring *TP53* inactivation and including both GCB and ABC subtypes; the C3 cluster, containing mutations in BCL2 and chromatin modifiers such as *KMT2D*, *CREBBP*, and *EZH2*, often corresponding to the GCB subtype; and the C4 cluster, comprising mutations in immune evasion molecules, BCR signaling intermediates, NF-κB modifiers, and members of the RAS/JAK/STAT pathway, primarily composed of GCB-like DLBCLs.

While these classification systems differ, there are significant overlaps. For instance, the MCD subgroup from Chapuy and the C5 cluster from Schmitz both feature *MYD88* and *CD79B* mutations. Similarly, the BN2 subgroup and the C1 cluster include *BCL6* and *NOTCH2* mutations, while the EZB subgroup and the C3 cluster are both associated with *EZH2* mutations and the GCB subtype.

1.6.3. Tumor microenvironment

DLBCL typically develops within a specialized tumor microenvironment composed of various cellular and noncellular components interacting with malignant B cells[88]. Among the cellular compartment there are T and B lymphocytes, TAMs, NK cells, dendritic cells, and others. The TME controls a variety of biological processes such as pathogenesis, progression, metastasis, and drug resistance via mechanisms like sustained proliferation and immune escape[89].

In fact, DLBCL cells often evade the immune system through several mechanisms. One way is by altering immune recognition, which involves the loss or reduction of MHC I proteins. Genetic inactivation of ß2M is observed in approximately 30% of DLBCL cases, while copy number loss of *HLA I* at chromosome 6p21 occurs in roughly 20% of cases[90]. DLBCL cells also create a supportive microenvironment by losing MHC II expression, often mediated by inactivation of the *CIITA*. These immune evasion mechanisms impair antigen presentation to T cells and leads to poor T cell infiltration[91,92].

Macrophages are the most abundant non-tumoral immune cells infiltrating the DLBCL TME[93]. While previous studies have explored the impact of TAMs on patient outcomes, the specific roles of M1 and M2 macrophage infiltration in the prognosis of DLBCL remain unclear[94,95,96]. Some research indicates that the presence of tumor-infiltrating macrophages is associated with poor prognosis in aggressive DLBCL[97,98]. However, recent research demonstrated M1 macrophages are more prevalent in DLBCL samples compared to controls, suggesting a shift towards a pro-inflammatory state[93].

1.6.4. Treatment

1.6.4.1. First line treatment

The standard treatment for DLBCL typically involves immunochemotherapy, most commonly R-CHOP (rituximab, cyclophosphamide, doxorubicin, vincristine, and prednisone). The addition of rituximab has significantly improved outcomes, with 5-year overall survival rates of 70% to 80% for low-risk patients (IPI < 2), who often require only four cycles of R-CHOP for limited disease[99]. However, approximately 50% of high-risk patients (IPI > 2) relapse after initial R-CHOP treatment, possibly due to treatment resistance or low CD20 expression. Recent trials have shown that replacing vincristine with polatuzumab vedotin (an antibody-drug conjugate targeting CD79b) in R-CHOP improves progression-free survival in these high-risk patients, making it the preferred regimen in this population[100,101,102].

1.6.4.2. T-cell therapies for R/R DLBCL patients

For patients with R/R DLBCL, treatment options have expanded beyond traditional chemotherapy. Salvage chemotherapy followed by autologous stem cell transplantation (ASCT) remains a standard approach; however, novel therapeutic options, including chimeric antigen receptor T-cell (CAR-T) therapies and bispecific antibodies, have shown promise for patients who are not candidates for ASCT or who relapse post-transplant[103]. CAR-T cell therapy is an immunotherapy where T cells from patients are genetically modified to express a chimeric antigen receptor (CAR) that targets specific cancer antigens. The CD19-targeted CAR-T is the most commonly used in R/R DLBCL. This CAR binds to CD19 on tumor cells, activating the T cells directly. This interaction enables targeted cytotoxicity and destruction of cancer cells, bypassing the need for cross-presentation[104].

Bispecific antibodies offer another therapeutic option for patients with R/R DLBCL. These antibodies function by bridging T cells and malignant B cells, effectively bringing them into close proximity. Blinatumomab is an approved bispecific antibody that targets both CD19 on the surface of malignant B cell and CD3 on T cells, facilitating the direct activation of T cells and promoting their cytotoxicity against the B cells, potentially

leading to effective tumor cell destruction. This and other similar bispecific antibodies have shown efficacy in various B-cell malignancies and are currently under investigation for their effectiveness in treating DLBCL[105,106].

1.6.4.3. Macrophage-directed therapies in DLBCL

Despite the clinical benefits of T-cell-directed therapies for R/R patients, CR is only achieved in a subset of cases. Resistance often develops due to inadequate T-cell infiltration or impaired T-cell function[107,108,109]. Approximately 20 to 30% of R/R DLBCL patients fail to achieve a durable response after CAR-T therapy, with a key contributing factor being an immune microenvironment characterized by low T-cell infiltration and dysfunctional T cells[108,110].

Given these challenges, macrophage-directed therapies have emerged as a potential strategy. Previous research demonstrated that the presence of $CD68^+$ macrophages was linked to favorable prognosis in patients treated with R-CHOP, while it correlated with poor outcomes in the absence of rituximab, meaning that macrophages are playing an important role in the treatment response in DLBCL[101]. Although these therapies have demonstrated limited efficacy as monotherapies in certain cases and may not sufficiently induce phagocytosis on their own, there is a growing interest in their use in combination therapies. In fact, blockade of CD47 and LILRB1 have demonstrated an increase therapeutic efficacy of rituximab against DLBCL cells[111,112,113]. The rationale behind this approach is that CD47/SIRPα blockade can disrupt the "don't eat me" signal, while rituximab can opsonize tumor cells, providing a synergistic anti-tumor effect[114]. This strategy highlights the potential for developing macrophage-directed therapies, especially for patients who are resistant to rituximab and T-cell-mediated treatments. However, there is a need to develop new macrophage-directed therapies that can be used in conjunction with existing treatments to boost macrophage antitumor activity, overcome immune resistance, and improve outcomes for DLBCL patients.

1.7. Primary central nervous system lymphoma

1.7.1. Definition and epidemiology

Primary central nervous system lymphoma (PCNSL) is a rare and aggressive extranodal NHL that is confined within the central nervous system (CNS), including the brain, leptomeninges, spinal cord, and/or eyes, without any clinical sign of systemic disease. In brain lesions, the parenchyma is affected in approximately 80-90% of cases. Meningeal involvement, known as leptomeningeal disease, occurs in around 15-20% of patients, either independently or alongside parenchymal lesions.

PCNSL annual incidence rate ranges from 0.3 to 0.6 cases per 100,000 individuals in nationwide population-based studies; however, its incidence increases among elderly patients[115,116,117]. The median age at diagnosis for PCNSL is around 60 years, with a slightly higher prevalence in males. PCNSL accounts for approximately 1-2% of all NHLs, 4-6% of all extranodal lymphomas, and 4-6% of all primary brain tumors[118].

According to the WHO-HAEM5, PCNSL is classified under a new category called large B-cell lymphomas (LBCL) of immune-privileged sites. This classification encompasses aggressive B-cell lymphomas that arise as primary tumors in immune sanctuaries, including the CNS, the vitreoretinal compartment, and the testes. These lymphomas share common molecular features, including specific genetic alterations and immunophenotypic characteristics. According to the International Consensus Classification (ICC), PCNSL is considered a primary DLBCL of the CNS[71,119–121]

1.7.2. Diagnosis

The diagnosis of PCNSL relies on imaging and histopathology. Magnetic resonance imaging (MRI) is the preferred imaging technique to assess the tumor's location and extent, with contrast-enhanced computed tomography (CT) as an alternative if MRI is contraindicated. After imaging, a stereotactic CNS biopsy is necessary to confirm PCNSL and discard other brain conditions with similar imaging features. In fact, stereotactic biopsy is the gold standard method for parenchymal affection.

Cerebrospinal fluid (CSF) analysis, obtained via lumbar puncture before or after the biopsy, includes cytology, protein analysis, and flow cytometry, which is highly sensitive

for detecting malignant cells. Additionally, analyzing circulating tumor DNA (ctDNA) in the CSF offers a more precise tool for monitoring PCNSL than plasma-based tests, improving diagnosis and disease management.

1.7.3. Prognosis

For primary central nervous system lymphoma (PCNSL), two widely used prognostic scoring systems have been established. The first, developed by the Memorial Sloan-Kettering Cancer Center (MSKCC), categorizes patients into three groups based on age and Karnofsky Performance Status (KPS)[122]. Patients over 50 years old with a KPS below 70 are reported to have the poorest outcomes.

The second system, from the International Extranodal Lymphoma Study Group (IELSG)[123], which is similar to the Nottingham/Barcelona score[124], identifies five independent prognostic factors associated with poor outcomes and reduced overall survival (OS). These factors include age over 60 years, an ECOG Performance Status of 2-4, elevated serum LDH levels above the upper normal range, elevated CSF protein levels, and involvement of deep structures such as the basal ganglia, corpus callosum, brain stem, or cerebellum.

Each factor is assigned 1 point, and patients are grouped according to their total score: 0-1, 2-3, or 4-5 points. The corresponding 2-year OS rates for patients with 0-1, 2-3, or 4-5 unfavorable factors are 80%, 48%, and 15%, respectively[125].

1.7.4. Genetic alterations

Genome-wide studies have identified several recurrent genetic alterations in PCNSL that distinguish it from DLBCL, suggesting a distinct pathogenesis[126]. A significant number of PCNSL cases exhibit an ABC-like phenotype; however, this does not have clear prognostic significance in PCNSL, unlike in systemic DLBCL.

PCNSL is characterized by the constitutive activation of signaling pathways involving the BCR and NF-κB. The *MYD88*^{L265P} mutation is particularly prevalent in PCNSL, found in approximately 75-80% of cases, and plays a central role in this activation, leading to downstream signaling that promotes lymphoma cell survival and proliferation by

impairing terminal B cell differentiation, disrupting normal cell cycle regulation, enhancing immune evasion, and inhibiting apoptosis. When *MYD88*^{L265P} is combined with *CD79B* mutations, which occur in around 50% of PCNSL cases, these outcomes are amplified, further driving the malignant behavior of PCNSL cells[127]. The significant association between *MYD88*^{L265P} and *CD79B* mutations suggests a collaborative effect in activating the NF-κB pathway. These characteristic mutations of PCNSL are genetic hallmarks of the MCD/C5 subtype[87].

PCNSL typically shows fewer *MYC*/*BCL2* rearrangements compared to systemic DLBCL; however, it frequently presents with gains or amplifications of the *MYC* and *BCL2* loci, leading to overexpression of these oncogenic proteins[128]. *BCL6* translocations, observed in roughly 20-30% of cases, are also more common in PCNSL than in other DLBCL subtypes, suggesting a role in its unique pathobiology[129].

Moreover, in contrast to the majority of systemic DLBCLs, PCNSLs and other immune-privileged site lymphomas exhibit relatively few copy number alterations (CNAs). Systemic DLBCL primarily shows genomic instability characterized by multiple low-frequency CNAs affecting *p53*/cell cycle components and additional *TP53* mutations. In contrast, PCNSL rarely has *TP53* mutations but frequently perturbs *p53* function through upstream alterations such as *CDKN2A* loss[130].

Another important aspect of PCNSL pathogenesis is ASHM, which occurs more frequently in PCNSL than in systemic DLBCL. These alterations afect genes encoding immunoglobulins, like the *IGHV4-34*, which is present in up to 40% of cases; and proto-oncogenes, such as *PIM1*, *PAX5*, *BTG2*, and *MYC*. These mutations contribute to the development and progression of PCNSL by promoting genetic instability and aberrant signaling pathways[131].

The mechanisms of tumor immune escape in PCNSL are also significant. These mechanisms include deletions of the *HLA* locus (6p21), observed in about 60% of cases, copy-number losses of *B2M* (15q21.2), and chromosomal rearrangements involving *CIITA*. Chromosomal translocations involving the *CD274* gene, and less frequently, genomic amplifications of *CD274* and *PDCD1LG2,* which lead to overexpression of PD-L1 and PD-L1, have also been documented. These genetic changes

lead to overexpression of immune checkpoint proteins[87,132]. All these immune escape mechanisms are correlated with poor outcome and lower survival.

1.7.5. Tumor microenvironment

PCNSL is considered a lymphoma growing in an immune-privileged site—the brain—where immune responses are tightly regulated. It is protected by the blood-brain barrier (BBB), which selectively restricts the entrance of immune cells. Microglia, the tissue-resident macrophages in the CNS and the only type of resident immune cell in the brain, contribute to this immune privilege by presenting low expression of MHC molecules or co-stimulatory molecules[133,134], and secreting immunosuppressive cytokines, such as TGF-β and IL-10, which help modulate and suppress potential immune responses[135]. These mechanisms, all important for avoiding inappropriate inflammatory reactions in the brain, also make the CNS a permissive environment for lymphoma development.

Despite this, it is now accepted that PCNSL exhibits substantial immune cell infiltration, which have prognostic implications[136,137].

Recent studies have highlighted the heterogeneity of the TME in PCNSL, which is still being fully characterized. Infiltrating $CD4^+$ T cells typically localize around lymphomatous areas, whereas $CD8^+$ T cells are more concentrated within the tumor[136]. Notably, a correlation has been observed between PD-1 expression in TILs and favorable outcomes, while the absence of $PD1^+$ TILs is linked to relapse or disease progression[138,139,140]. T cell exhaustion, increased immune checkpoint molecule expression, and immune evasion signals have also been described[141].

The role of TAMs in PCNSL has gained significant attention, as macrophages are the most prevalent non-tumoral immune cells infiltrating the TME. In mouse models, an increase in APCs—including microglia, infiltrating macrophages, and dendritic cells—was observed near the tumor, alongside substantial T cell infiltration[142]. PD-L1 expression in tumor cells and a higher density of TAMs have been linked to better OS, a pattern also seen in other lymphomas in immune-privileged sites[143,144]. However, other studies have not found any correlation between high TAM infiltration and better OS[137].

Both M1 and M2-like macrophages have been identified within the TME, where they play key roles in CNS lymphoma progression[137,145]. Recent work from our group demonstrated that PCNSL is characterized by significant macrophage infiltration, with these cells expressing elevated levels of PD-1 and SIRPα in M2 macrophages[146].

1.7.6. Treatment

First-line treatment in PCNSL typically involves high-dose methotrexate-based chemotherapy (HD-MTX)[147,148]. For consolidation therapy, fit patients often receive high-dose chemotherapy followed by autologous stem cell transplantation (ASCT), while whole-brain radiotherapy (WBRT) may be used for unfit patients[149]. However, WBRT is now used more selectively due to potential long-term cognitive effects. Although initial response rate to treatment is high, approximately 35% to 60% of patients experience relapse, with most recurrences occurring within the first two years of diagnosis[150]. For relapsed cases, several salvage therapies may be considered, including HD-MTX rechallenge, novel targeted therapies such as Bruton's tyrosine kinase (BTK) inhibitors, and immune checkpoint inhibitors[151]. Despite these treatment options, the prognosis for relapsed PCNSL remains poor, with 5-year survival rate for patients is estimated to be around 25%, highlighting the need for more effective therapies and treatment strategies[150].

The addition of rituximab in PCNSL treatment has also been studied[152]. PCNSL as other B-cell neoplasms expresses CD20; however, the use of rituximab in this setting is sometimes debated. A phase III trial compared chemotherapy with and without rituximab, followed by further chemotherapy and low-dose radiation for patients under 60. The trial found no significant improvement in event-free survival with rituximab, though there was a slight, non-significant trend toward better progression-free survival (PFS)[153]. In contrast, adding rituximab to HD-MTX chemotherapy improved 5-year OS, with 40% of patients surviving compared to 28% in those who received chemotherapy alone[154]. A key challenge impacting rituximab's effectiveness in PCNSL is its limited ability to penetrate the brain. Due to its large molecular size, the delivery of rituximab is largely confined to areas with significant tumor burden where the BBB is highly

compromised. This restricted access to smaller or more diffuse tumor regions may explain the reduced efficacy observed in some patients.

1.7.6.1. Novel therapeutic options

PCNSL has a higher rate of recurrence and a worse prognosis than systemic DLBCL; thus, novel therapeutic modalities are needed. Essentially, the tumor immune microenvironment significantly influences the pathobiology of PCNSL. Therefore, it is reasonable to explore therapeutic strategies that target both malignant cells and the supportive immunosuppressive tumor microenvironment. Anti-PD-1 blockade has shown promise in preclinical murine models of PCNSL[155]. Currently, nivolumab and pembrolizumab, alone and in combination with R-CHOP, are being evaluated in clinical trials to assess their effectiveness and safety in PCNSL. Preliminary results from small studies and case series suggest potential therapeutic activity, particularly in patients with relapsed or resistant cases. However, these early findings are based on limited data, and durable responses have not yet been consistently demonstrated[156,157].

Overall, the efficacy of immune checkpoint therapies in PCNSL remains largely anecdotal, with a paradoxical aspect to their use: while these therapies aim to enhance T cell activity, PCNSL frequently exhibits loss of MHC class I expression, potentially limiting T cell recognition of tumor cells. This contradiction highlight the need for deeper insights into the tumor microenvironment to fully assess the potential benefits and limitations of immune checkpoint inhibitors in PCNSL treatment.

Exploring novel agents that can cross the blood-brain barrier, as well as immunotherapies targeting immune evasion mechanisms or engaging other immune effector cells in the brain, such as macrophages, is crucial for advancing the treatment of PCNSL.

1.8. Secondary central nervous system lymphoma

Secondary central nervous system lymphoma (SCNSL) occurs when the CNS becomes involved as a site of relapse in patients with systemic DLBCL. This complication affects approximately 5% of DLBCL patients, though the incidence can rise to 10-15% in high-risk subgroups, including those with high ECOG scores, elevated LDH levels, and multiple extranodal sites at diagnosis. SCNSL typically presents early, with CNS relapse occurring within a median of 6 to 10 months after the initial lymphoma diagnosis, often during or shortly after frontline therapy. Prognosis is poor, with survival rates of only 3 to 6 months following CNS involvement, underscoring the need for early detection and aggressive intervention[158].

Although large-scale studies can demonstrate a reduction in the risk of CNS relapse with the introduction of rituximab for the treatment of DLBCL, the impact is small, likely reflecting the poor CNS penetration of rituximab through the BBB[153,159]. In the pre-rituximab era, most relapses occurred in the leptomeninges[160]. However, with the addition of rituximab, CNS relapses occur more commonly within the brain parenchyma, accounting for 60% of all relapses as opposed to 15-20% for leptomeningeal relapses[161,162].

1.8.1. Clinical risk factors of CNS relapse

The CNS International Prognostic Index (CNS-IPI) is the gold standard method in clinical practice for stratifying patients and predicting CNS relapse, combining various clinical features for a comprehensive risk assessment[163]. Evaluation of specific extranodal sites in multivariate analysis along with the 5 IPI factors has yielded kidney/adrenal as critical sites for CNS relapse, and thus, the final model of CNS-IPI score includes 6 risk factors. It defines three risk categories into low risk (0-1 factors), intermediate risk (2-3 factors), and high risk (≥4 factors), and defines a 2-year risk of CNS recurrence of approximately 0.6%, 3.5%, and 10%, respectively. Importantly, it is reported that patients with 5 and 6 risk factors have a risk of CNS recurrence up to 15% and 30%, respectively[164].

The CNS-IPI represents the first model to estimate the risk of CNS relapse. However, despite its robustness and prior validation[165], the performance of this model remains suboptimal, with half of the events occurring in patients classified as having low to intermediate scores.

1.8.2. Biomarkers associated with CNS relapse

To better predict CNS involvement in DLBCL, attention has recently shifted towards integrating biological features, such as *MYC, BCL2* and *BCL6* translocations, and cell-of-origin subtype, into the CNS-IPI score. Klanova et al. demonstrated that the combination of both high CNS-IPI score and ABC or unclassified subtype was associated with a two-year CNS relapse rate of 15.2%, as opposed to 0.5% for low risk and GCB subtype[166]. Additionally, recent research has reported that double-hit or triple-hit lymphomas are associated with a 13% higher risk of CNS recurrence at three years[167,168]. Yet, clear conclusions regarding the integration of biological characteristics into risk models are still lacking.

1.8.3. CNS prophylaxis treatment

CNS prophylaxis is commonly administered to DLBCL patients with a high-risk CNS-IPI, particularly those with more than two extranodal sites, such as testicular or kidney/adrenal involvement, or with dual expression of MYC and BCL2[169]. In the pre-rituximab era, intrathecal methotrexate (IT-MTX) was the standard prophylaxis, based on experience with other lymphomas. IT-MTX is effective for leptomeningeal disease but has limited CNS penetration and is less suitable for parenchymal involvement. However, in the rituximab era, IT-MTX did not significantly reduce the incidence of CNS relapse in DLBCL, likely due to increasing rates of parenchymal involvement. Intravenous HD-MTX has emerged as a preferred option across various guidelines due to its ability to penetrate the brain, although it carries a risk of significant neurological toxicity[170].

Nevertheless, the use of CNS prophylaxis in DLBCL remains controversial. Large retrospective studies have yielded mixed conclusions regarding its efficacy, and the

absence of prospective randomized controlled trials leaves uncertainty about its true value. Despite this, CNS prophylaxis continues to be widely used in clinical practice[171]. Improved diagnostics for early detection of CNS relapses and the development of newer therapeutics for CNS prophylaxis are needed to enhance treatment outcomes for SCNSL patients.

2. Hypothesis

PCNSL often employs mechanisms such as MHC class I downregulation and PD-L1 overexpression to escape T cell recognition and attack. Since MHC I on cancer cells can inhibit macrophage activity through the LILRB1 receptor, CNS lymphoma cells that downregulate it may become more susceptible to macrophage-mediated cytotoxicity. Additionally, PD-1 expression in macrophages reduces their phagocytic capacity, potentially hindering their ability to combat PD-L1$^+$ CNS lymphoma cells effectively. Given that macrophages constitute the predominant immune cell population within the tumor microenvironment of PCNSL, we hypothesize that these cells play a crucial role in mediating the anti-tumor response to immune checkpoint inhibitors, particularly in cases characterized by genetic alterations that promote T cell immune evasion.
Furthermore, we propose that harnessing macrophage-mediated anti-tumor responses could serve as an effective therapeutic strategy for other types of non-Hodgkin lymphoma characterized by MHC class I downregulation, which often renders them resistant to conventional T cell-based therapies. This approach may overcome the limitations posed by impaired antigen presentation and expand treatment options for patients with refractory lymphomas

Relapse in the CNS is a significant challenge for DLBCL patients. Although several clinical and molecular scores have been developed to identify patients at risk of CNS relapse at diagnosis, their accuracy is still limited. This highlights the need for a deeper understanding of the factors involved in secondary CNS lymphoma and the identification of new biomarkers capable of predicting CNS involvement. We hypothesize that a comprehensive multiomics analysis of the (epi)genetic, transcriptomic, and immune characteristics at the time of diagnosis in systemic DLBCL tumors could uncover specific features that predispose these tumors to migrate to the CNS.

3. Objectives

The **main objective** of this thesis is to study the immune dynamics in CNS lymphoma and develop macrophage-directed immunotherapeutic strategies to boost the immune response in B-cell lymphomas. Additionally, it seeks to identify molecular and immunological markers that can predict CNS involvement in DLBCL.

The **secondary objectives** are the following:

- To assess the roles of macrophages and T cells within the immune-evasive tumor microenvironment of primary CNS lymphoma that lack MHC I expression, and to evaluate their response to PD-1 and CD47 blockade therapy.

- To identify potential targets and therapeutic strategies that effectively enhance macrophage activity against B-cell lymphoma cells, particularly in cases where MHC class I downregulation impairs T cell-mediated anti-tumor responses.

- To analyze the immune, genomic, transcriptomic, and epigenomic characteristics of systemic DLBCL tumors at diagnosis to identify key features associated with CNS relapse.

4. Material & Methods

4.1. Cell Lines

A20 (BALB/c B-cell lymphoma) and Raji (human Burkitt lymphoma) cell lines were obtained from ATCC. Toledo (human DLBCL) cell line was obtained from Koch Institute High Throughput Services Core. SUDHL-4 (human DLBCL), was obtained from the Koch Institute High Throughput Services Core. SUDHL-8 (human large B-cell lymphoma), HBL-1 (AIDS-related NHL), and Daudi (human Burkitt lymphoma) cells were provided by Catherine Wu's laboratory (Dana-Farber Cancer Institute). All cell lines, except HBL-1 cell line, were cultured in RPMI (Thermo Fisher) supplemented with 10% ultra-low IgG fetal bovine serum (FBS) (Thermo Fisher), 100 units/mL penicillin, 100 µg/mL streptomycin, and 292 ug/mL L-glutamine (Thermo Fisher). HBL-1 cell line was cultured in PriGrow V (abm) supplemented with 10% ultra-low IgG FBS, 1X GlutaMAX and 1% Penicillin/Streptomycin. Cell lines were maintained in humidified incubators at 37 °C with 5 % carbon dioxide.

4.1.1. Fluorescent and bioluminescent cell lines

StayGold+ (SG+) cell lines were generated by transduction of cells with a lentivirus encoding hStayGold (Genbank LC593679.1) under the control of an EF1-α promoter (Vectorbuilder) followed by selection with puromycin. GFP+ cell lines were generated by lentiviral transduction of cells using CMV-GFP-T2A-Luciferase pre-packaged virus (Systems Bio). Transduced cells were then sorted for stable GFP expression. To generate a stable mScarlet Toledo line, a DNA fragment encoding the monomeric mScarlet red fluorescent protein was synthesized (IDT) and cloned into an AAVS1-homology donor vector previously published[63], using HiFi DNA Assembly (NEB) following restriction with XbaI and MluI digest of the targeting donor vector and inclusion of homology arms on the synthesized mScarlet fragment. The AAVS1-mScarlet donor template vector was introduced in the cells along with an AAVS1-targeting Cas9 PX458 (#48138-Addgene) plasmid containing the sgRNA sequence: GGGGCCACTAGGGACAGGAT using nucleofection according to the manufacturer's specifications (Lonza 4D Nucleofector, B-cell protocol) at a DNA mass ratio of 4:1 donor to Cas9 plasmid. The cells were selected

using puromycin driven by the endogenous AAVS1 transcription via a splice acceptor and 2A chysel sequence upstream of the puromycin cassette in the AAVS1-homology donor construct. Cells were then expanded and further enriched for reporter expression using fluorescence-assisted cell sorting. Cells were frozen immediately after FACS enrichment, banked, and thawed for use in experiments.

For luciferase expression, cells were stably transfected with luciferase (Fluc2 gene). For this, cells were electroporated the presence of 5 pM of pGL4_Luc2_CMV_neo plasmid; 48 hours after electroporation 2000 mg/ml G418 was added to culture media. After two weeks of selection, the bioluminescence of cells was analyzed by bioluminescence imaging (BLI) using IVIS® Spectrum system and Living Image software (PerkinElmer).

4.1.2. Generation of knockout cell lines

MHC I knockout (KO) A20 and Raji variants were made by CRISPR-Cas9 genome editing using a Cas9 endonuclease. Mouse TAP1 gRNA (GCGGCACCTCGGGAACCAACAGG), human B2M gRNA (CGTGAGTAAACCTGAATCTTTGG), Cas9 endonuclease and universal tracrRNA were obtained from Integrated DNA Technologies (IDT). The crRNA:tracrRNA complex was ensembled following the manufacturer's protocol and delivered by electroporation using the Neon Transfection System (Thermo Fisher).

4.2. Macrophage isolation and culture

Primary murine macrophages were derived from syngeneic BALB/c mice as previously described[172]. In brief, long bones from mice were collected and bone marrow was mechanically extracted using a mortar and pestle. Cells were washed with PBS then subjected to ACK lysis (ThermoFisher) to deplete red blood cells. Unfractionated bone marrow cells were plated on Petri dishes (Corning) with 20 ng/mL murine macrophage colony-stimulating factor (M-CSF) (Peprotech) for at least 7 days to differentiate into macrophages. Macrophages were washed, removed from plates using TrypLE

(Invitrogen) and cell lifting, and used for experiments or replated as necessary. Macrophages were generally used for experiments between days 7-21 of culture.

Primary human macrophages were derived from peripheral blood monocytes of anonymized healthy human blood donors. Leukocyte reduction collars from anonymized blood donors were obtained from the Crimson Core Biobank (Brigham and Women's Hospital). Monocytes were isolated using StraightFrom Whole Blood $CD14^+$ microbeads (Miltenyi) using an AutoMACS Pro or AutoMACS Neo Separator (Miltenyi). Purified monocytes were cultured in IMDM (ThermoFisher) + 10% low IgG FBS (ThermoFisher) + 1x penicillin, streptomycin, and glutamine (ThermoFisher) containing 20 ng/mL human M-CSF (Peprotech) for 7 days to differentiate into macrophages. Macrophages were generally used for experimentation between days 7-21 of culture and removed from plates by trypsinization and cell lifting before replating as necessary.

4.3. Primary samples

Study 3 included 48 patients diagnosed with systemic DLBCL between 2007 and 2019 at the Department of Hematology from Vall d'Hebron University Hospital (Barcelona, Spain) and Arnau de Vilanova University Hospital (Lleida, Spain). All patients received R-CHOP-like regimens as first-line therapy. Patients were retrospectively categorized into three groups according to disease relapse withing the first two years after diagnosis: relapse in the central nervous system (CNS Relapse; N=11), relapse in systemic sites (Systemic Relapse; N=21) and patients without any relapse (No Relapse; N=16). Systemic Relapse and No Relapse groups together were defined as No CNS Relapse group (N=37). We collected FFPE samples from DLBCL tumors obtained at diagnosis for subsequent analysis. This study was approved by the Institutional Clinical Research Ethics Committee of the Vall d'Hebron Research Institute, and all patients provided written informed consent in accordance with the Declaration of Helsinki.

4.4. DNA and RNA Isolation

For study 3, DNA and RNA were obtained from DLBCL formalin-fixed paraffin-embedded (FFPE) lymph nodes at diagnosis. Total DNA and RNA from samples were

extracted using the Cobas DNA Sample Preparation Kit and the High Pure FFPET RNA Isolation Kit, respectively (Roche Molecular Systems Inc., Drive Pleasanton, CA, USA), following the manufacturer's protocol. Subsequently, obtained DNA and RNA samples were quantified fluorometrically (Qubit, Thermo Fisher Scientific, Waltham, MA, USA).

4.5. Co-culture assays

4.5.1. Long-term assays

For study 2, long-term co-culture of murine or human macrophages and lymphoma cells was performed using fluorescently labeled target cells. Phenol-red free IMDM (Thermo Fisher) supplemented with 10% ultra-low IgG fetal bovine serum, 100 units/mL penicillin, 10 µg/mL streptomycin, and 292 ug/mL L-glutamine, and 20 ng/mL M-CSF was used.

Lyoplate Mouse and Lyoplate Human Cell Surface Marker Screening Panel plates (BD) were centrifuged at 300 x g for 5 minutes before reconstitution with 140 µl of IMDM, using the ASSIST multichannel automatic pipette (Integra).

To set up co-cultures, 20 µl containing $1x10^4$ macrophages and $2x10^3$ target cells (4:1 E:T ratio) were added to each well of a 384-well plate using the ASSIST Plus multichannel automatic pipette (Integra). Subsequently, 20 µl from each Lyoplate well was added to achieve a working concentration of 6.55 µg/ml. Finally, an additional 20 µl medium alone or medium containing anti-CD47 (clone B6H12, BioXcell) or anti-CD20 (clone MB20-11 and Rituximab, BioXcell) antibodies were added to the wells. This achieved a final working concentration of 10 µg/mL of anti-CD47 or anti-CD20 as appropriate. Cells were then co-cultured for 156h (~6.5 days), with whole-well imaging of phase contrast and green and red channels performed every 8 hours using an Incucyte S3 system. Automated imaging analysis was performed using Incucyte Analysis Software.

4.5.2. Phagocytosis assays

CFSE+ Raji and mScarlet+ Toledo cells were used as target cells. Labeling of Raji cells with carboxyfluorescein succinimidyl ester (CFSE) (ThermoFisher) was performed as

following: Raji cells were harvested and washed in phosphate-buffered saline. The cells were then resuspended in a CFSE solution at a final concentration of 5 μM and incubated at 37°C for 10 minutes. After incubation, the cells were washed twice with complete medium to remove excess dye and co-cultured with murine macrophages at a target macrophage ratio of 4:1. Cells were co-cultured in the presence or absence of different antibodies at a final concentration of 10 μg/mL. Cells were co-cultured for 2 hours in serum-free IMDM in round-bottom ultra-low attachment 96-well plates (Corning). After the incubation period, cells were washed and analyzed by flow cytometry. Macrophages were identified using APC anti-SIRPα and target cells were identified by CFSE. Phagocytosis was quantified as the percentage of macrophages that contained CFSE signal. Phagocytosis was normalized to the maximal response. Dose-response curves were generated using Prism version 9.2.0 (GraphPad).

4.6. Bispecific antibody generation

4.6.1. Scfv Library and Plasmid Generation

Antibody sequences were obtained from publicly available sources and contains the following targets: CD20 (Rituximab, IMGT 161), CD85 (US Patent Application Pub. No.: 20230235055A1), CD71 (Delpacibart, IMGT 1374), CD38 (Daratumumab, IMGT 301), CD40 (Dacetuzumab, IMGT 232), CD47 (CV1), CD47 (WTa2d1), CD24-1, CD24-2 (US Patent Application Pub. No.: 20210213055A1), CD184 (Ulocuplumab, IMGT 483), PD-1 (Nivolumab, KEGG D10316). The sequences were numbered using the Kabat numbering system and their VH and VL regions were fused through a (GGGGS)X3 linker. The sequence was reverse- translated and optimized for the *Homo sapiens* codon usage table. Gene blocks ordered from Twist Biosciences containing these sequences were engineered with flaking 5' and 3' multiple cloning sites containing EcoRI/BamHI and NotI. The cloning was carried over using restriction enzyme digestion followed by T4 DNA ligation and bacterial transformation. Individual colonies were subjected to Nanopore sequencing (Quintara Biosciences) to verify correct gene insertion. The ZymoPURE™ Plasmid Miniprep Kit (endotoxin levels ≤ 1 EU/μg of

plasmid DNA) was used to extract plasmid DNA from transformed bacteria, which was subsequently used for transfection.

4.6.2. Purification of Recombinant Antibodies

Purified pairs of IgG1-Knob and IgG1-Hole plasmids were co-transfected to a final concentration of 1 μg/ml of each into 900 μl of Expi293F cells at $3x10^6$ cells/ml (Thermo Fisher) in 96 deep-well plate (USA Scientific) with ExpiFectamine 293 Transfection Kit (Thermo Fisher Scientific) following the manufacturer's recommendation and incubated at 37°C, 8% CO2 with shaking at 900 rpm for 7 days. Cells were pelleted at 3,000 xg for 20 min and the antibody supernatants were diluted 2-fold with PBS and used for further analysis.

4.6.3. Recombinant protein production and purification

WTa2d1xCD38 plasmids were produced using ZymoPure MaxiPrep kit following manufacturer instructions. Plasmid concentration and purity were assessed using Nanodrop (Thermo Fisher) and 1 μg/ml of each was employed to transient transfect Expi293F cells (Thermo Fisher) following manufacturer instructions. Posteriorly, the culture was pelleted at 15,000 xg for 15 min and the supernatant was loaded in a Protein A column (Cytiva) equilibrated with TBS (pH 7.2). The column was washed with 25 ml of TBS and the protein was eluted with 100mM glycine and 100mM NaCl solution (pH 3.0). The eluate was brought to physiological pH with 1M Tris (pH 8.0) and the solution was buffer exchanged to PBS using either dialysis bags (ThermoFisher) or spin-columns (Cytiva). Protein concentration was obtained using a Nanodrop (Thermo Fisher by taking the absorbance at 280 nm.

4.7. Immunoassays

4.7.1. Flow cytometry

In study 1, brain cell suspension was blocked with 1 μg rat serum IgG per 10^6 cells (Sigma-Aldrich) for 15 min at 4ºC before the incubation with mAbs for 20 min at 4ºC. The

following mAbs were used for the identification of mouse macrophages and lymphoma cells: anti-mouse/human CD11b-PerCP Cy5.5 (Clone M1/70), anti-mouse CD45-BV510 (Clone 30-F11), anti-mouse CD206-PE/Cy7 (Clone C068C2), anti-mouse CD279-PE (PD-1, Clone 29F.1A12), anti-mouse F4/80-APC/Cy7 (Clone BM8), anti-mouse Gr1-FITC (Clone RB6-8C5), anti-mouse CD20-APC (Clone SA275A11), anti-mouse H-2Kd-PE (Clone SF1-1.1), and anti-mouse CD3-AF700 (Clone 17A2) were all purchased from Biolegend; anti-mouse CD172a-APC (SIRPα, Clone P84), anti-human CD47-FITC (Clone B6H12) and anti-human CD274-PE (PD-L1, Clone MIH1) were obtained from eBioscience. Dead cells were discarded using the LIVE/DEADTM Fixable Violet Dead Stain Cell kit (Invitrogen). Mouse TAMs were identified as CD45+ Gr1low/- $CD11b^+$ $F4/80^+$; M1 mouse TAMs as CD206- and M2 mouse TAMs as $CD206^+$. All gates were based on fluorescence minus one (FMO) or isotype controls. Flow cytometry was performed in a NaviosTM cytometer (Beckman Coulter) and data were analyzed using the FlowJo v10 software (TreeStar).

4.7.2. Binding assays

In study 2, to evaluate specific binding interactions, $1x10^5$ target cells were added in 100 µl to each well of the Lyoplate plate containing 20 µl of purified antibody. The plate was then incubated on ice for 30 minutes to facilitate binding. For murine binding, biotinylated goat anti-mouse, anti-rat, and anti-Syrian hamster antibodies, at a concentration of 1.25 µg/ml each, were added at 100 µl per well, while biotinylated anti-Armenian hamster antibody, at a concentration of 0.6 µg/ml, was added at the same volume, to each corresponding well. The plate was then incubated for an additional 30 minutes on ice. After washing, plates were incubated with Alexa Fluor 647 streptavidin, diluted 1:4000, to achieve a final concentration of 0.5 µg/ml, for 30 minutes on ice, followed by another round of washing. For human binding, Alexa Fluor 647 Goat anti-mouse Ig and Goat anti-Rat Ig were directly added as first step in each according well (dilution 1:200), following the same incubation times. Cells were then resuspended with 100 µl of FACS Staining Buffer (BD) for flow cytometry analysis, performed using a BD LSR Fortessa flow cytometer. The mean fluorescence intensity (MFI) of the bound

streptavidin-labeled antibodies was measured to quantify the extent of binding. Data analysis was conducted using FlowJo (version 10.9), and the MFI was calculated accordingly.

4.7.3. Immunohistochemistry

Immunohistochemistry (IHC) was conducted on FFPE tissue samples from the spleen, liver, and brain of mice. Antigen retrieval, immunohistochemical detection and counterstaining were performed at an Autostainer Link 48 (DAKO) using antibodies against mouse CD20 (LS-B12186-50, LSBio), mouse CD3 (Clone SP7, ThermoFisher) and mouse Iba-1 (Clone EPR16588, Abcam). Slides were scanned using NanoZoomer 2.0 HT Digital slide scanner C9600 and visualized using NDP.view 2 (Hamamatsu Photonics K.K).

4.7.4. ELISA

Immulon 4HBX Flat Bottom plates (Thermo Fisher) were coated with 1:1000 dilution in PBS of anti-human IgG Fc (Jackson Immunoresearch) overnight at 4 °C. The following day, the plate was washed three times with PBST and blocked with 1% BSA in PBST for one hour at room temperature. The plate was then washed with PBST, loaded with the diluted transformed supernatants from Expi293F cells, and incubated for another hour at room temperature. Upon washing again, anti-human IgG H+L (Jackson Immunoresearch) was added to the plate at 1:100,000 dilution in 2% (w/v) non-fat dry milk in PBST and incubated for another hour at room temperature. Finally, another set of washes was performed and 1-Step Turbo TMB Elisa Substrate (ThermoFisher) was added to the plate and the reaction was quenched with 10% phosphoric acid after 3 min. The absorbance was assessed at 450 nm.

4.8. Multiomic techniques

4.8.1. Targeted next generation sequencing

Next generation sequencing (NGS) was performed using a custom capture-based panel, targeting exonic regions of 190 recurrently mutated genes in hematological neoplasms as well as regions across the genome recurrently affected by copy number variants (CNV) (Appendix Table 1). Libraries were generated using the SureSelectQXT Target Enrichment chemistry (Agilent Technologies, Santa Clara, CA, USA) and 50 ng of DNA as input, following the manufacturer's recommendations, and then sequenced on a HiSeq 2500 instrument (Illumina, San Diego, CA, USA), following a 2 x 150bp paired-end reads standard protocol. Data analysis was performed using an in-house bioinformatics pipeline, including alignment against the reference genome build hg19 with BWA v0.7.17 and Samtools v1.9, and base and indel recalibration with GATK v3.7.0 and abra2 v2.23. Variant calling was performed with VarScan2 v2.4.3 and Mutect2 v4.1.0.0. A minimum of 5 reads supporting the variant allele were required to call a mutation. Variants were annotated and filtered according to location (exonic and splicing), variant type (nonsynonymous single nucleotide variants and indels), read depth (>50x), minor allele frequency (MAF < 0,01 according to gnomAD) and variant allele frequency (VAF ≥ 5 %). Visual analysis was performed with Integrative Genomics Viewer to remove sequencing artifacts. CNV analysis was performed with CNVkit v0.9.6.dev0 and regions with copy number neutral loss of heterozygosity (LOH) were detected using Samtools v.1.9. Finally, we input our data into the LymphGen classifier, which categorized DLBCL into molecular subgroups defined as MCD (characterized by *MYD88L265P, CD79B* mutations, and immune evasion), ST2 (featuring *SGK2* and *TET2* mutations), EZB (characterized by epigenetic dysregulation), and BN2 (with *NOTCH2* activation and frequent *BCL6* rearrangements) and A53 (characterized by aneuploid with *TP53* inactivation), as previously described.[173]

4.8.2. RNA sequencing

The purity (Nanodrop), integrity, and concentration of RNA samples were analyzed using high-resolution capillary electrophoresis (Bioanalyzer 6000 nano/Bioanalyzer 6000 pico/Fragment Analyzer DNF-471) Agilent 2100 Bioanalyzer system (RNA6000 Nano and RNA6000 Pico kits), and 5300 Agilent Fragment Analyzer system (DNF-471 kit, and fluorometric quantification (Qubit BR/Qubit HS kits). Directional libraries of Total RNA were generated following the protocol of the KAPA RNA Hyperprep kit with RiboErase (Roche) for FFPE samples. A Bioanalyzer 2100 capillary electrophoresis system (Agilent Technologies, Santa Clara, CA, USA) and real-time PCR assay were used to verify the library insert size and concentration; and adapters with different barcodes to sequence multiple samples in a single lane. The libraries were sequenced using the NovaSeq6000 system (Illumina, San Diego, CA, USA) with paired-end reads of 2x50bp. More than 50 million paired reads were generated for each sample (>100 million total reads). For the analysis, RNA sequencing (RNA-seq) reads were mapped with STAR/2.7.8a[174] against the GRCh38 human reference with ENCODE parameters. Gene quantification was performed with RSEM/1.3.0[175] with default parameters using the gencode.37 annotation. Differential expression (DE) was performed with limma using the voom transformation[176] and adjusting by sex; genes with Log2FoldChange (FC) ≥ 0.5 and raw p-value (p) ≤ 0.05 were considered significant. Gene set enrichment analysis (GSEA) was performed using the limma t moderated ranked gene list with fgsea R package[177] with Reactome pathway database, Hallmarks gene set collection from MSigDB, and Gene Ontology (GO) terms. The normalized enrichment score (NES) was calculated for each gene set, and gene sets with adjusted p-value (Padj) ≤ 0.25 or p-value ≤ 0.05 were considered significant.

Cell type profiling was performed with CIBERSORTx[178], using the logCPM gene matrix and the Cell Fractions module with the LM22 signature matrix as a reference. CIBERSORTx, which uses a deconvolution algorithm to analyze gene expression profiles, takes into account the expression of 547 genes to estimate the abundance of 22 different immune cell types.

4.8.3. NanoString immune profiling

Cell-of-Origin (COO) molecular subtype was determined in all simples using the Research Use Only version of the Lymphoma Subtyping Test (LST) on the nCounter Analysis System (NanoString Technologies, Inc., Seatlle, WA, USA), which measures 15 signature genes and 5 housekeeping genes, as described previously[179]. The nCounter® PanCancer Immune Profiling Panel, used for targeted gene expression analysis, was performed in 36/48 samples. The panel consists of 730 immune-related genes and 40 housekeeping genes[180]. To determine COO, a Linear Predictor Score (LPS) was calculated for each RNA sample using a weighted sum of the gene expression. The LPS was compared against thresholds to define LPS value ranges for the assignment of ABC or GC subtype, or Unclassified[83,181]. For gene expression using the nCounter® PanCancer Immune Profiling Panel, the acquired data underwent log base 2 transformation and normalization, with housekeeping genes selected through the nSolver 2.6 package. Statistically significant differentially expressed genes (DEGs) were mined based on the difference in expression values between CNS Relapse group and No Relapse or No CNS Relapse group using linear models from the "LIMMA" package in the R language. Volcano plots of DEGs were generated using the "ggplot2" package in the R language, and Benjamini-Hochberg's method was used as control for the false discovery rate (FDR). P-value $\leq$ 0.05 and | log2FC | $\geq$ 0.5 were critical values for screening DEGs. Cell type abundance was also assessed using the panel, based on previously established gene expression specific to certain immune cell populations[182,183]. This method assumes each cell type's characteristic genes are consistently expressed, allowing abundance to be measured as the average log-scale expression of these genes.

4.8.4. DNA Methylation

Genome-wide DNA methylation profiling was performed at the Carreras Leukaemia Research Institute's Genomics Unit using the Methylation EPICv1.0 BeadChip (Illumina, Inc., San Diego, CA, USA) as described previously[184]. Following Illumina's recommendations, the DNA quality of each FFPE sample was checked using the Infinium FFPE quality control (QC) kit by performing a quantitative PCR with 2 ng of

FFPE DNA. 300 ng of FFPE DNA from samples passing the integrity quality control were bisulfite-converted using the EZ DNA Methylation-Gold™ Kit (Zymo Research, CA, USA) following the manufacturer's instructions. Bisulphite-converted FFPE DNA was restored using the Infinium HD FFPE DNA Restore Kit and the ZR-96 DNA Clean & Concentrator-5 kit (Zymo Research, CA, USA). The Methylation EPICv1.0 BeadChip platform allows over 850,000 methylation sites per sample to be interrogated at single-nucleotide resolution. 4 μl of bisulphite-converted DNA were used for processing and were hybridized in the array following the manufacturer's instructions. Illumina methylation data was preprocessed using the R environment (version 4.3.2) with the minfi Bioconductor package (version 1.48.0). Raw signal intensities were normalized applying a background correction method with dye-bias normalization using ssNoob method (single-sample normal-exponential out-of-band). The DNA methylation levels were represented as β-values ranging from 0 to 1, which is calculated as the ratio of methylated signal. Next, we removed failed CpGs (detection p value ≥ 0.01), probes annotated with genetic variants, cross-reactive probes, and those located on sex chromosomes. Annotation information from the Illumina BeadChip was utilized to categorize CpGs into promoter regions (TSS1500, TSS200, 5'UTR, and 1stExon) and gene body regions (Body, and 3'UTR).

Differentially methylated CpGs were identified using the limma Bioconductor package (version 3.58.1). CpG sites with median β-value difference ≥ |0.33| and Padj ≤ 0.05 were selected. ORA (Over-Representation Analysis) was used to analyze methylation-regulated expressed genes by R software. The DEGs (differentially expressed genes), DMPs (differentially methylated probes), and DMGs (differentially methylated genes) were analyzed using the DESeq and ChAMP R packages. The functional correlation of DEGs was analyzed by GO, Reactome and Hallmark Molecular Signatures Database (MSigDB) terms. Correlation analysis between methylation level and mRNA expression was conducted with R software.

4.9. *In vivo* studies

4.9.1. Macrophage/Microglia depletion

Pexidartinib (PLX3397) (Selleckhem) is a tyrosine kinase inhibitor targeting the colony-stimulating factor 1 receptor (CSF1R) used to deplete microglia in mouse brains. It was added to chop, specifically to an open standard diet (D20031201) (Research Diets, Inc) at a concentration of 290 mg/kg. Mice were exposed to the D20031201-PLX3397 diet for twenty days before intracerebral injection of tumoral cells and continued on the same diet until reaching the endpoint. The same procedure was followed with the D20031201 diet alone for the control group.

Clodronate liposomes were used to selectively deplete systemic macrophages. Clodronate, a bisphosphonate, is encapsulated within liposomes, which are phagocytosed by macrophages. Once internalized, clodronate is released, leading to macrophage apoptosis. For this study, intraperitoneal administration of clodronate liposomes (Liposoma) was initiated at a concentration of 0.5 mg/ml per 10 grams of body weight, starting two days prior to tumor cell injection. Maintenance doses were then administered every three days to ensure ongoing macrophage depletion.

4.9.2. PCNSL syngeneic models and drug treatment

All animal experiments were approved by the local Ethical Committee for the Use of Experimental Animals. Mice were initially anesthetized with isoflurane (1-2%), followed by subcutaneous injection of meloxicam (5mg/kg) for analgesia. A total of 10^5 A20 cells in 5 µl of PBS were injected intracerebrally into eight-week-old BALB/c female mice, using a Hamilton syringe with a 26-gauge needle at a rate of 1 µl/min, guided by stereotactic coordinates (1 mm anterior, 1.8 mm lateral right to the bregma, and 2.5 mm deep from the dura) on a Stoelting Just For Mouse™ stereotaxic platform.

A total of 96 immunocompetent (IC) mice were randomly assigned and divided into two groups (N=48 each). One group received WT A20 cell injections and the other MHC I KO A20. Each group was further randomized and subdivided into four cohorts (N=12

each), receiving vehicle treatment (PBS), anti-PD1 treatment, anti-CD47 treatment or the combination of both.

Additionally, a total of 48 macrophage/microglia-depleted (MMD) mice were randomized and divided into two groups (N=24 each). In the same manner, one group received WT A20 cell injections and the other received MHCI KO A20. Each of these groups was further randomized and split into two subgroups (N=12 each), receiving either vehicle treatment (PBS) or anti-PD1 treatment.

Intravenous treatment administration started four days after tumor induction, with a frequency of twice per week at doses of 200μg. For survival experiments, mice received a total of seven injections. Euthanasia was performed upon reaching humane endpoints, including weight loss, circling behavior, motor impairments, and increased head size. To investigate immune infiltration in the brain, brains were harvested 12 days post-tumor inoculation, following the administration of three treatment injections.

Tumor growth was monitored by BLI using an IVIS® Spectrum system (PerkinElmer) twice a week starting on day 3 post-tumor injection. Tumoral size was analyzed and quantified using Living Image software (PerkinElmer), and the total photons per second (ph/s) were recorded.

4.9.3. Brain dissociation

For endpoint experiments in PCNSL syngeneic models, mice brains were collected in cold RPMI-1640 medium immediately after euthanasia. The two hemispheres were then separated with a razor blade. One hemisphere was dedicated to immunohistochemistry, while the other was processed for flow cytometry and RNA sequencing. Brain single cell suspension was obtained using the Tissue Neural Dissociation Kit (Papain) (Miltenyi Biotec, Cat#130-092-628) following the manufacturer's protocol. Briefly, half brain tissue was harvested and mechanically cut into small pieces. The tissue was enzymatically digested using papain from the dissociation kit for 30 minutes at 37°C, with gentle agitation. After enzymatic digestion, the tissue was triturated to ensure a single-cell suspension. The suspension was filtered through a 70 μm cell strainer to remove debris.

Cells were washed and resuspended in PBS supplemented with 0.5% BSA for further analysis.

4.9.4. DLBCL and PCNSL xenograft models

NSG mice were obtained from Jackson labs (Strain: #005557) and used for experiments when approximately 6-12 weeks of age. Age and sex matched mice were engrafted subcutaneously with $1x10^6$ GFP+ Raji cells in 50% (v/v) Matrigel Matrix (Corning) and PBS. Mice were randomized to treatment cohorts and then subjected to intraperitoneal treatment with vehicle control, 100 μg WTa2d1xCD38, or 100 μg rituximab biosimilar (BioXCell). Mice were treated 5-7 times per week for 14 days. Tumor dimensions were measured by caliper twice per week and used to calculate tumor volumes using an ellipsoid formula: length x width x width x $\pi/6$.

Eight-week-old female NSG mice (Charles River Labs, Strain: #614) were used to develop a model of PCNSL, as previously described. Mice were then randomized into treatment groups and received intravenous injections of either vehicle control or 200 μg of WTa2d1xCD38 starting on day 3 post tumor injection, administered three times per week for a total of six injections. Tumor growth monitorization was performed via BLI as previously described.

For survival experiments, mice were euthanized when endpoint criteria were met, including neurological symptoms (seizures, circling or hind limb paralysis) or a significant weight loss (>20%).

4.10. Statistical Analysis

In study 1, results are expressed as the mean ± standard error of the mean (SEM) with 95% confidence interval (CI) of at least four independent experiments or subjects. The statistically significant differences between groups were analyzed using the Mann-Whitney test or one or two-way ANOVA, and $P < 0.05$ was considered significant. Survival curves were generated using the Kaplan Meier method, and statistically compared by the log-rank test. $P < 0.05$ was considered significant. Analyses were

performed using the biostatistics software package SPSS version 22 (IBM, Chicago, IL, USA). Results were graphed with GraphPad Prism 6 software.

In study 2, GraphPad Prism (v10.2) was used to perform correlation and grouped analysis. We performed a Pearson correlation test and a linear regression to evaluate the relationship between the functional and biochemical properties of the antibodies. A two-way ANOVA with correction for multiple comparisons at the indicated time point was used to detect the differences between different sample groups in both *in vivo* and *in vitro* datasets. If necessary, Tukey's multiple comparisons test was performed to distinguish the differences within groups. For paired group analysis, a Student two-tailed paired T-test was performed to elucidate the differences in grouped data. Significant differences were determined as $p < 0.05$. For the long-term co-culture and *in vivo* experiments, the results are expressed as mean ± SEM (with 95% CI), whereas for the remaining experiments, the results are expressed as mean ± standard derivation (SD).

For other statistical analyses, Python (v.3.10) was used. The datasets were normalized using sklearn MinMaxScaler function and Seaborn was used to calculate Euclidean distance and perform hierarchical clustering of the different therapeutic combinations in the human system. For K-means clustering, the dataset was first normalized using sklearn StandardScaler (z-score normalization) and then fitted using skelarn's K-means clustering function. The silhouette method was used to identify the optimal number of clusters.

In study 3, time to progression was assessed as the time between diagnosis and relapse. Supervised analysis for transcriptomic and epigenetic analysis were done by comparing CNS relapse vs. No relapse groups; and CNS relapse vs. No CNS relapse groups (Systemic relapse + No relapse). DEGs with p-value ≤ 0.05; gene sets with FDRq-value ≤ 0.25 or p-value ≤ 0.05; and CpG sites with median β-value difference ≥ |0.33| and adjusted p-value ≤ 0.05, were considered significant. All statistical analyses were carried out using GraphPad Prism. Differences in proportions and binary/categorical variables were calculated from two-sample Z-tests or Fisher's exact test. Mann–Whitney *U* test was used for differences in distributions between two population groups unless otherwise noted. *P* values were corrected for multiple comparisons using the Benjamini–Hochberg method when applied.

5. Results

5.1. Part I

Understanding immune evasion in primary central nervous system lymphoma: macrophage and T cell interactions in response to immunotherapy

This research aimed to assess the distinct roles of macrophages and T cells in modulating tumor growth and their contributions to effectiveness of anti-PD-1 immunotherapy in primary CNS lymphoma.

5.1.1. *In vivo* PCNSL model set up

The murine A20 DLBCL cell line was used as a model to replicate primary central nervous system lymphoma in a syngeneic immunocompetent model by intracerebral injection in BALB/c mice, due to the absence of available murine PCNSL cell lines. Strong positive expression of PD-L1, CD47 and MHCI surface proteins in A20 cells were detected by flow cytometry (data not shown). To downregulate expression of MHC class I in malignant cells, we employed CRISPR-Cas9 technology to precisely target and disable the TAP1 gene. TAP1 encodes a transporter that plays a critical role in loading peptides onto MHC class I molecules. By downregulating TAP1, we reduce MHC class I expression on the surface of malignant cells. Validation of the KO was performed through Sanger sequencing, confirming the disruption of the targeted locus (data not shown). Flow cytometry was employed to subsequentially assess MHCI surface expression, confirming a significant reduction in comparison to wild-type cells (Figure 9).

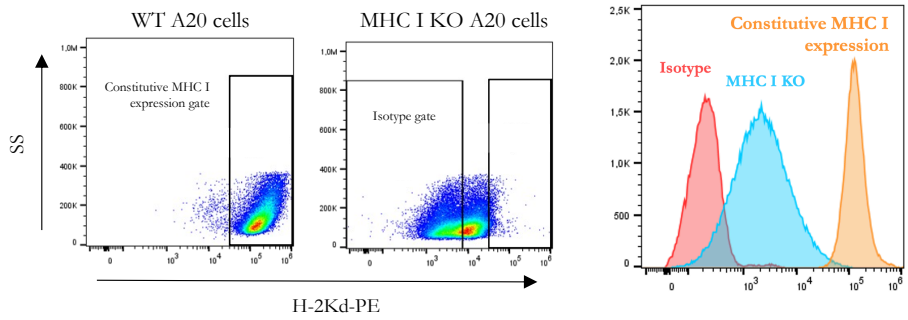

Figure 9 | Validation of MHC I knockout by CRISPR-Cas9 using flow cytometry. Dot plots and histogram showing surface expression of MHC I in A20 cells. Constitutive expression in WT A20 is shown, as well as the expression results after the CRISPR.

To study the role of macrophages in the context of CNS lymphoma, we established a macrophage-depleted mouse model by targeting both systemic macrophages and brain microglia. Systemic macrophages were eliminated using clodronate liposomes, while microglia were targeted with the CSF1R inhibitor Pexidartinib. To assess the efficacy of these treatments, we performed Iba-1 staining via IHC on mouse brain, spleen, and liver slides at various timepoints. Our findings revealed a significant reduction of microglia in brain at day 21 (Figure 10A) and systemic macrophages within the spleen and liver

following three injections (Figure 10B), with sustained depletion over time observed using the same dosing regimen (data not shown). We also checked the depletion of macrophages and microglia in mice bearing primary CNS lymphoma and assessed the expression of CD11b using flow cytometry. Our results revealed a significant reduction in both myeloid cell populations within the tumor microenvironment under inhibitory treatment. While the depletion was not complete and a residual membrane staining is observed, we believe these cells likely remain inactive due to the inhibitory effects of the treatment. (Figure 10C).

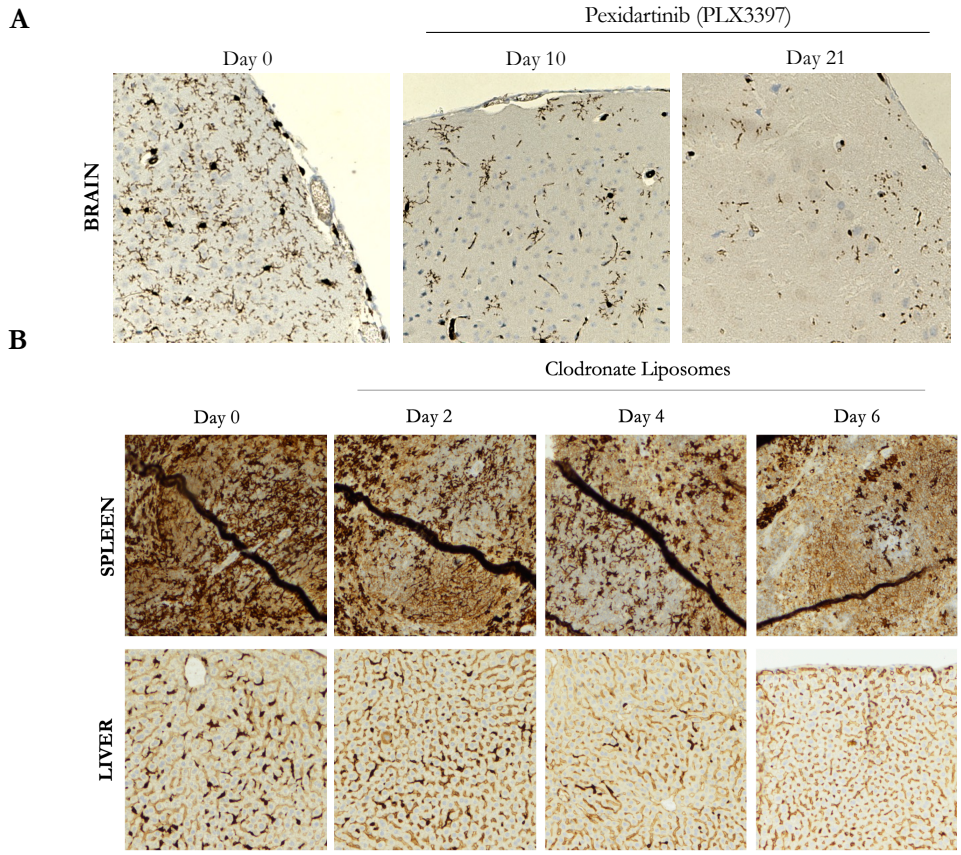

Figure 10 | Microglia and macrophage staining. A, IHC of Iba-1-stained microglia in FFPE brain sections from mice treated with the anti-CSF1R drug Pexidartinib (PLX3397) at baseline (day 0), day 10, and day 21 post-treatment. **B**, IHC of Iba-1-stained macrophages in FFPE spleen and liver sections from mice treated with clodronate liposomes, stained the day after each injection (up to 3 injections total). Images were captured at 10x magnification. IHC = Immunohistochemistry; FFPE = Formalix-fixed paraffin-embedded

We also checked the depletion of macrophages and microglia in mice bearing primary CNS lymphoma and assessed the expression of CD11b+ using flow cytometry. Our results revealed a significant reduction in both myeloid cell populations within the tumor microenvironment under inhibitory treatment. While the depletion was not complete and a residual membrane staining is observed, we believe these cells likely remain inactive due to the inhibitory effects of the treatment (Figure 11).

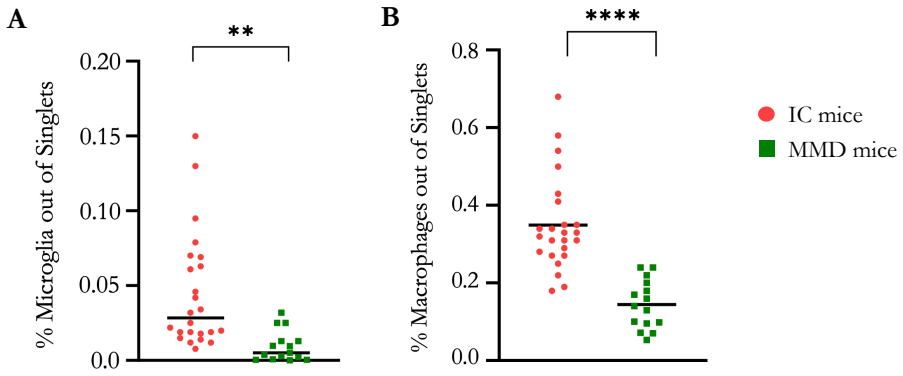

Figure 11 | Detection of CD11b⁺ microglia and macrophages by flow cytometry after PCNSL induction. A,B. Microglia (**A**) identified as $CD45^{low}CD11b^{+}$ cells and macrophages (**B**) identified as $CD45^{high}CD11b^{+}$ cells in brain tissue. Plots show percentages of cells (out of singlets) in PCNSL-induced immunocompetent mice (red) and mice treated with Pexidartinib + Clodronate liposomes (green).

To study CNS lymphoma induction in mice, we injected a total of 10^5 malignant B cells into the brain. Tumor growth was detectable by bioluminescence imaging starting from day 7 post-inoculation, and generally progressed over time, although in some cases tumor growth was reduced or did not progress (Figure 12A). In our model, mice with PCNSL had a median survival of 39 days. By IHC, multifocal tumor infiltrates affected both cerebral hemispheres and were predominantly localized in the brain parenchyma, where lymphoma cells tended to form dense clusters, although in some cases the meningeal compartment was also affected (Figure 12B).

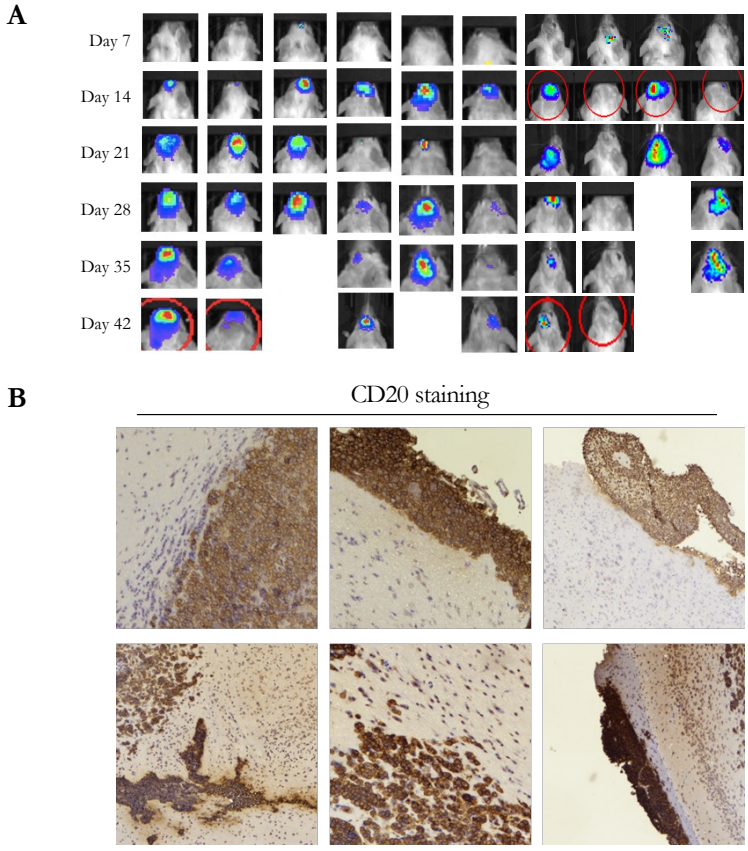

Figure 12 | Tumoral growth of malignant B cells in a PCNSL syngeneic mouse model. A, Bioluminescence imaging of mice bearing PCNSL, captured from day 7 to day 42 post-tumor injection at 7-day intervals. Red crosses indicate deceased mice. **B,** CD20 immunohistochemical staining of brain sections with PCNSL, highlighting the presence of tumor cells.

5.1.2. MHC I loss induces a more aggressive disease and reduces overall survival

To study the influence of MHC I expression in PCNSL, we induced the disease in IC mice by injecting luciferase-stable WT or MHC I KO A20 cells into the brain and monitored tumor growth by BLI, and survival. MHC I-negative tumors exhibited a more aggressive phenotype, with significant differences in tumor growth apparent as early as day 7 post-implantation, and continuing through later stages, compared to WT tumor growth (Figure 13A). To determine if the advantage in proliferation was intrinsic to the cancer cells carrying the knockout mutation, we cultured them in vitro under identical conditions and at the same concentration. We then compared their growth by counting cells using beads and analyzing the samples by flow cytometry every 24 hours over a period of 4 days. The results indicated no significant differences in *in vitro* cell growth over time between wild-type A20 cells and knockout A20 cells (Figure 13B). This suggests that MHC I-negative lymphoma cells may possess a proliferative advantage within the brain microenvironment, where T cells are unable to exert a cytotoxic effect against them. In this context of absence of the MHC I-LILRB1 inhibitory signaling pathway, we hypothesize macrophages may exhibit increased antitumoral activity. However, this potential increase of macrophage activation would not be reflected in the aggressiveness of MHC I-negative PCNSL, possibly because, unlike T cells, these may require further stimulation.

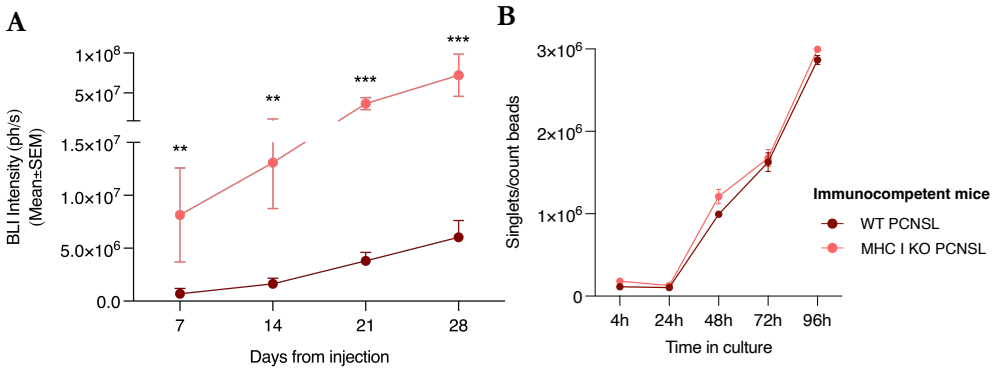

Figure 13 | In vivo and in vitro growth of WT and MHC I KO A20 cells. A, Graph depicting tumor growth of A20 cells in the brains of IC mice with PCNSL, measured by BLI over time. Sample size is n = 12 per group. Measurements were taken every 7 days for a total duration of 28 days (until all mice were alive). Data are presented as mean BLI intensity (ph/s) ± SEM. **B,** *In vitro* growth of both cell lines was assessed by counting viable cells every 24 hours using flow cytometry with beads. Data is represented as mean ± SEM. Dark red represents WT cells, while light red indicates MHC I KO cells. IC = Immunocompetent; BLI = Bioluminescence imaging; SEM = Standard error of the mean

Wild-type PCNSL tumors are more effectively regulated by T cells, resulting in slower tumor growth over time compared to their MHC I knockout counterparts. This faster growing tumor translated into a significantly longer survival of wild-type tumor-bearing mice compared to MHC I knockout tumor-bearing mice (median survival: 39 days (WT, dark red line) vs. 26 days (MHC I KO, light red line); P=0.002, Kaplan-Meier)) (Figure 14A).

5.1.3. Macrophages and microglia control the initial tumoral growth

To uncover the role of macrophages and microglia in primary CNS lymphoma, we also injected WT or MHC I KO A20 lymphoma cells into the brains of MMD mice. Tumor growth and survival were assessed. The results demonstrated that both WT and MHC I KO tumors exhibited accelerated growth and a significantly more aggressive phenotype in the absence of macrophages and microglia in the tumor microenvironment. This enhanced aggressiveness was evident when compared to the same tumors growing in immunocompetent mice, with significant differences observed at 14 and 21 days post-tumor implantation. These findings highlights the important role of macrophages in modulating tumor progression and highlight the potential importance of macrophage-mediated immune responses in controlling tumor growth in this model. (Figure 14B).

This suggests that both macrophages and microglia play an important role in controlling the initial tumoral growth of CNS lymphoma cells in the brain.

Survival analysis showed significant differences between growth of each tumor in IC mice compared to in MMD mice (Figure 14A). Both WT and MHC I KO tumors had approximately the same low median survival rates, meaning that depletion of macrophages/microglia is sufficient to induce a very aggressive disease, even in WT tumors. To understand the aggressiveness of MHC I KO tumors, it is important to note that survival of mice bearing MHC I KO PCNSL with a fully intact immune cell compartment (light red line) closely mirrors survival of mice carrying WT tumors growing in absence of macrophages and microglia (dark green line).

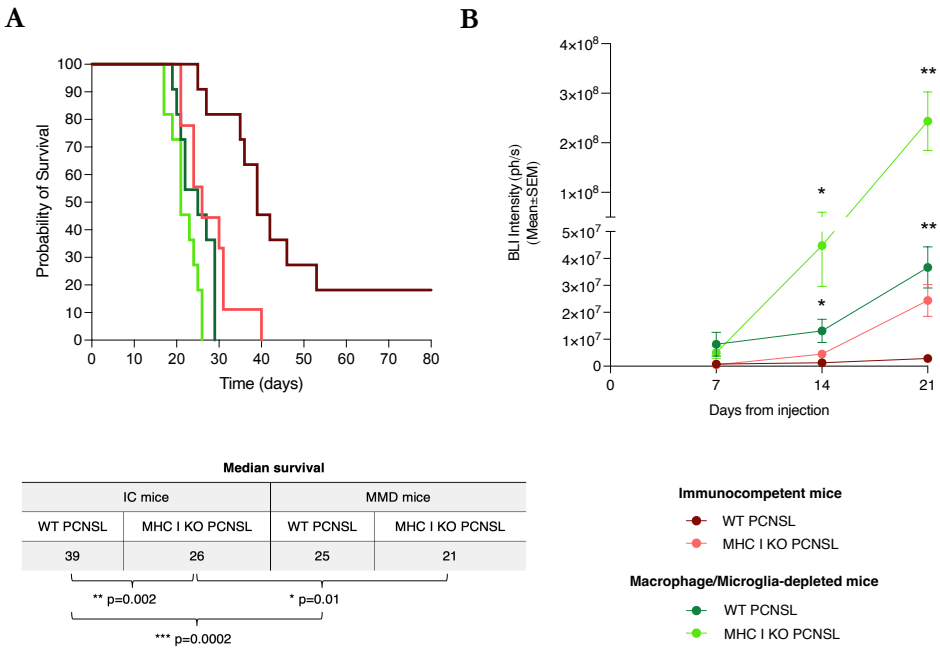

Figure 14 | Survival and tumoral growth of mice bearing PCNSL. Results are organized into two groups: IC and MMD. Within each group, mice were induced with either WT PCNSL (dark red for IC and dark green for MMD) or MHC I KO PCNSL (light red for IC and light green for MMD). **A,** Kaplan-Meier survival plot representing the probability of survival over 80 days. Median survival days for each group are indicated. Significant differences in survival are represented by p-values determined using the Log-rank test. **B**, Tumoral growth curves displayed as the mean bioluminescence intensity ± SEM for each group over time until day 21 (when all mice were alive). Mann-Whitney tests were conducted to compare type of PCNSL growing in MMD mice with each respective type of PCNSL in IC mice at every timepoint, with significant differences indicated by * ($p<0.05$) and ** ($p<0.01$). SEM = Standard error of the mean; IC = Immunocompetent; MMD = Macrophage/microglia-depleted

5.1.4. PD-1 blockade immunotherapy is more effective when macrophages are present in the TME

The observation that loss or downregulation of MHC class I surface expression in malignant cells led to a more aggressive disease in our syngeneic mouse model of PCNSL, along with evidence that macrophages can control malignant cell growth in this microenvironment, has led us to hypothesize that anti-PD-1 treatment could exert anti-tumoral effects even in scenarios where MHC class I is downregulated, by activating the phagocytic activity of macrophages. Thus, to study the roles of macrophages and T cells

in this scenario, we treated both IC and MMD mice, carrying WT and MHC I KO PCNSL, with a PD-1 blocking antibody.

Results showed that in IC mice, WT CNS lymphoma tumors showed significant differences in tumor growth became evident from day 14 post-tumor injection. However, in MHC I KO CNS lymphoma, no significant differences in tumor growth were observed between anti-PD-1-treated mice and the vehicle group at any timepoint, though a modest treatment response advantage was noted (Figure 15A). In mice depleted of macrophages and microglia, no significant differences were observed between the control and anti-PD-1 treatment groups at any timepoint, regardless of the tumor type (Figure 15B).

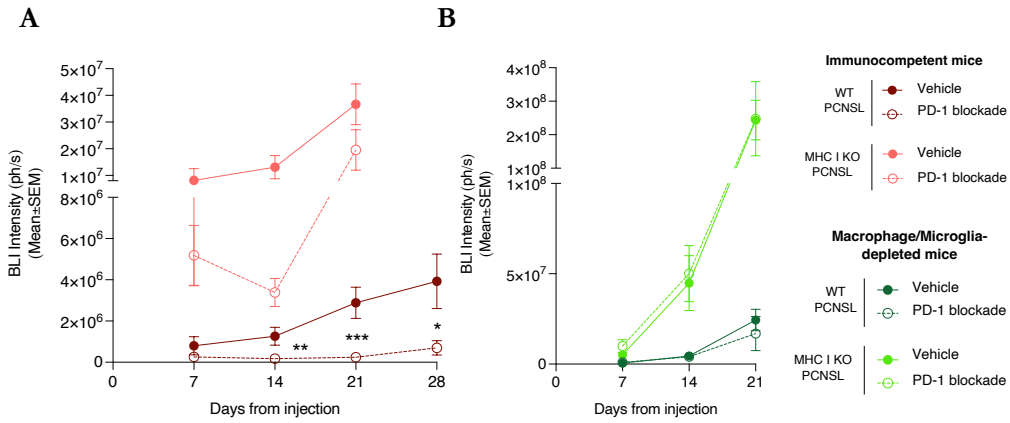

Figure 15 | Tumoral growth in mice bearing PCNSL treated with anti-PD1. Tumor growth curves are shown for each group over time, up to day 21 or 28 (until all mice are alive). Solid lines represent non-treated groups, while dashed lines represent groups treated with anti-PD-1. Data is presented as mean bioluminescence intensity ± SEM. The legend provides color-coded lines for the different groups. SEM = Standard error of the mean; IC = Immunocompetent; MMD = Macrophage/microglia-depleted

When comparing only anti-PD-1-treated groups, we observe a higher efficacy of the treatment in both tumors when macrophages are present in the TME, showing significant differences as early as day 14. Nonetheless, MHC I KO tumors have a lower response to treatment in general in comparison to WT tumors (Figure 16).

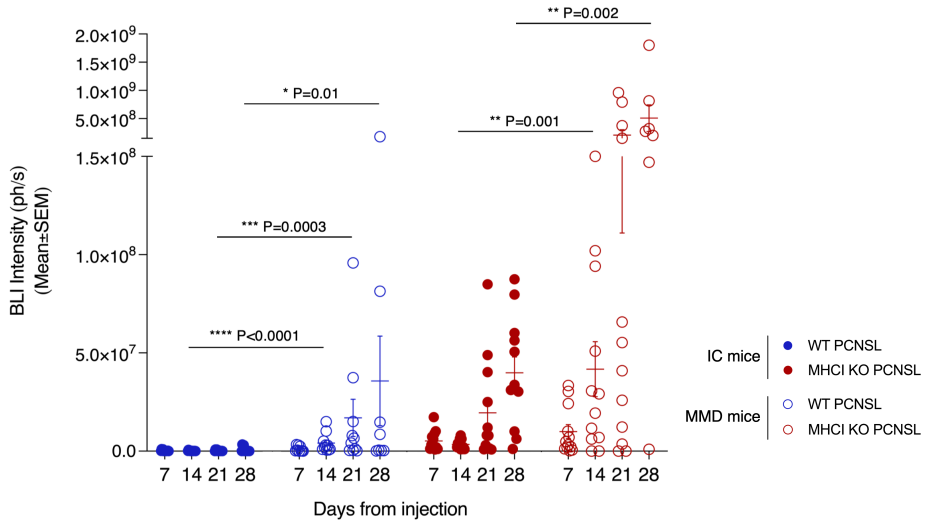

Figure 16 | Tumoral growth in anti-PD-1-treated mice bearing PCNSL. This plot displays the mean bioluminescence intensity ± SEM for each mouse in each group over time until day 28 (when all mice were alive). Solid dots represent tumors in IC mice, while empty dots indicate tumors in MMD mice. Blue dots correspond to WT PCNSL, and red dots represent MHC I KO PCNSL. Mann-Whitney tests were conducted to compare groups, with significant differences indicated by p-values. SEM = Standard error of the mean; IC = Immunocompetent; MMD = Macrophage/microglia-depleted

Overall, these results conclude that in the absence of macrophages and microglia, PD-1 blockade is less effective, suggesting that these cells actively participate in the anti-tumoral response to the anti-PD1 treatment. Results also support our hypothesis that MHC I KO tumors exhibit a diminished response to PD-1 blockade due to the inactivity of T cells.

In terms of survival, PD-1 blockade significantly prolonged survival in IC mice bearing both WT and KO tumors (Figure 17A). However, mice with WT tumors demonstrated higher survival rates. Notably, the survival effect of anti-PD-1 treatment in KO tumors was comparable to that of non-treated WT tumor-bearing mice. Interestingly, in mice without macrophages (Figure 17B), only those bearing WT PCNSL tumors showed a significant survival advantage. MHC I KO tumor-bearing mice did not respond to anti-PD-1 treatment in the absence of macrophages. These results together with the also observed diminished response to treatment in terms of tumoral growth confirm the hypothesis that MHC I-negative CNS lymphomas can only be controlled by macrophages. PD-1 blockade alone is insufficient to reduce the aggressiveness of MHC

I KO CNS tumors, indicating that disrupting the PD-1-PD-L1 interaction does not fully engage macrophages to eliminate the tumors.

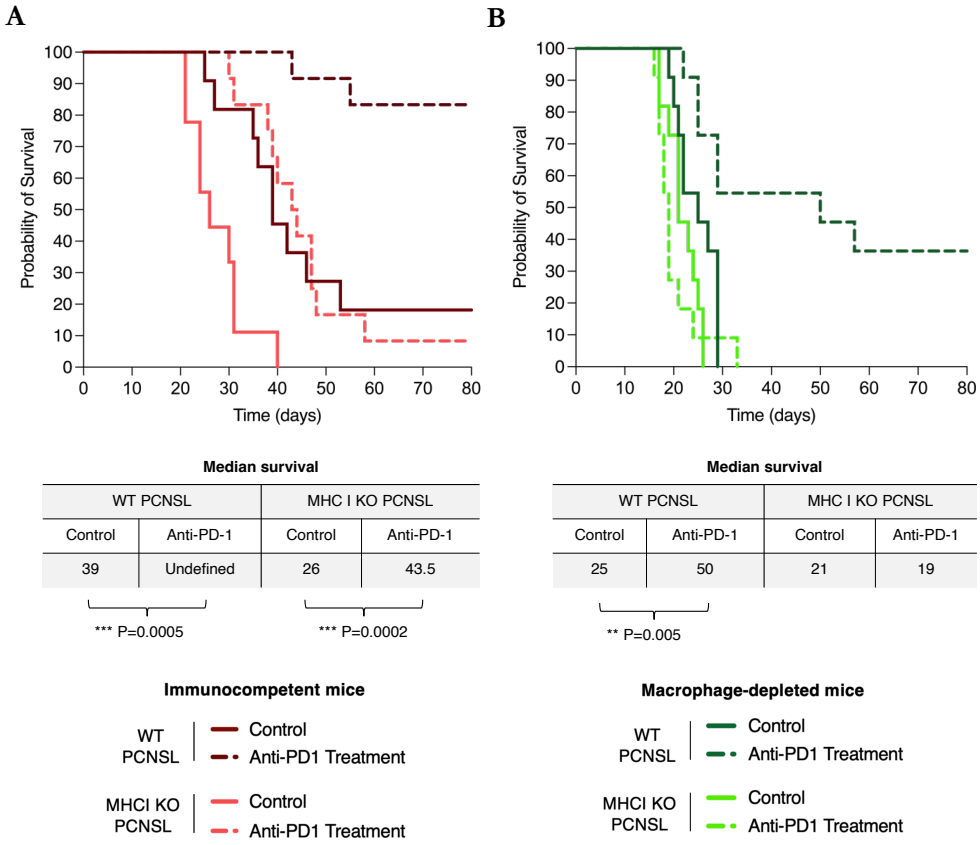

Figure 17 | Kaplan-Meier survival curves of mice bearing PCNSL. A,B, These survival plots illustrate the probability of survival over 80 days for mice with PCNSL. Mice were divided into two groups: immunocompetent mice (A) and macrophage/microglia-depleted mice (B). Within each group, mice were injected with either WT A20 cells (dark red for IC and dark green for MMD) or MHC I KO A20 cells (light red for IC and light green for MMD), and treated with anti-PD-1 treatment. Median survival days for each group are indicated below the curves. Significant differences in survival are represented by p-values determined using the Log-rank test. IC = Immunocompetent; MMD = Macrophage/microglia-depleted

5.1.5. Blocking CD47-SIRPα pathway is not enough to engage a complete macrophage anti-tumoral response in MHC I-negative CNS lymphomas

To explore immunotherapies that fully activate macrophage anti-tumoral activity in MHC I-negative CNS lymphomas, we repeated the experimental procedure, treating mice with either anti-CD47—targeting the key macrophage immune checkpoint CD47-SIRPα pathway—alone or in combination with anti-PD1.

Interestingly, significant differences in survival were observed only in MHC I-negative PCNSL mice compared to controls, suggesting that macrophages are more active against KO tumors. However, overall survival in MHC I KO PCNSL was lower than in WT tumors, with anti-CD47 treatment resulting in worse outcomes than PD-1 blockade alone (Figure 18A). It is important to note that CD47 blocking antibodies exhibited toxicity due to high CD47 expression in red blood cells, which may have hampered their effectiveness against the tumor.

When treated with both CD47 and PD-1 blocking antibodies, we did not observe any synergistic effect in any of the models (Figure 18B).

Overall, these results indicates that MHC I-negative CNS lymphomas remain highly aggressive under CD47 blockade, and this immune checkpoint inhibition is insufficient to improve outcomes in these tumors. An important observation from these results is that macrophages respond, at least partially, to these immunotherapies, indicating their potential as effector immune cells in treating MHC I-negative CNS lymphomas. Additional immunotherapies need to be explored to fully activate macrophage-mediated cytotoxicity against these tumors.

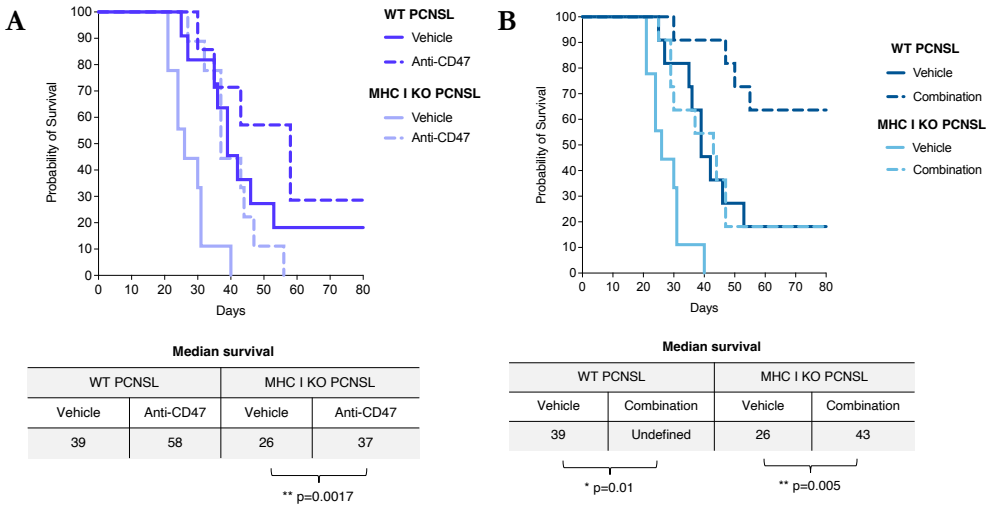

Figure 18 | Kaplan-Meier survival curves of mice bearing PCNSL. A,B, These survival plots illustrates the probability of survival over 80 days for mice with WT PCNSL and MHC I-negtive PCNSL.. Mice were treated with anti-CD47 treatment (A), or combination of anti-PD-1 and anti-CD47 treatments (B). Within each group, mice were injected with either WT A20 cells (dark red for IC and dark green for MMD) or MHC I KO A20 cells (light red for IC and light green for MMD). Median survival days for each group are indicated below the curves. Significant differences in survival are represented by p-values determined using the Log-rank test. IC = Immunocompetent; MMD = Macrophage/microglia-depleted

5.1.6. Macrophages and microglia drive immune suppression

To further characterize macrophages and T cells involved in the anti-tumor response, we extracted brains on day 12 and analysed the infiltrating immune cell populations using flow cytometry and IHC. Tumoral B cells constituted the majority of CD45+ cells, and showed greater predominance in MMD mice, particularly those bearing MHC I KO tumors (Figure 19A). Our analysis revealed significant immunophenotypic differences among malignant B cells and infiltrating macrophages and T cells, which were strongly associated with the genetic subtype of PCNSL and the immune composition of the TME. However, we observed no substantial immunophenotypic variations between untreated and treated PCNSL.

PD-L1 and CD47 expression in tumoral cells was significantly lower in MMD mice compared to IC mice (Figure 19B,C), suggesting that microglia and/or macrophages likely play a role in inducing the expression of these markers. The immunosuppressive

function of microglia is well-documented and may contribute to the maintenance of elevated immune checkpoint expression within the brain microenvironment. Additionally, we observed that MHC I-negative malignant cells expressed lower levels of PD-L1 and CD47 in comparison to WT PCNSL tumors, which indicates a lower susceptibility to immunosuppressive signals.

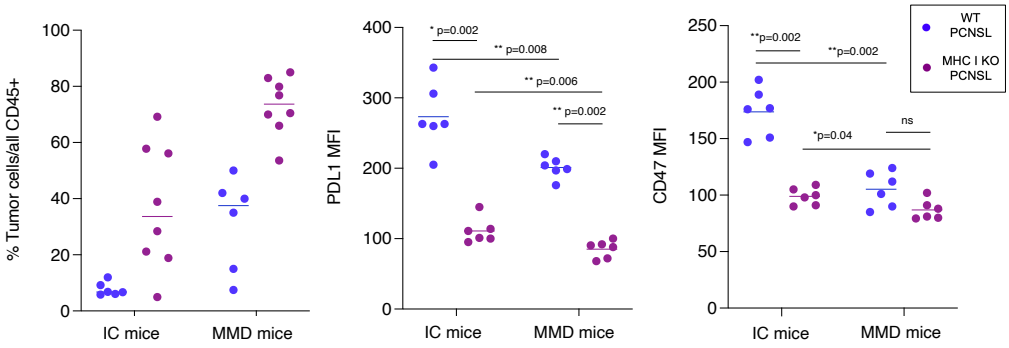

Figure 19 | Characterization of tumor cells in non-treated mice. A, Percentage of tumor cells within the CD45$^+$ population across different groups. **B,C,** Surface expression of PD-L1 (**B**) and CD47 (**C**) on tumor cells. Purple represents WT PCNSL, while maroon represents MHC I KO PCNSL. Significant differences between groups were determined using the n-Whitney test, with p-values indicated.

Across all PCNSL types, microglia emerged as the most prevalent non-tumoral immune cell throughout the brain parenchyma in immunocompetent mice (data not shown). IHC analysis revealed that infiltrating macrophages and microglia, detected by Iba$^+$ expression, were highly concentrated in proximity to CD20$^+$ tumoral cells, and exhibited significant larger morphologies and more extensive ramifications compared to their counterparts in non-tumoral areas (Figure 20). This observation aligns with findings previously reported by other researchers[142] and suggests a direct interaction and activation of macrophages and microglia within the tumor.

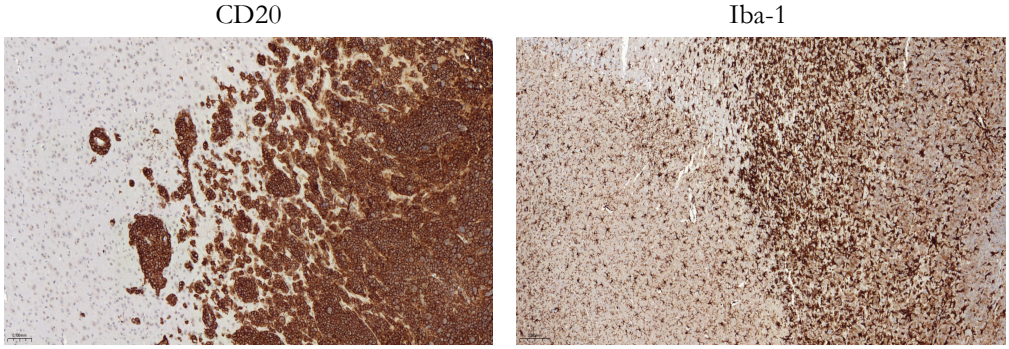

Figure 20 | Immunohistochemistry staining of brain samples. A, Section of brain tissue stained for $CD20^+$ tumora cells. **B,** The same region stained for Iba-1, showing the distribution of macrophages and microglia. Brains were extracted from immunocomptent mice.

By flow cytometry, we determined that infiltrating macrophages ($CD45^{high}F4/80^+CD11b^+$) mostly presented an M2-like phenotype ($CD206^+$) in all tumoral scenarios. PD-1 expression in these cells was significantly higher in WT PCNSL in comparison to MHC I KO PCNSL (Figure 21). SIRPα expression was also slightly higher although no significant differences were observed (Figure 21). We suggest that the observed higher PD-L1 expression in WT tumor cells likely leads to greater macrophage engagement with PD-1, triggering increased PD-1 expression on macrophages as a feedback mechanism. In contrast, MHC I KO tumors are less susceptible to T cell recognition, making the immunosuppressive feedback via PD-1/PD-L1 interactions less necessary or pronounced, which explains the lower PD-L1 expression observed.

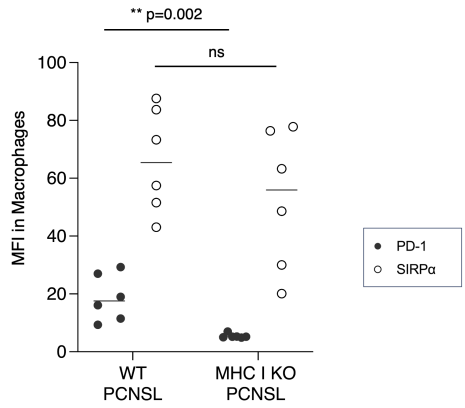

Figure 21 | Expression of PD-1 and SIRPα in macrophages. Expression of markers was performed by flow cytometry of brain samples from WT and MHC I KO tumor-bearing immunocompetent mice. Data is represented in MFI. Significant differences between groups were determined using the Mann-Whitney test, with p-values indicated.

In all groups $CD3^+$ T cell infiltration was predominantly localized either around the tumor and periphery, as previously described[133] (Figure 22A). Notably, T cells were absent in non-tumoral areas. A key limitation of the study was the inability to clearly distinguish $CD4^+$, $CD8^+$ T cells and Tregs beyond CD3 staining by flow cytometry.

Because the absence of an effective anti-tumor response in MHC I-negative tumors was not due to the absence of infiltration of T cells in the brain, we checked PD-1 expression in T cells as a marker of activation. We found a significantly lower PD-1 levels in T cells within MHC I KO tumors compared to WT tumors in both mouse models (Figure 22B), indicating reduced T cell activation and anti-tumor effector function in the absence of MHC I.

A

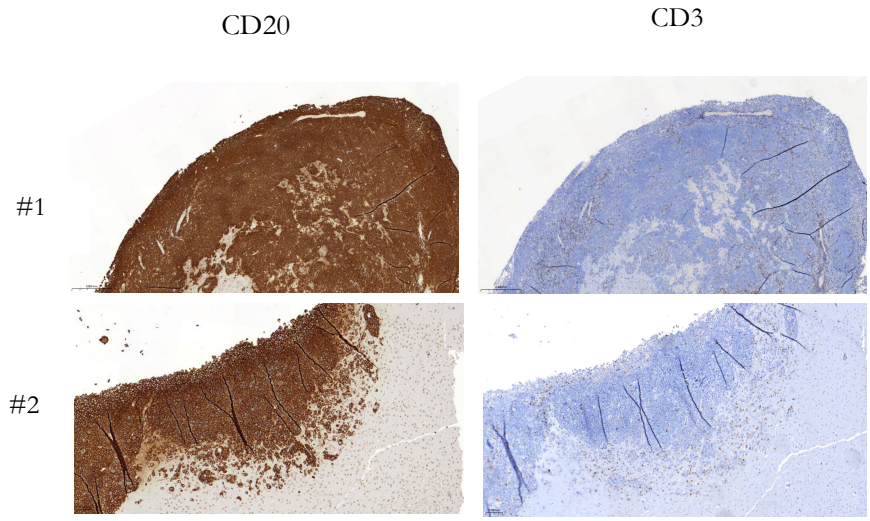

B

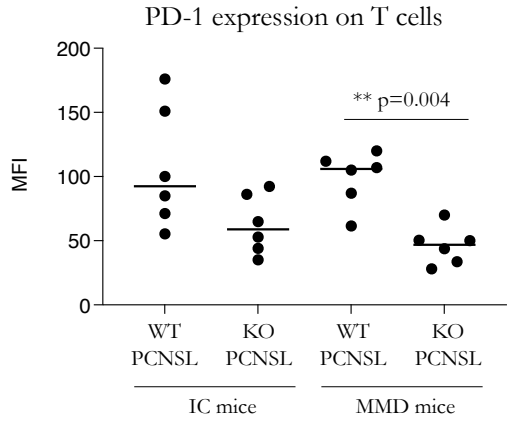

Figure 22 | A, Immunohistochemistry staining of brain samples. Two FFPE brain sections from untreated mice, stained for CD20 to identify tumor cells and CD3 to detect T cells. **B, MFI expression of PD-1 in T cells**. Expression was checked in non-treated immunocompetent and macrophage/microglia depleted mice bearing WT and MHC I PCNSL. Significant differences between groups were determined using the Mann-Whitney test, with p-values indicated.

5.2. Part II

Unbiased discovery of antibody therapies that stimulate macrophage-mediated destruction of B-cell lymphoma

This research aimed to explore novel macrophage-targeting strategies to enhance anti-tumor responses in B-cell lymphoma, specially in cases where MHC I is downregulated

5.2.1. Development of a high-throughput system to screen for macrophage-mediated cytotoxicity of B-cell lymphoma

The findings from the first part of this thesis conclude the need for developing novel therapeutic strategies to enhance macrophage-mediated responses against MHC I-negative lymphoma cells in PCNSL.

To identify unappreciated targets for macrophage-directed immunotherapy of B-cell lymphoma, we adopted a high-throughput assay to screen antibodies for their ability to stimulate macrophage-mediated cytotoxicity of lymphoma cells[185] (Figure 23). In our initial approach, we co-cultured mouse M2-like macrophages[172,186,187] with fluorescent MHC I KO A20 lymphoma cells. To the co-cultures we added an arrayed library of 173 purified monoclonal antibodies targeting different murine cell-surface antigens. We tested each antibody in duplicate across three different treatment conditions: (i) monotherapy (antibodies alone), (ii) combination with anti-CD47, or (iii) combination with anti-CD20. We performed automated microscopy and image analysis over a 7-day period to quantify the fluorescent area as a metric of lymphoma cell growth or elimination. For each treatment condition, we identified the antibodies that stimulated the greatest anti-tumor function.

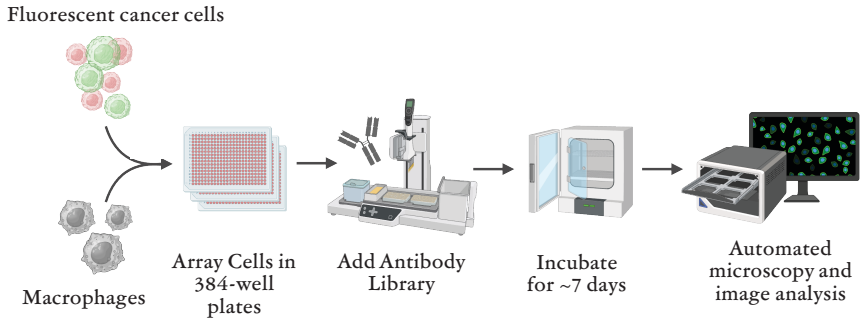

Figure 23 | Experimental design of an unbiased functional screen to identify monoclonal antibodies that provoke macrophage-mediated cytotoxicity of lymphoma cells. Primary murine macrophages were co-cultured in 384-well plates with StayGold+ MHC I A20 cancer cells (a murine B-cell lymphoma cell line). The wells were subjected to three treatment conditions: control ("monotherapy"), 10 μg/mL anti-CD47 antibody, or 10 ug/mL anti-CD20 antibody. An arrayed library of purified monoclonal antibodies targeting murine cell surface antigens (n = 173 antibodies) was overlaid at a concentration of 6.55 μg/mL. The cells were incubated for 156 h (~6.5 days) and the StayGold+ area was quantified by automated microscopy and whole-well image analysis every 8 hours.

Consistently across all conditions, we observed that antibodies to CD24, CD95 (FAS), CD40, CD184 (CXCR4), and CD79b were able to elicit robust macrophage-mediated cytotoxicity of the A20 cells (Figure 24A-D). We also performed quantitative surfaceome profiling by evaluating the ability of each antibody to bind to the surface of the A20 cells by flow cytometry. Furthermore, our results indicate that some antibodies may preferentially act on the macrophages in the co-culture system (e.g., Ly-6A/E, 4-1BBL), suggesting they modulate immune checkpoints (Appendix Figure 1). In total, these studies identified several unappreciated targets for innate immunotherapy on A20 cells that may present new therapeutic opportunities for lymphoma.

We observed a modest correlation between antibody binding and the anti-tumor response by macrophages (Figure 25A-C). For example, CD24 was the highest detected surface antigen in our assay and it induced the greatest anti-tumor response. However, many targets existed as outliers, suggesting that the degree of binding to lymphoma cells alone is not sufficient to predict whether an antibody can elicit macrophage-mediated cytotoxicity.

Overall, these findings revealed novel antibody-based therapies that enhance macrophage activity against MHC I-negative lymphoma cells. In addition to their application in primary CNS lymphoma, we believe that these new macrophage-mediated therapies could potentially overcome resistance to T-cell-mediated therapies across a broad range of B-cell lymphomas. This is particularly relevant given that one of the primary reasons for unresponsiveness to T-cell therapies is the lack of MHC I expression in malignant cells[188,189].

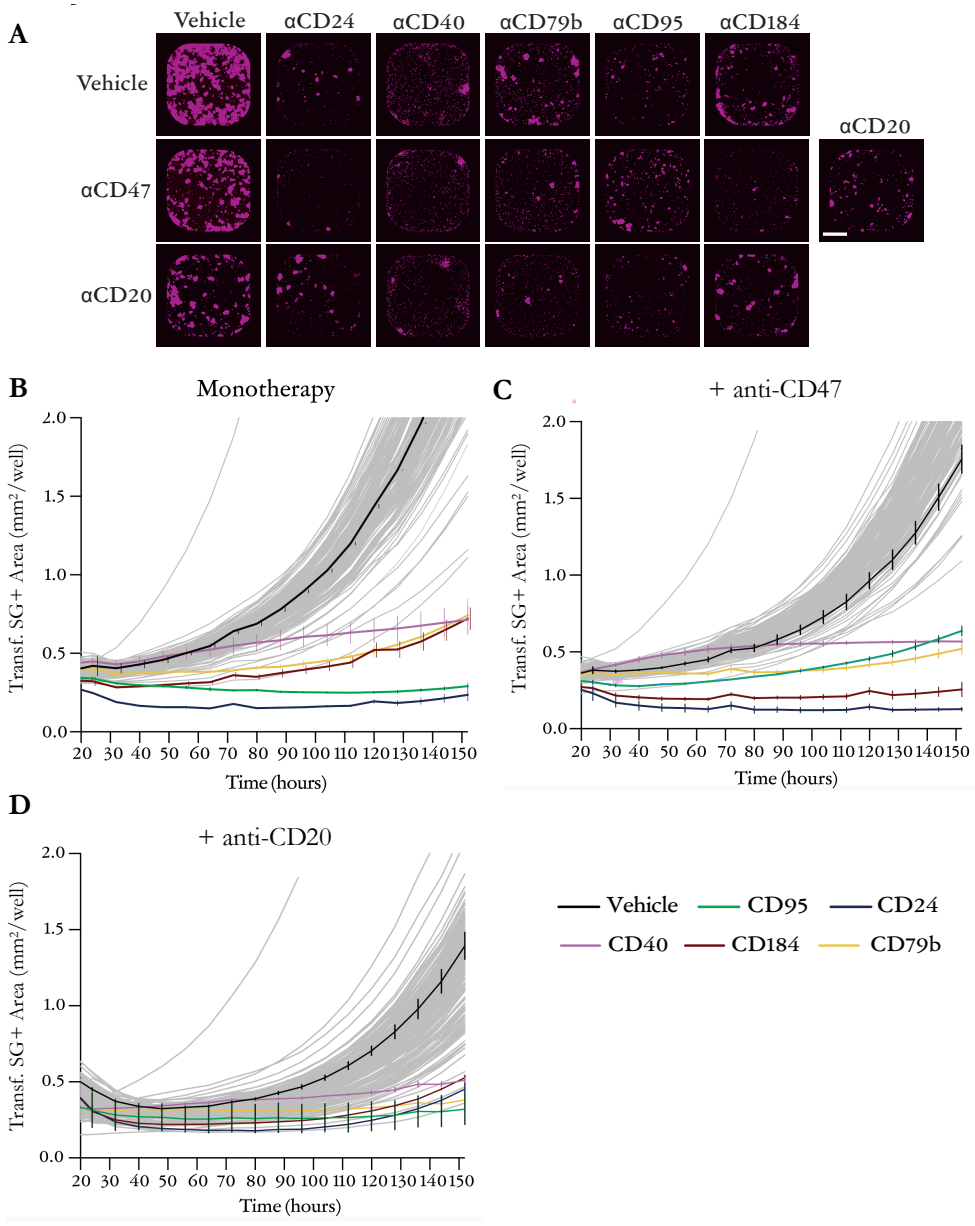

Figure 24 | A, Representative whole-well images at the last time point (156 h) showing StayGold+ lymphoma area (purple) from wells treated with the indicated antibodies that were found to stimulate macrophage-dependent cytotoxicity of A20 cells. Scale bar, 800 μm. **B-D,** Results of co-cultures with the antibody library showing growth of StayGold+ A20 MHC I KO cells under monotherapy conditions (**B**), in combination with anti-CD47 (**C**), or in combination with anti-CD20 (**D**). Each curve represents the transformed SG+ area (mm²/well) over time. Curves are the mean of two individual co-culture wells. Black curve indicates mean -/+ SEM of control wells. Colored curves indicate antibodies against CD24, CD40, CD79b, CD95 and CXCR4. SEM = Standard error of the mean.

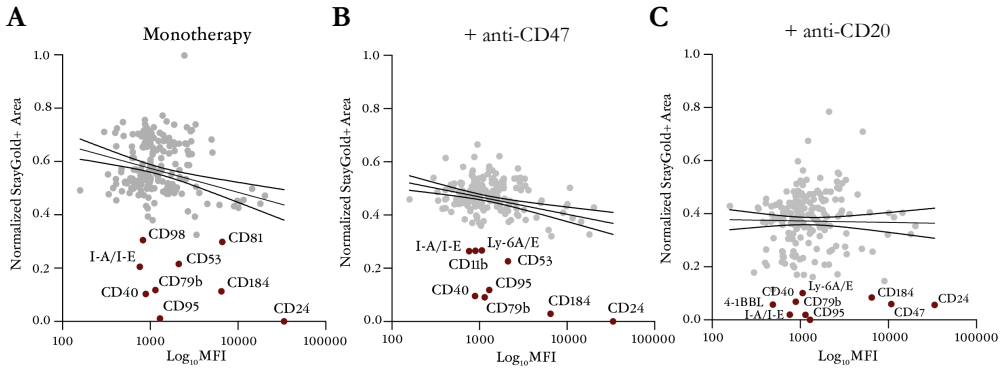

Figure 25 | Correlation between antibody binding and efficacy. A-C, Scatter plots depicting results of quantitative surfaceome profiling by flow cytometry for each library antibody binding to A20 lymphoma cells (x-axis) versus anti-lymphoma function at the last imaging time point (t = 156 hours, y-axis). Lower fluorescent area values indicate greater macrophage anti-lymphoma activity. Highlighted in red are the antibodies exceeding the 95th percentile in functional activity and are defined as hits. Black curve indicates the linear relationship with 95% CI boundaries between the functional efficacy and binding in the monotherapy condition (**A**, r=-0.2334, p=0.0011), in combination with anti-CD47 (**B**, r=-0.2339, p=0.0011), and in combination with anti-CD20 (**C**, r=-0.009, p=0.8987). CI = Confidence Interval.

5.2.2. Discovery of targets and antibodies for macrophage-mediated cytotoxicity of human B-cell lymphoma

To enhance our understanding and determine whether we could similarly identify targets of antibody-dependent phagocytosis in the human system, we also evaluated an arrayed library of 241 purified monoclonal antibodies targeting various human cell-surface antigens. The library included antibodies to 92 antigens that were shared with the murine library (Appendix Figure 2). We used primary human macrophages and co-cultured them with GFP+ Raji cells, an aggressive Burkitt lymphoma cell line. As with the murine system, we tested all of the antibodies in three conditions: (i) monotherapy (antibodies alone), (ii) combination with anti-CD47, and (iii) combination with anti-CD20 (Figure 26A-C). We identified functional antibodies that were consistent across all three treatment conditions. Of note, a strong association was observed with antibodies targeting MHC molecules on the lymphoma cells, including antibodies to MHC I (HLA A,B,C, β2M), and MHC II (HLA-DR-DQ-DP, HLA-DR) components. Moreover, we identified CD147, CD71, CD98, CD22 and CD38 blocking antibodies as top hits across multiple treatment conditions.

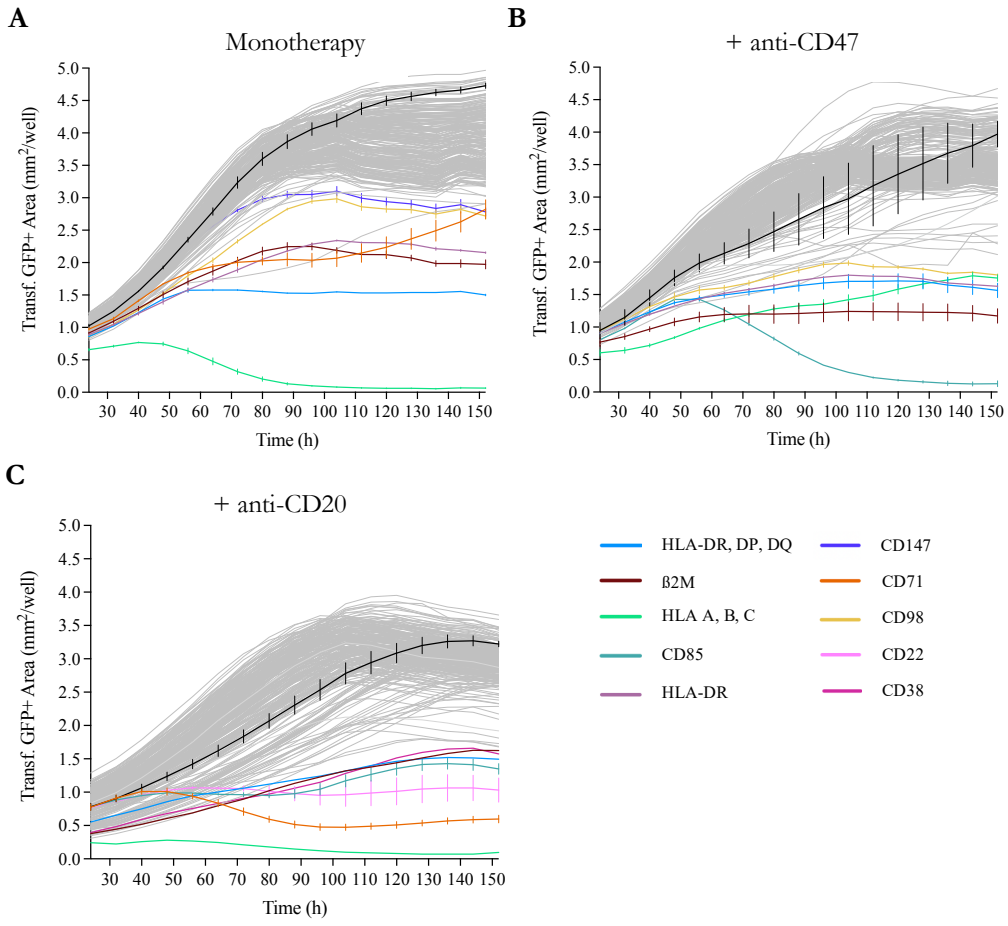

Figure 26 | An unbiased antibody screen identifies targets for macrophage-directed immunotherapy for human B-cell lymphoma. Primary human macrophages were co-cultured in 384-well plates with GFP+ Raji cells (a human Burkitt lymphoma cell line). The wells were subjected to three treatment conditions: control, 10 μg/ml anti-CD47 antibody, or 10 μg/mL anti-CD20 antibody. An arrayed library of purified monoclonal antibodies targeting human cell surface antigens (n = 241 antibodies) was overlaid at a concentration of 6.55 μg/mL. The cells were then incubated for 156 h (~6.5 days) and the GFP+ area was quantified by automated microscopy and whole-well image analysis every 8 hours. **A-C**, Growth of GFP+ Raji cells in co-culture with macrophages under monotherapy conditions (**A**), in combination with anti-CD47 (**B**), or in combination with anti-CD20 (**C**). Each curve represents the growth of lymphoma cells treated with a different antibody. Curves are the mean of two individual co-culture wells. Black curve indicates the mean -/+ SEM of control wells. Colored curves indicate top antibody hits against MHC-related antigens, CD85, CD98 and CD71. SEM = Standard Error of the Mean.

Again, we observed a modest correlation between the degree of antibody binding and elimination of the lymphoma cells in culture with some notable standouts (Figure 27A-C). As an example, an anti-CD85j (LILRB1) antibody had no substantial effect as a single agent, but exhibited the greatest anti-tumor response in combination with anti-CD47 (Figure 27A,B). These observations confirm the role of MHC I/LILRB1 pathway as a macrophage immune checkpoint that regulates macrophage activity[63]. Moreover, this suggests that this screening platform can be useful to identify antibodies that act by either opsonizing the lymphoma cells, exerting a functional effect directly on the macrophages, and/or cross-linking macrophages and lymphoma cells to promote phagocytosis.

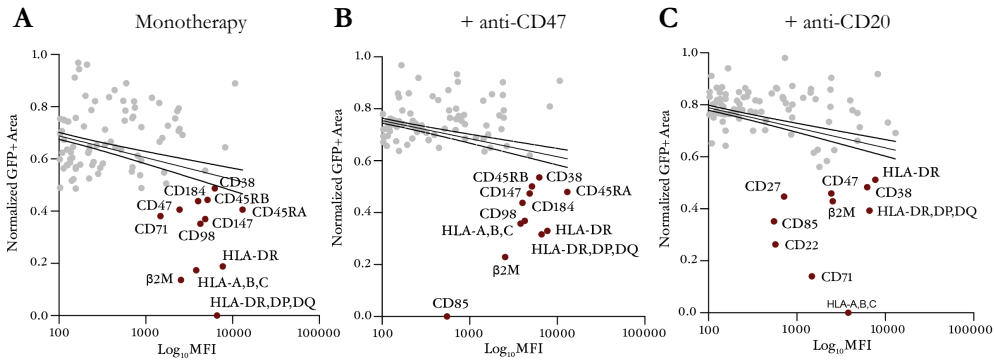

Figure 27 | A-C, Scatter plots depicting results of quantitative surfaceome profiling by flow cytometry for each library antibody binding to GFP+ Raji lymphoma cells (x-axis) versus functional anti-lymphoma effectiveness at the last imaging time point (t = 156 hours, y-axis). Lower fluorescent area values indicate greater macrophage anti-lymphoma activity. Highlighted in red are the antibodies exceeding the 95th percentile in function activity and are defined as hits. Black curve indicates the linear relationship with 95% CI boundaries between the functional efficacy and binding in the monotherapy condition (**A**, r=-0.3364, p<0.0001), in combination with anti-CD47 (**B**, r=-0.3646, p<0.0001), and in combination with anti-CD20 (**C**, r=-0.4105, p<0.0001). CI = Confidence Interval

5.2.3. Antibody combinations to maximize macrophage-mediated cytotoxicity of B-cell lymphoma

Together, our murine and human studies identified several therapeutic targets and corresponding antibodies that could stimulate macrophage-mediated cytotoxicity of lymphoma cells. Since combinations of therapeutic antibodies have shown promise in ongoing clinical trials for patients with lymphoma, particularly combinations of anti-

CD47 and anti-CD20 antibodies[112], we next evaluated whether combinations of antibodies to the targets we identified could elicit more robust anti-tumor responses *in vitro* in the murine and human systems.

Given the central importance of MHC I molecules in regulating macrophage phagocytosis, and with our primary focus on determining macrophage-mediated therapies for MHC I-negative lymphomas, we examined both WT and MHC I KO cell lines. Using syngeneic mouse macrophages and A20 lymphoma cells, we evaluated the combination of the top five antibodies from the murine screen—anti-CD24, CD95 (FAS), CD40, CD184 (CXCR4), and CD79b—along with antibodies against CD47, CD20, and PD-1 as comparisons. We individually combined all of these for a total of 28 different antibody combinations to identify those that exhibit the greatest activity for stimulating macrophage anti-lymphoma functions (Figure 28A-C). We found that the A20 MHC I KO line was more vulnerable to ADCP but otherwise similar trends were observed across the wild-type and MHC I KO lines. Additionally, we found that there were several antibody combinations that were substantially more effective than even the combination of anti-CD20 and anti-CD47. In particular, most combinations with anti-CD24 or anti-CD95 antibodies caused elimination of nearly all lymphoma cells from the co-cultures. These findings suggest highly active antibody combinations can be identified that maximize the ability of macrophages to attack and eliminate lymphoma cells.

Similarly, we also evaluated 28 different antibody combinations in the human system. We tested wild-type Raji cells, Raji MHC I KO cells, and Toledo cells (a human DLBCL cell line). The combinations included the top antibody hits from the human screen (anti-CD85, CD71, and CD147), the mouse system (anti-CD24 and CD40), and a shared antibody (anti-CD184), along with CD47 and CD20-targeting antibodies.

From these efforts, we identified over a dozen antibody combinations that were highly active across all three cell lines tested. Among the most effective of these combinations was anti-CD85j (LILRB1) combined with either anti-CD47, anti-CD147, or anti-CD71 (Figure 29). Together, these findings indicate that highly active combination therapies can be identified, and the effectiveness of these combinations may be comparable to or exceed that of anti-CD20 combinations. Furthermore, the MHC I KO line was generally more sensitive to macrophage-dependent killing in response to antibodies, again

highlighting the importance of MHC I molecules in protecting lymphoma cells from macrophage phagocytosis.

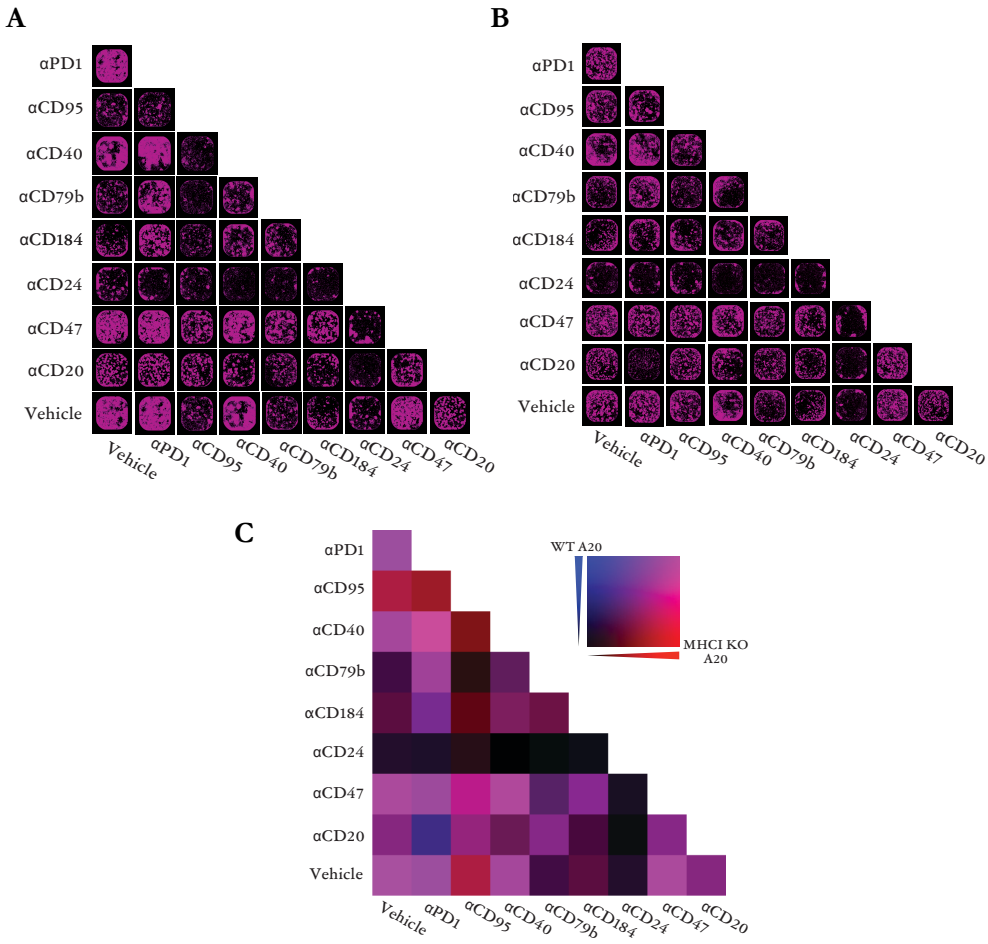

Figure 28 | Identification of antibody combinations that elicit maximal macrophage-mediated cytotoxicity of B-cell lymphoma. A,B, Primary murine macrophages were co-cultured with StayGold+ WT or MHC I KO A20 cells. Seven different antibodies identified from our screen and anti-PD-1 were tested alone or in combination as indicated. StayGold+ area was measured over time as a representation of growth or elimination of lymphoma cells. Images at the last time point (156 h) are shown for each antibody combination for SG+ WT A20 (**A**) and SG+ MHC I KO A20 cells (**B**). **C,** Heat map representing SG+ area at last time point (152 h) for WT (blue) and MHC I-negative (red) A20 cells. Merged data is shown in purple. For both cell lines, lighter color indicates greater SG+ area while darker color indicates lesser SG+ area. Data represents the mean of 2 individual co-cultures per antibody combination. SG = StayGold

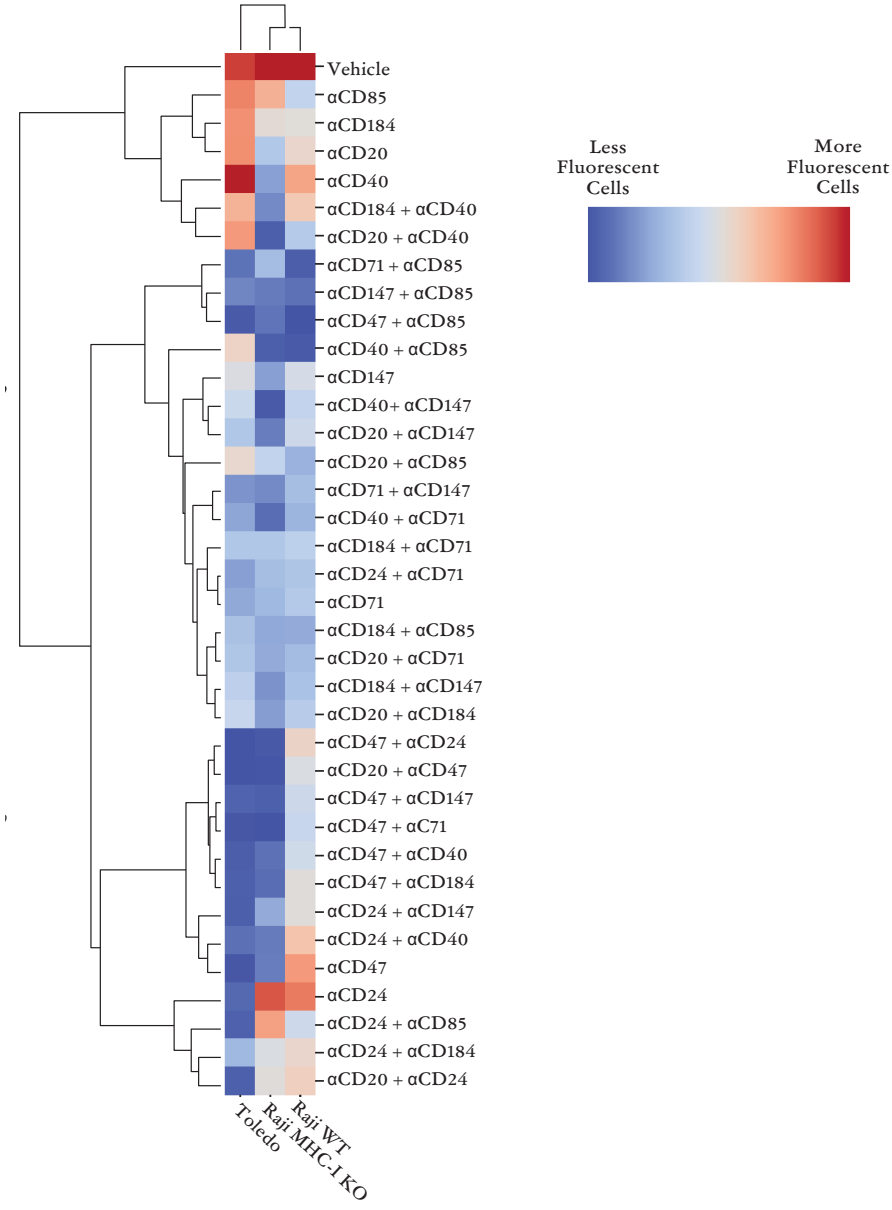

Figure 29 | Unbiased hierarchical clustering. Antibody combination studies were performed using primary human macrophages and GFP+ WT Raji, GFP+ Raji MHC I KO, and mScarlet+ Toledo cells treated with 8 different antibodies alone or in combination as indicated. Heatmap depicts the mean normalized fluorescent area of the last time point (152 h) from 2 individual co-culture wells. Unbiased hierarchical clustering was used to identify antibodies, combinations and cell lines with similar anti-lymphoma properties when co-cultured with macrophages.

5.2.4. Development of a rapid system to create and evaluate bispecific antibodies for macrophage-mediated cytotoxicity

Our unbiased screening efforts and combination studies indicate that additional targets exist on lymphoma cells that can be leveraged to stimulate robust anti-tumor responses by macrophages. Some of these molecules may act as macrophage immune checkpoints, while others may serve as optimal targets of ADCP. Regardless of the mechanism of action, we reasoned that antibodies to the targets identified from our mouse and human screens could be adapted to a bispecific format to maximize anti-lymphoma responses by macrophages and generate therapies that would exhibit robust single-agent activity against lymphoma cells. We therefore developed a strategy to rapidly generate a total 156 bispecific macrophage-activating antibodies and screen them for the ability to stimulate macrophage-mediated cytotoxicity of lymphoma cells. To begin, we curated a library of available antibody sequences to targets identified from our screens (Figure 30). We formatted these into single-chain fragment variable (scFvs) constructs, then fused them to a human IgG1 knob or hole Fc construct[190]. This heterodimeric scFv-Fc format permits the rapid combinatorial production and screening of bispecifics since each binding arm is encoded by a single chain that can be readily combined with other binding elements.

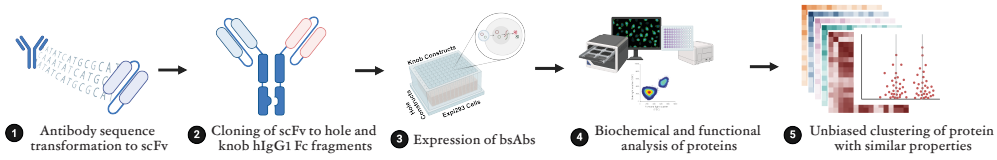

Figure 30 | Multiplex generation of bispecific antibodies that stimulate macrophage destruction of human B-cell lymphoma. Experimental setup for the generation and functional characterization of a combinatorial matrix of bsAbs. scFvs were created based on publicly available antibody sequences, fused to modified human IgG1 Fc regions containing knob or hole mutations for bispecific assembly, and a combinatorial library of bsAbs was expressed in Expi293 cells. The resulting bsAbs were tested for functional activity and binding to multiple lymphoma cell lines and red blood cells. ELISA was performed to evaluate antibody expression. Finally, the properties of macrophage-mediated cytotoxicity, binding, and expression by ELISA were used for K-Means unbiased clustering of the antibodies with similar biochemical and functional properties. bsAb = Bispecific antibody; scFv = Single-chain variable fragment

Based on the results of our screening assays, we targeted CD47, CD24, CD79b, CD184, CD40, CD95, CD38, CD71, CD85j (LILRB1), and CD20. For targeting CD47, we tested two different single-domain binding modules: CV1 (a high-affinity SIRPα decoy protein), and WTa2d1 (a low affinity SIRPα decoy protein)[191]. We also targeted PD-1 as a comparison. We crossed all of these binding arms with each other in two reciprocal formats (i.e., knob-hole and hole-knob), expressed them in Expi293F cells, and then evaluated the resulting antibodies for expression, binding, and function. We tested each bsAb in co-culture assays using primary human macrophages and three different human B-cell lymphoma cell lines: Raji, Toledo, and SUDHL-8 (Figure 31 and 32).

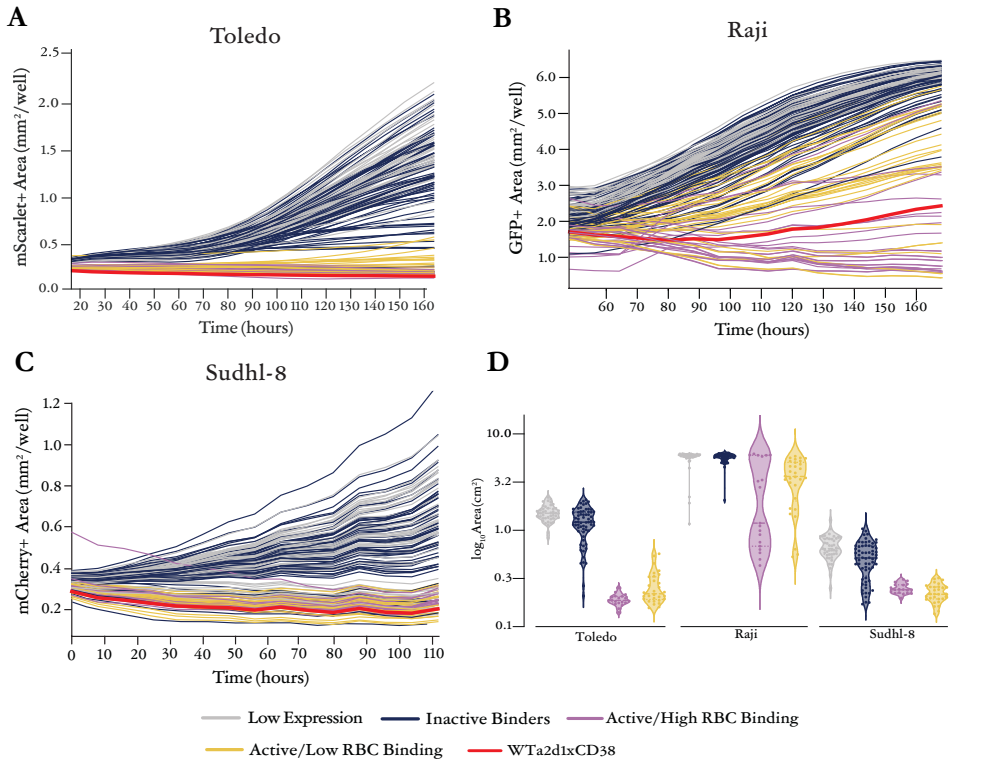

Figure 31 | Bispecific antibody screening. A-C, Growth of human lymphoma cells (**A**, mScarlet+ Toledo; **B**, GFP+ Raji; **C**, mCherry+ SUDHL-8) in co-culture with primary human macrophages. Each curve depicts lymphoma growth in the presence of a different bsAb. Curves represent mean of 2 independent co-culture wells. Each color represents a different cluster of proteins based on functional properties. **D**, Violin plot of fluorescent area at the last time point for each lymphoma cell line for each unbiased cluster of bsAbs. bsAb = Bispecific antibody

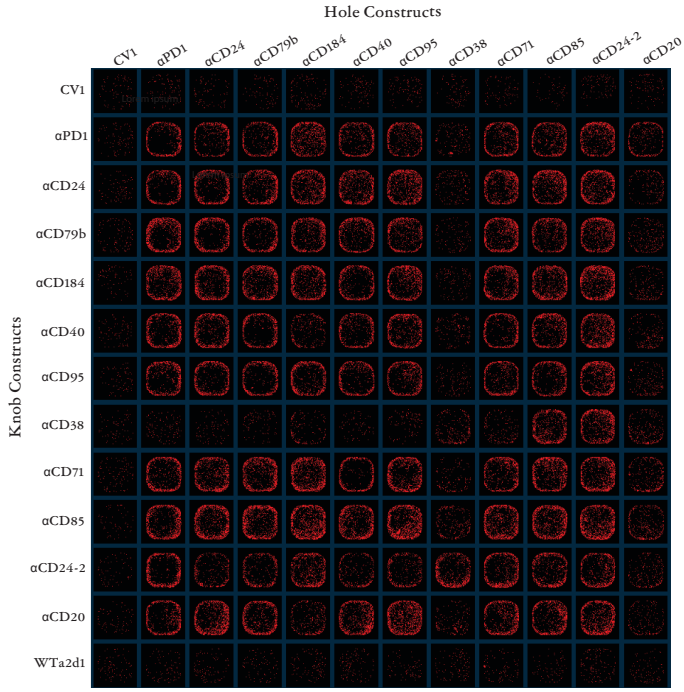

Figure 32 | Representative images from each well taken at last time point of the co-culture with macrophages and mScarlet+ Toledo cells and each bsAb from the combinatorial library. Rows indicate hole constructs, columns indicate knob constructs. bsAb = bispecific antibody

We also examined the expression of each bsAb by ELISA and their binding to each of the cell lines (Figure 33).

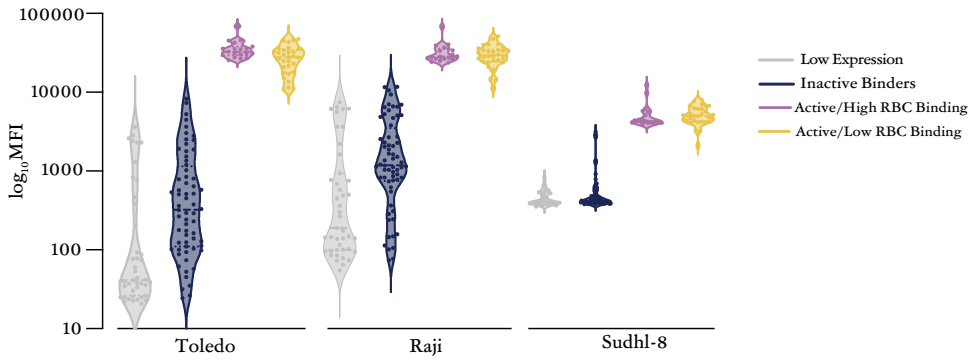

Figure 33 | Violin plot depicting binding of the antibodies to each lymphoma cell line (represented as $\log_{10}$ MFI) as indicated based on clustering. MFI = Mean fluorescence intensity

Furthermore, since on-target red blood cell toxicity has been observed with some anti-CD47 antibodies in clinical trials[112,192], we also examined the ability of each bispecific to bind to human RBCs. Across all of these assays, we found that four distinct categories of bispecific emerged from unsupervised clustering analysis: (i) Bispecifics that were highly active and exhibited minimal red blood cell binding ('Active/Low RBC binding'), (ii) Bispecifics that were highly active and exhibited intense red blood cell binding ('Active/High RBC binding'), (iii) Bispecifics with limited activity, variable lymphoma binding, and low or absent red blood cell binding ('Inactive binders'), and (iv) Bispecifics that did not fold or express well ('Low Expression'). Bispecifics formulated with a CV1 binding arm exhibited robust anti-tumor effects but strong binding to red blood cells. Many bispecifics formulated with WTa2d1, CD20, or CD38 binding arms exhibited desirable properties of robust anti-lymphoma activity with minimal red blood cell binding. Other binding targets exhibited limited functional activity or did not express well (Figure 34).

Across all three cell lines tested, we found that a WTa2d1xCD38 bispecific was consistently among the most effective agents for stimulating macrophage-mediated cytotoxicity of B-cell lymphoma cells and exhibited minimal red blood cell binding. Overall, these properties indicate this bispecific agent may be an ideal therapeutic for stimulating innate immune cells to attack and eliminate B-cell lymphoma.

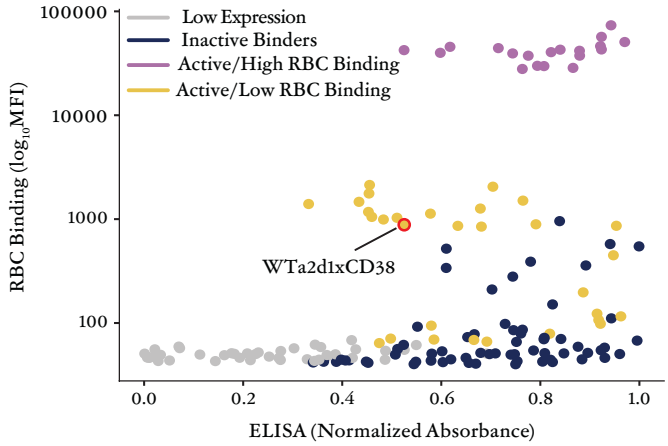

Figure 34 | Correlation between bispecific antibody clusters and their binding affinity to human red blood cells (RBC) as assessed by ELISA and Log_{10}MFI. MFI = Mean fluorescence intensity; RBC = Red blood cell

5.2.5. WTa2d1xCD38 bispecific antibody is an optimal therapeutic candidate for B-cell lymphoma

Given the favorable properties observed using the WTa2d1xCD38 bispecific, we further evaluated the biochemical and functional qualities of this agent. We found that the predicted structure of this bispecific included an expected association via the T22Y (knob) and Y86T (hole) mutations as previously described[190]. Moreover, by mass spectrometry, approximately 94% of the protein assembled in the expected bispecific format (Figure 35A). In on-cell binding assays, we found that each arm is able to bind to its respective antigen (Figure 35B) and that WTa2d1xCD38 binds to Raji, Toledo and human macrophages cells with an EC_{50} of 11.03, 0.37, and 2.90 nM, respectively (Figure 35C), indicating high-affinity binding to lymphoma cells and macrophages with potential to bridge the two cell types.

We then evaluate the efficacy of the WTa2d1xCD38 bispecific antibody across a broader spectrum of lymphomas and specifically assess its performance against MHC I-deficient cells. We conducted macrophage co-culture assays using a panel of nine distinct human B-cell lymphoma cell lines, including both MHC I-expressing lines and MHC I KO variants, in response to the bispecific at different concentrations. The results demonstrated that the bispecific antibody exhibited significantly enhanced macrophage-mediated cytotoxicity against MHC I KO cell lines compared to their WT counterparts. The IC50 values ranged from 73 pM for SUDHL-8 to 33 pM for its MHC I KO variant, and from 3.17 nM for HBL-1 to 0.68 nM for its MHC I KO counterpart (Figure 35D). These findings indicate a marked increase in bsAb efficacy against MHC I-deficient lymphoma cells.

Our comparative analysis using rituximab as a control revealed that the WTa2d1xCD38 bispecific antibody demonstrated superior potency and efficacy *in vitro* across nearly all cell lines tested (Figure 36A,B). Moreover, in phagocytosis assays, the bispecific elicited higher ADCP than both rituximab and anti-CD47 antibodies (Figure 37).

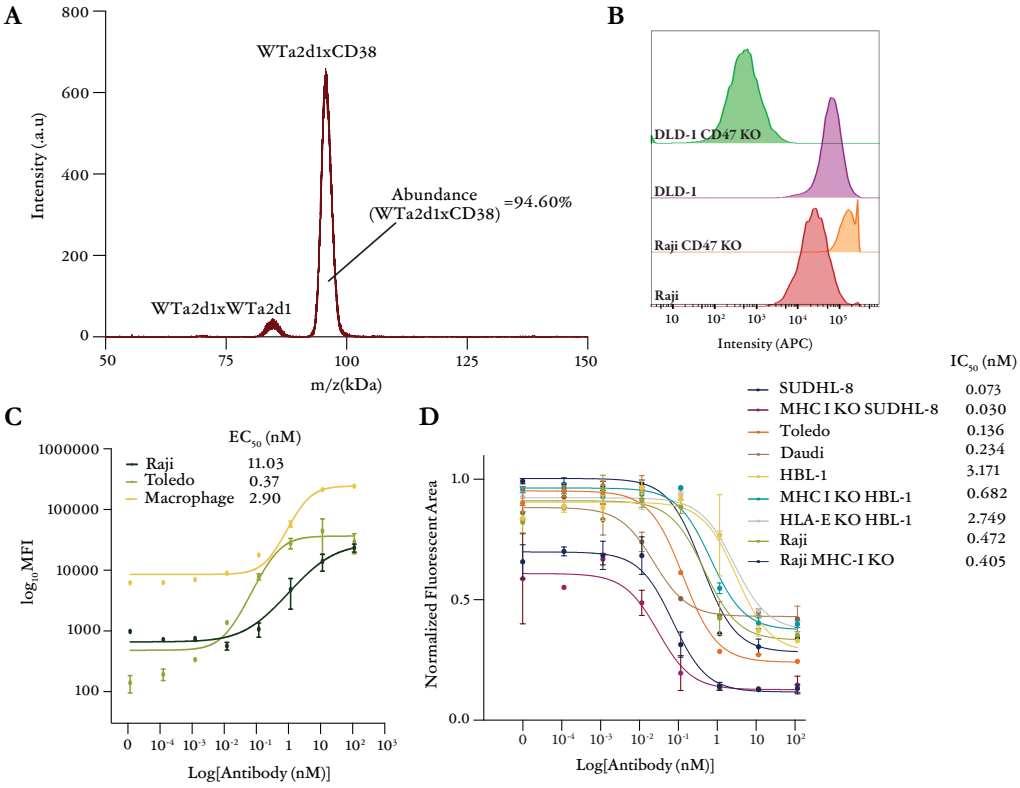

Figure 35 | Biophysical characterization, antigen binding, and functional potency of WTa2d1xCD38. **A**, Maldi-TOF analysis of the protein population of the purified bsAb. Based on the theoretical mass of the possible homo and heterodimers, the two main peaks were assigned to Wta2d1xWta2d1 and Wta2d1xCD38 species. The abundance of WTa2d1xCD38 was calculated as 94.60% based on the peak area. **B**, Histogram showing binding of the bsAb to WT versus CD47 KO cell lines which highlights the ability of the two antibody arms to bind to their respective antigens. Binding was detected with an APC-conjugated anti-human IgG secondary antibody. DLD-1 is a colorectal cancer cell line that expresses CD47 but not CD38. **C,** Binding of WTa2d1xCD38 to the indicated human lymphoma cell lines and macrophages combined from 3 donors indicates the cell-based affinity for the antibody. **D**, Co-culture assays using primary human macrophages were used to determine the potency of WTa2d1xCD38 across nine different human B-cell lymphoma cell lines, including the indicated wild-type and MHC I KO variants. Each curve represents an 8-point titration performed in duplicate for each cell line. Fluorescent area was compared at the last imaging time point and normalized based on the maximum value for each cell line. bsAb = Bispecific antibody; MFI = Mean fluorescence intensity

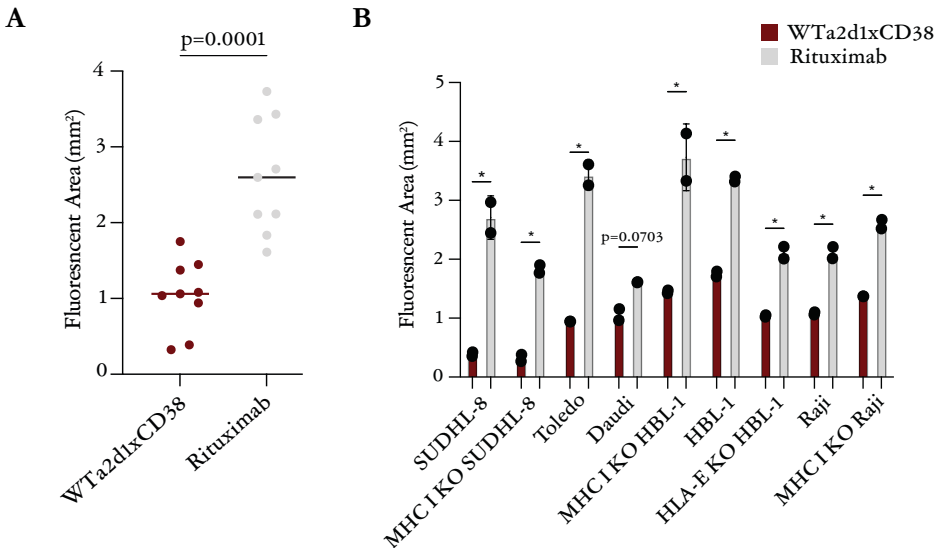

Figure 36 | WTa2d1xCD38 stimulates maximal macrophage-mediated cytotoxicity of B-cell lymphomas. A, Comparison of the fluorescent area at the last time point for different B-cell lymphoma cell lines when treated with 10.54 μg/mL of WTa2d1xCD38 or rituximab. Each point represents the mean value for a different cell line performed in duplicate. Student two tailed paired T-test was used to evaluate the difference between the two groups. **B,** Comparison of the fluorescent area at the last time point from co-culture assays using the indicated lymphoma cell lines treated with either WTa2d1xCD38 or rituximab. *p-value<0.0001 for the indicated comparisons by two-way ANOVA with correction for multiple comparisons.

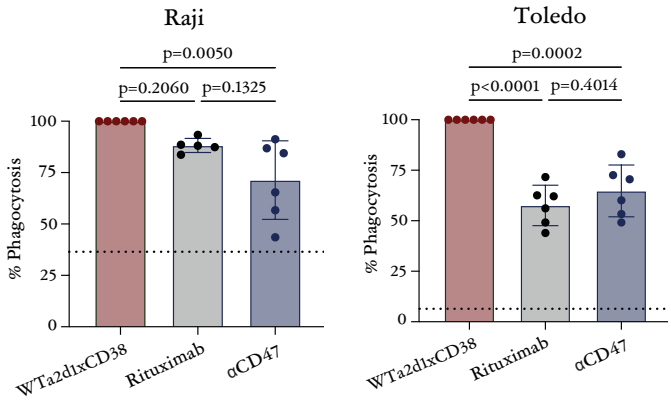

Figure 37 | Macrophage phagocytosis of Raji and Toledo cells when co-cultured for 2 hours in the presence of the WTa2d1xCD38, rituximab, or an anti-CD47 antibody (clone B6H12). All of the values were normalized against the bsAb and the experiment was performed two independent times with three individual co-culture wells per condition. The dotted lines indicate the mean of the negative control condition performed in one experiment with three co-culture wells. Two way ANOVA with Tukey's multiple comparison test was used to evaluate the difference between the groups.

Then, we assessed the contributions of the FcγRs in mediating responses to WTa2d1xCD38. We found that CD16-, CD32-, or CD64-blocking antibodies were able to decrease the activity of the bsAb in co-culture assays with macrophages, but the degree of inhibition varied based on the B-cell lymphoma cell line and the specific Fc receptor (Figure 38A,B). These findings suggest the human IgG1 isotype is important for the effects of WTa2d1xCD38, but also that Fc-independent effects may contribute to its mechanism of action.

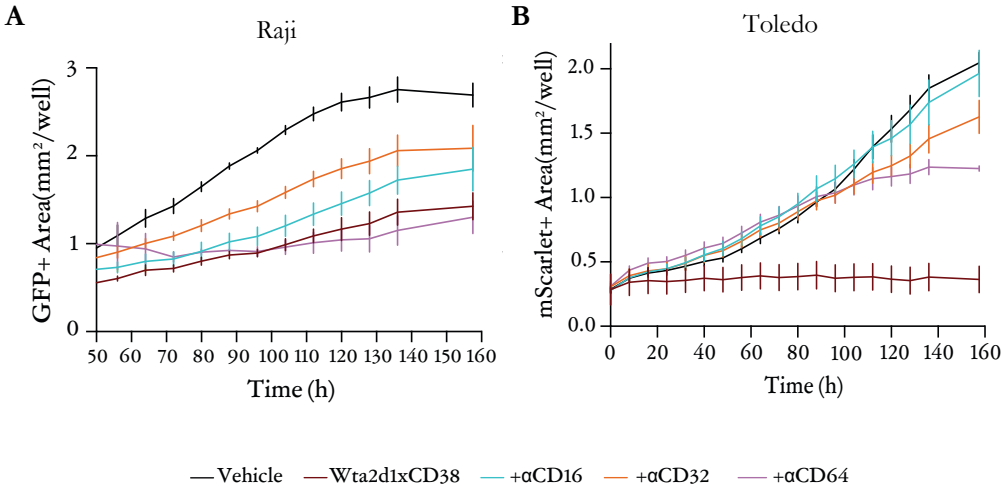

Figure 38 | WTa2d1xCD38 efficacy under Fc gamma receptors inhibition. A,B Co-culture with human macrophages pooled from multiple donors with Raji (**A**) and Toledo (**B**) lymphoma cells as targets. Co-cultures were treated with 1 μg/ml WTa2d1xCD38 and 10 μg/ml antibodies to different Fc gamma receptors as indicated. Curves indicate mean -/+ SEM. SEM = Standard error of the mean

Finally, to understand whether WTa2d1xCD38 could also exhibit therapeutic effects in vivo, we evaluated its efficacy in two xenograft models of aggressive B-cell lymphoma in NSG mice. These mice lack adaptive immune cells but contain myeloid cells capable of responding to macrophage-directed therapies[193]. First, we engrafted Raji cells subcutaneously into the flanks of NSG mice (Figure 39A). After establishing tumors, we randomized the mice into three treatment groups: vehicle control, 100 μg WTa2d1xCD38, or 100 μg Rituximab as a standard-of-care benchmark. We found that

tumor growth was dramatically inhibited by treatment with either WTa2d1xCD38 or rituximab, compared to the vehicle control group (Figure 39B). No significant difference was observed between the WTa2d1xCD38 and Rituximab treatments, indicating that WTa2d1xCD38 is as effective as the benchmark treatment in this model. Additionally, treatment with WTa2d1xCD38 significantly prolonged survival compared to the control group, similar to Rituximab (Figure 39C).

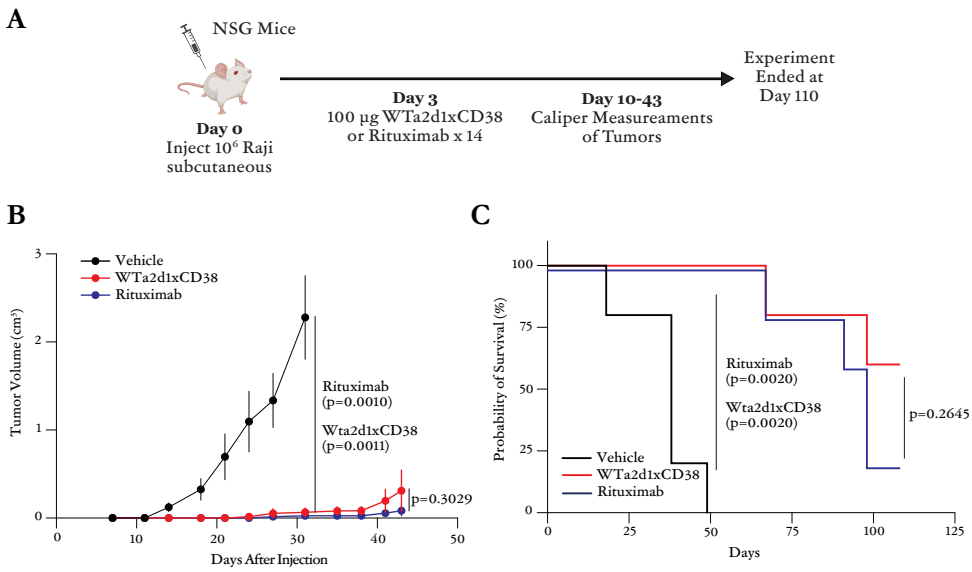

Figure 39 | WTa2d1xCD38 exhibits anti-tumor efficacy in xenograft models of B-cell lymphoma. A, Experimental setup of a xenograft experiment using Raji cells engrafted subcutaneously into the flanks of NSG mice. **B**, Growth curves of Raji lymphoma tumors in NSG mice treated with the indicated therapies over time (n = 5 mice per treatment cohort). Tumor growth was evaluated by caliper measurements. Mice were treated with control, 100 µg WTa2d1xCD38, or 100 µg Rituximab for 14 days. **C**, Survival analysis of the indicated treatment cohorts. The median survival of Vehicle and Rituximab groups were 38 and 98 days, respectively, whereas the WTa2d1xCD38 was not reached. Log-Rank test was used to evaluate the difference in the probability of survival. Note Rituximab curve is minimally nudged for visualization.

In a second study, we stereotactically engrafted Raji cells into the brains of NSG mice as a model of PCNSL (Figure 40A). We randomized mice to treatment with vehicle control, rituximab or WTa2d1xCD38. Again, we found that WTa2d1xCD38 inhibited tumor growth and significantly prolonged survival compared to the control group and rituximab (Figure 40B,C). Together, these findings indicate that WTa2d1xCD38 robustly stimulates anti-tumor responses and could be a highly active therapy for patients with B-cell lymphomas.

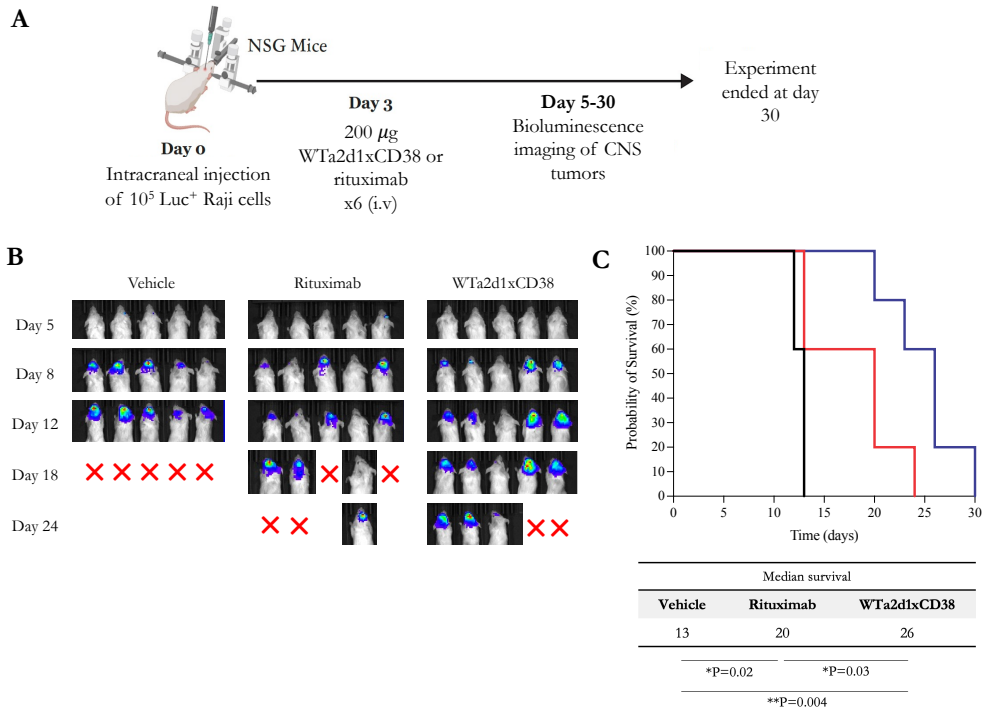

Figure 40 | WTa2d1xCD38 exhibits anti-tumor efficacy in xenograft models of PCNSL. A, Experimental setup of the xenograft CNS lymphoma model experiment using Raji cells engrafted stereotactically into NSG mice brains. **B**, BLI using luciferase reporters of CNS tumors throughout the experiment period (n = 5 mice per treatment cohort). Mice were treated with vehicle control, 200 μg of rituximab or 200 μg of WTa2d1xCD38 three times per week. **C**, Survival analysis comparing the vehicle control, rituximab and WTa2d1xCD38 treatment cohorts. Log-Rank test was used to evaluate the difference in the probability of survival between vehicle and treatment conditions. BLI = Bioluminescence imaging

5.3. Part III

Transcriptomic and (Epi)genetic Hallmarks of Central Nervous System Tropism in Diffuse Large B Cell Lymphoma

This research aimed to identify molecular features of DLBCL at diagnosis that predicts CNS relapse through a comprehensive multiomic analysis.

5.3.1. Study cohort

We included tumoral samples from 48 patients diagnosed with DLBCL who relapsed within 2 years after initial diagnosis. Detailed information is summarized in Table 1. Patients were categorized in 3 groups according to site of relapse: 11 patients presented CNS relapse, 21 patients presented systemic relapse, and 16 patients didn't present relapse. All samples were obtained at diagnosis. The median age at diagnosis was 58.6 years (range, 22-98), with no statistically significant differences in age, stage, CNS-IPI, or COO between the groups.

Among the 11 patients who experienced CNS relapse, the median time to relapse was 12 months (range, 1-24). None of them exhibited CNS involvement affection at diagnosis, as confirmed by PET imaging and CSF analysis. Regarding the site of relapse in the CNS, 5 patients (45.5%) had brain parenchyma involvement, while 6 (54.5%) had leptomeningeal involvement.

The Lymph2Cx assay revealed varying distributions of ABC and GCB subtypes, while FISH analysis identified distinct patterns of *MYC*, *BCL2*, and *BCL6* rearrangements across patient groups. *MYC* rearrangements were exclusively detected in patients with CNS relapse, affecting 27.3% of this group. However, it's important to note that MYC rearrangement data was incomplete for some patients in other groups. *BCL2* rearrangements were characteristic of patients experiencing relapse (both CNS and systemic), but were not observed in patients without relapse. Notably, only one case of double-hit lymphoma was identified, occurring in the CNS relapse group. *BCL6* rearrangements were observed in all groups, and no triple-hits were detected. The data for *BCL2* and *BCL6* rearrangements was not available for all patients across all groups, potentially limiting the comprehensiveness of these findings.

CNS-IPI scores and the use of CNS prophylaxis varied by risk category, with higher-risk patients more likely to receive prophylaxis, though its application was not consistent across all groups. The prophylaxis received was TIT, and in some cases combined with MTX.

Clinical feature	CNS relapse (N=11)	Systemic relapse (N=21)	No relapse (N=16)
Age, median (range), y	**62.2 (38-86)**	**64.7 (28-86)**	**65.3 (22-98)**
≥60, n (%)	5 (45.4)	13 (61.9)	15 (93.7)
Stage 3 or 4, n (%)	**10 (90.9)**	**18 (85.7)**	**8 (50.0)**
COO by Lymph2Cx, n (%)			
ABC	4 (36.4)	8 (38.1)	6 (37.5)
GCB	6 (54.4)	12 (57.1)	10 (62.5)
Unclassified	1 (9.0)	1 (4.8)	0 (0)
MYC translocation, n (%)	**3 (27.3)**	**0 (0)¶**	**0 (0)†**
BCL2 translocation, n (%)	**3 (42.8)***	**5 (55.5)§**	**0 (0)***
BCL6 translocation, n (%)	**2 (28.5)***	**2 (22.2)§**	**2 (12.5)***
Double-hit	1	0	0
Triple-hit	0	0	0
CNS-IPI score, n (%)			
Low (0-1)	3 (27.3)	2 (9.5)	6 (37.5)
Intermediate (2-3)	6 (54.5)	15 (71.4)	6 (37.5)
High (≥4)	2 (18.2)	4 (19.0)	4 (25.0)
CNS prophylaxis, n (%)	**6 (54.5)**	**9 (42.8)**	**3 (18.7)**

*Available for 7 patients

¶Available for 16 patients

§Available for 9 patients

†Available for 14 patients

Table 1 | Clinicopathologic characteristics of DLBCL patients with CNS Relapse, Systemic Relapse, and No Relapse.

5.3.2. Differential genetic features of DLBCL associated with CNS relapse

To identify the differential genetic features of DLBCL tumors that will relapse in the brain, we performed targeted NGS using a custom lymphoma-related gene panel of 190 genes (Appendix Table 1), on 7 CNS Relapse, 13 Systemic Relapse and 11 No Relapse samples. LymphGen subtype was assessed in all cases, but no specific subtype was enriched in any of the groups. The mean number of somatic mutations per case was 9 (range 0-32). Affected genes and type of mutation per patient are depicted in Figure 41.

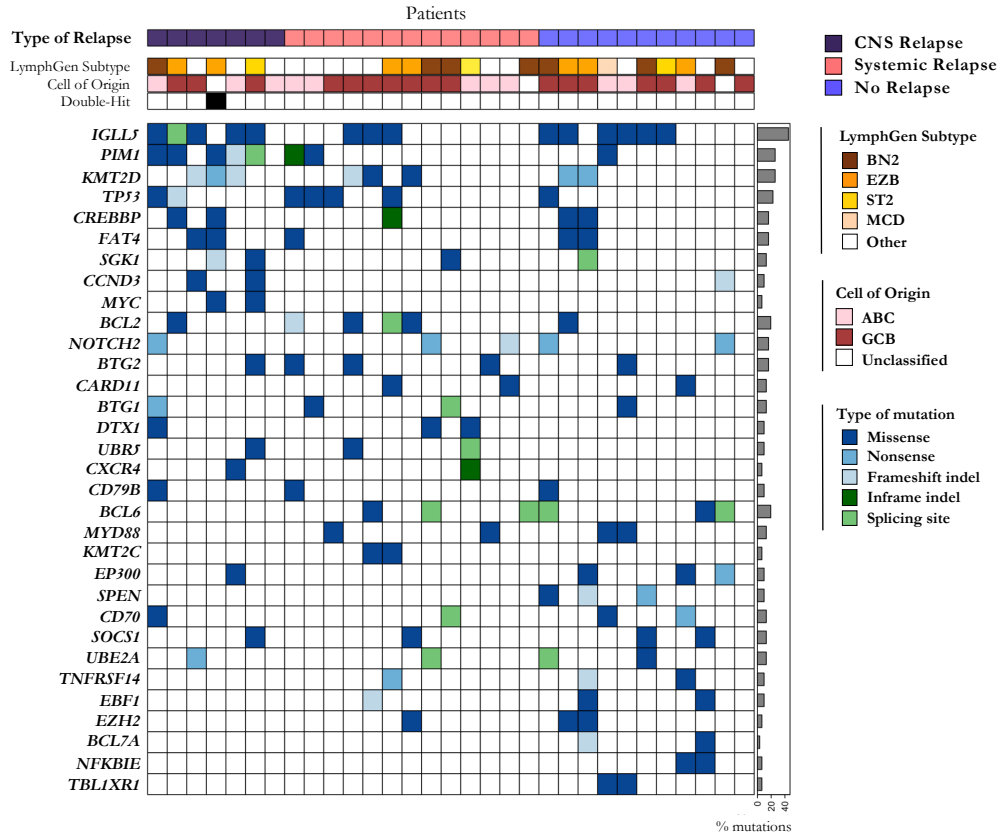

Figure 41 | Mutational profiling. a, Oncoplot showing the clinicopathologic characteristics and mutations detected by targeted NGS (custom panel) at diagnosis. Only genes mutated in more than 10% of patients are included. Types of mutations are classified as Missense, Nonsense, Frameshift indel, Inframe indel, and Splicing site. LymphGen Subtype, cell of origin, and double-hit information are shown. The prevalence of each mutated gene across all patients is displayed as bar plots. NGS = Next generation sequencing

Among the 7 CNS-relapsed samples, *IGLL5* and *PIM1* were the most frequently mutated genes (71%), followed by *KMT2D* (43%), and *TP53*, *CREBBP*, *FAT4*, *SGK1*, *CCND3*, and *MYC* (28.6%). Both *IGLL5* and *PIM1* are targets of aberrant somatic hypermutation in DLBCL, which contributes to lymphomagenesis and are related to primary CNS lymphoma[194,195]. *TP53* and *BCL2* (30.7%) were the most frequently mutated genes in the systemic-relapsed group; while *IGLL5* (54.5%), and *BCL6*, *SPEN* and *EP300* (27%) were the most frequent in the non-relapsed group.

Risk of CNS relapse was significantly associated with *PIM1* mutations (*P*=0.0007, Fisher's exact test), which was mutated in only 15% of systemic-relapsed patients and 9% of non-relapsed patients (Figure 42). Two patients experiencing CNS relapse despite low CNS-IPI scores at diagnosis displayed mutations in *PIM1* and *CREBBP*, with one patient being a double-hit and additionally harboring mutations in *MYC* and *KMT2D*, and the other in *TP53* and *BCL2*.

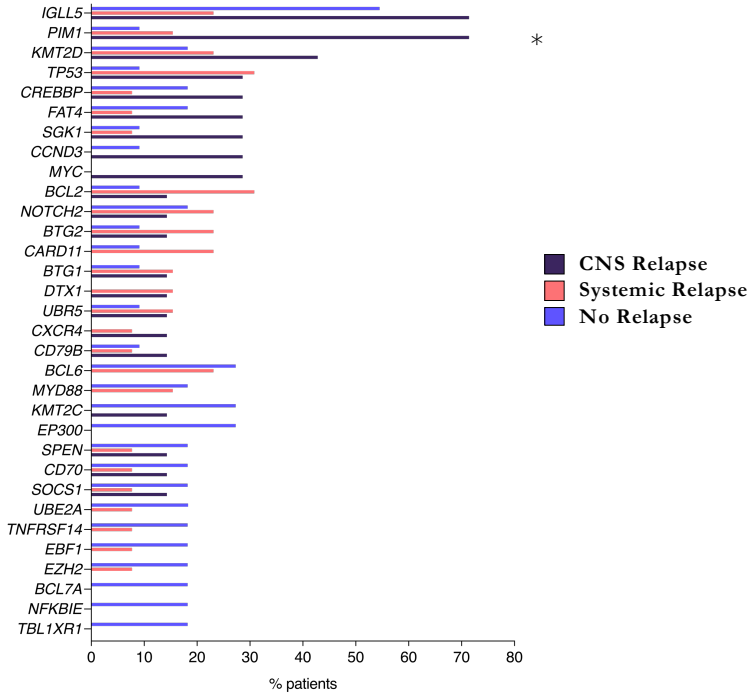

Figure 42 | Mutational profiling. Prevalence of mutated genes within each group of patients. Only genes mutated in more than 5% of patients in each group are included. *PIM1* gene was significantly associated with CNS relapse after adjustment for multiple testing.

5.3.3. Transcriptomic profiling of DLBCL with CNS tropism

To identify specific transcriptomic profiles related to CNS infiltration, we conducted bulk RNA-seq in 11 CNS Relapse, 19 Systemic Relapse and 14 No Relapse samples. Unsupervised clustering analysis by principal component analysis (PCA) did not group samples according to site of relapse (Appendix Figure 3). In a supervised analysis, comparing CNS Relapse vs. No CNS Relapse, and CNS Relapse vs. No Relapse, we observed both significant upregulation and downregulation in expression of a subset of genes within the CNS Relapse group, characterized by $Log_2FC \geq 1$ and p-value ≤ 0.05 (Figure 43). A distinct differential gene expression pattern was also observed when comparing the CNS Relapse group to the Systemic Relapse group (Appendix Figure 4). Interestingly, over a hundred genes were found to be exclusively up- or downregulated in the CNS Relapse cohort when compared individually against both the Systemic and No Relapse groups. These same genes were not identified in other group comparisons (data not shown). These findings demonstrate a differential gene expression pattern, already evident at diagnosis, characteristic of tumors prone to spreading in the brain.

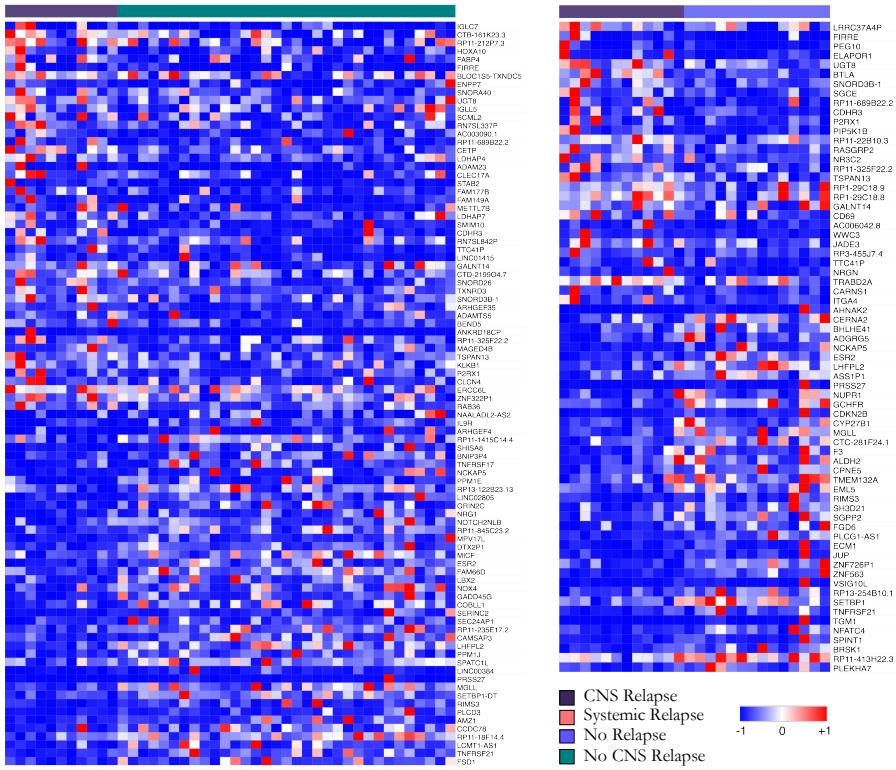

Figure 43 | Gene expression profiling. Heatmaps representing normalized expression of selected genes with significant differential expression (Log2FC ≥ 1 and p-value ≤ 0.05) when comparing CNS Relapse vs. No CNS Relapse (left heatmap) and CNS Relapse vs. No Relapse (right heatmap). Expression levels are indicated by a color gradient from red (high expression) to blue (low expression). Genes are arranged in descending order of expression within the CNS Relapse group.

GSEA for Reactome revealed a total of 346 enriched pathways in the CNS Relapse group, some related to increased B cell proliferation and epigenetic regulation, and decreased interferon-related pathways and FcR-mediated phagocytosis, among others (Figure 44A). Both Systemic and No Relapse groups together had only 48 enriched pathways in total. Moreover, using the Hallmark database we observed enrichment of multiple gene sets associated with aberrant cell growth and survival in the CNS-relapsed group when compared to non-CNS-relapsed group (Figure 44B), such as E2F TARGETS, G2M CHECKPOINT, MYC TARGETS V1, MYC TARGETS V2, MTORC1 SIGNALING and MITOTIC SPINDLE pathways. Furthermore, we again observed a reduction in interferon-related activity which may be associated with immune evasion.

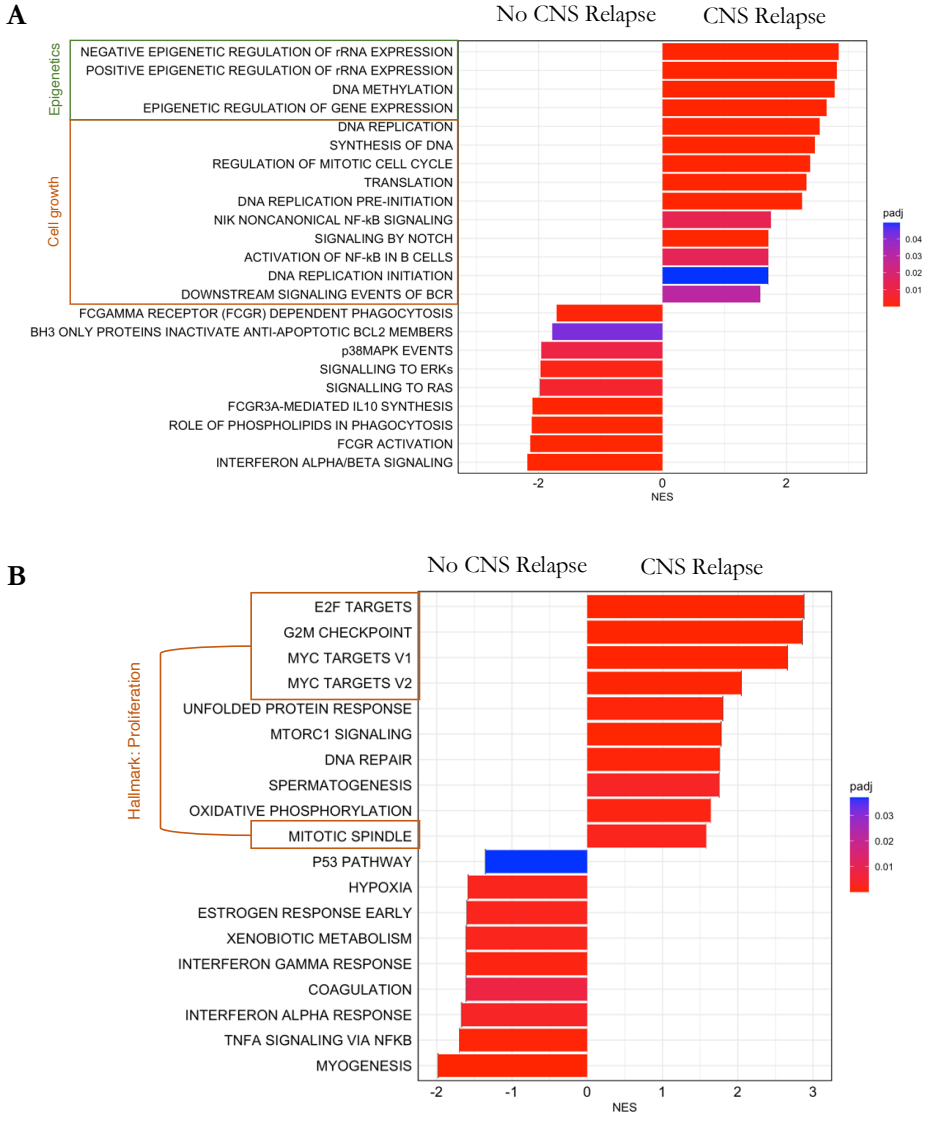

Figure 44 | A,B, GSEA analysis using Reactome (**A**) and MSigDB Hallmark (**B**) databases, comparing CNS Relapse vs. No CNS Relapse. A positive NES indicates enrichment in gene sets in the CNS Relapse group, while a negative NES indicates enrichment in the No CNS Relapse group. The color range indicates significant Padj ≤ 0.05. MsigDB = Molecular Signatures database; NES = Normalized enrichment score; Padj = Adjusted p-value

The same gene sets, along with additional ones, showed enrichment in the CNS-relapsed group compared to both the systemic-relapsed group and the non-relapsed group individually (Appendix Figure 5). GO enrichment analysis further revealed an upregulation of cell proliferation, through a higher expression in cell cycle-related genesets and others, in DLBCL samples with CNS tropism in comparison to all others (Appendix Figure 6). These enrichments were not observed when comparing the systemic-relapsed group to the non-relapsed group (data not shown). Overall, these results suggest that the increased proliferative and aggressive phenotype of DLBCL cells may contribute to the dissemination of extranodal disease in the CNS.

5.3.4. Immune gene expression signatures in DLBCL with CNS tropism

To validate our findings and further explore the immune characteristics of DLBCL tumors, we checked the expression of immune-related genes using the nCounter PanCancer Immune Profiling Panel (Nanostring), which allows for greater sensitivity in gene expression determination. It was performed in 10 CNS Relapse, 15 Systemic Relapse and 11 No Relapse samples. The CNS Relapse group, in comparison to the No Relapse group, showed an upregulation of relevant immune-related genes implicated in cell migration and adhesion (Figure 45A), including *FUT7* (FC=3.18; p=0.02), *ITGA4* (FC=2.2; p=0.0065), and *VCAM1* (FC=1.6; p=0.03); chemokine signalling as *IL7R* (FC=2; p=0.05) and *CCR6* (FC=3.4; p=0.01); and immune regulation like *TAL1* (FC=2.67: p=0.001), *LTB* (FC=3.32; p=0.009), *CD96* (FC=2.45; p=0.009), *CD1A* (FC=4.8; p=0.009), and *BTLA* (FC=2.3; p=0.02). Also, downregulation of genes related to cell death like *TNFRSF8* (FC=5.33; p=0.004), *TNFRSF18* (FC=3.15; p=0.01), *TNFSF4* (FC=1.77; p=0.01), and *GZMB* (FC=2.98; p=0.03), and immune regulation such as *CCL8* (FC=5.19; p=0.005), and *IRF8* (FC=2.07; p=0.01). When comparing the CNS Relapse group to both Systemic and No Relapse groups combined, some of these genes were still found to be upregulated (Figure 45B), like *CD1A* (FC=3.08; p=0.005), *LTB* (FC=2.5; p=0.02), and *ITGA4* (FC=1.7; p=0.03), and downregulated, such as *TNFRSF8* (FC=4.14; p=0.005), *TNFSF4* (FC=1.63; p=0.02), *CCL8* (FC=4.12;

p=0.005), *IRF8* (FC=1.88; p=0.01), and other interferon-related genes like *IFIT1* (FC=3.6; p=0.003), and *IFI27* (FC=3.65; p=0.003).

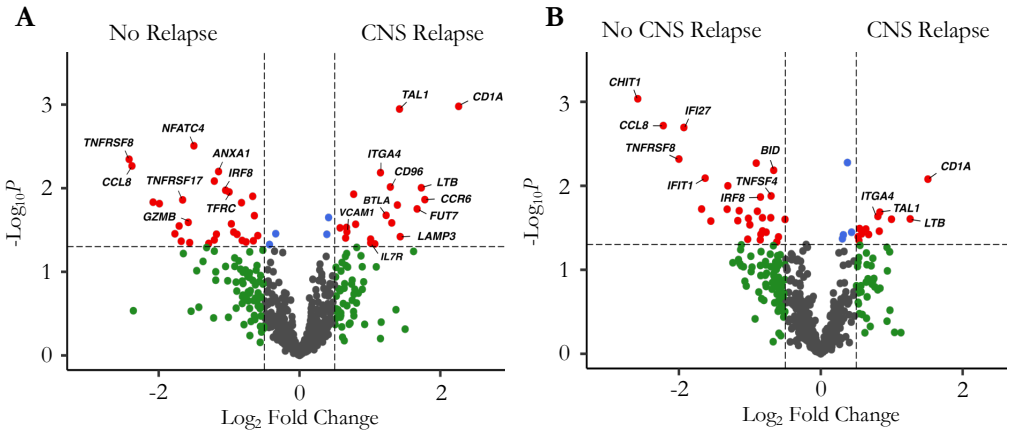

Figure 45 | Immune-related pan-cancer gene expression signatures. A,B, Volcano plots showing significantly differentially expressed genes when comparing CNS Relapse vs. No Relapse (**A**) and CNS Relapse vs. No CNS Relapse (**B**). Red dots denote significantly up- and downregulated genes with Log_2FoldChange ≥ 0.5 and p-value ≤ 0.05.

Interestingly, some of these genes that are upregulated in samples with CNS tropism (*ITGA4*, *CCR6*, *BTLA* and *IL7R*) (Figure 46) have been previously reported to be implicated in B cell CNS entrance in some hematological malignancies. These results suggest that, at diagnosis, malignant B cells with CNS tropism already exhibit a distinctive transcriptomic profile, potentially conferring them with a strategic advantage in infiltrating the central nervous system.

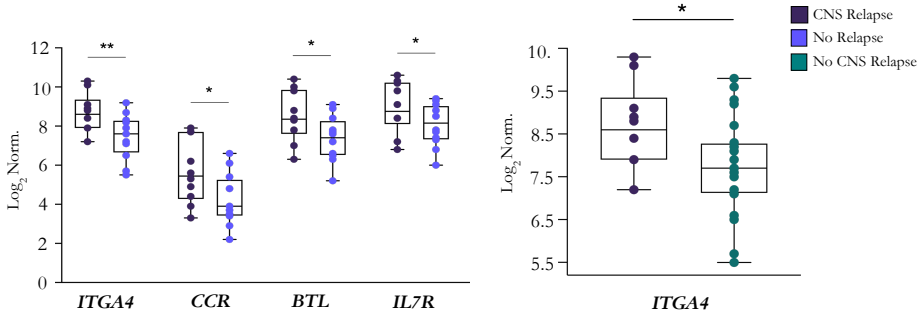

Figure 46 | Immune-related pan-cancer gene expression signatures. Normalized expression values of selected significantly upregulated genes in the CNS Relapse group compared to the No Relapse and No CNS Relapse groups. The Mann-Whitney test was used to determine significant differences in gene expression between the groups. Significance levels are indicated as follows: * p-value ≤ 0.05, ** p-value ≤ 0.01.

5.3.5. Immune cell composition of DLBCL tumors

To precisely define the immune cell composition of DLBCL tumors at diagnosis, we performed CIBERSORTx analysis using RNA-seq data. Results showed that the immune cell composition of DLBCL tumors at diagnosis did not differ depending on the site of relapse, with no statistical differences observed between CNS-relapsed samples and non-CNS-relapsed ones at diagnosis (Figure 47). B cells were the predominant cell type, constituting a median of over 45% of all cells, with B naïve cells being the most common maturation state. T cells made up a median of approximately 30% of the cell population, with CD4+ T cells being more abundant than CD8+ T cells. Total macrophages represented around 15% of the cells, with no significant differences observed between M0, M1, and M2 differentiation statuses. NK cells comprised less than 10% of the cell population. The remaining minority of cells included DCs, mast cells, eosinophils, and neutrophils.

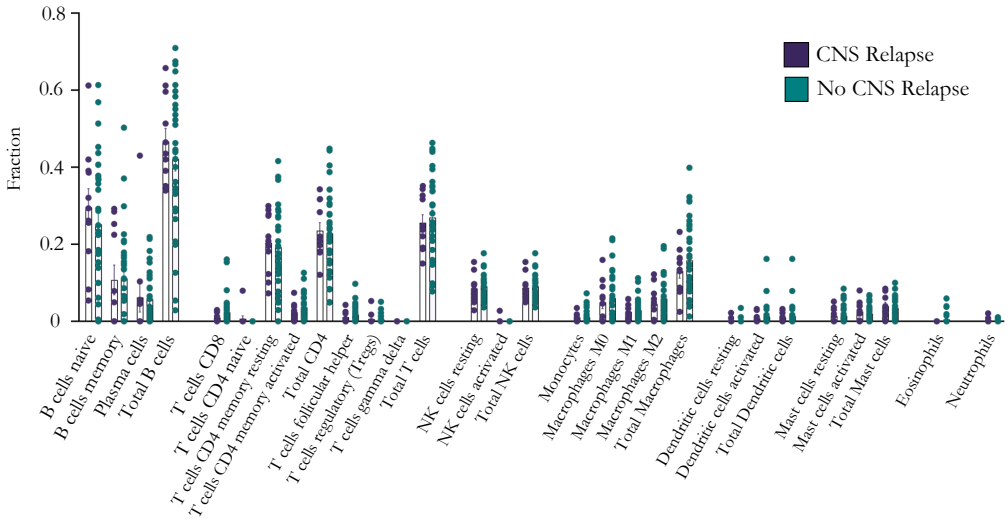

Figure 47 | Immune cell composition. The immune cell populations in each patient sample comparing CNS Relapse vs. No CNS Relapse. The profiling of immune cells was inferred by deconvolution analysis of RNA-seq with the LM22 immune cell gene signature, and the relative percentages of different cell types are shown in the bar plot.

5.3.6. Epigenomic signatures of DLBCL with CNS relapse

DNA methylation was performed in 7 CNS Relapse, 18 Systemic Relapse and 12 No Relapse samples. To delineate the distinct epigenomic characteristics of DLBCL tumors exhibiting CNS tropism, we conducted a comprehensive examination of CpG methylation status across all DNA in three distinct groups. Unsupervised analysis revealed clustering of CNS Relapse samples characterized by CpG hypomethylation (Figure 48). Specifically, through a supervised analysis of the CNS-relapsed related epigenome, we identified 343 differentially methylated CpG sites in comparison to both Systemic and No Relapse groups together. Conversely, there were no CpG sites that exhibited significant differential methylation when comparing CNS-relapsed samples to either the systemic-relapsed or non-relapsed groups individually, nor when comparing the Systemic Relapse group to the No Relapse group (data not shown).

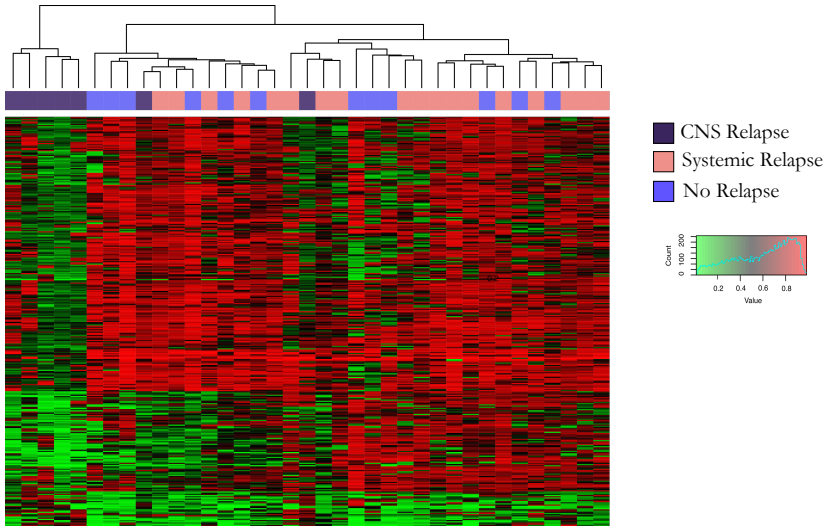

Figure 48 | DNA Methylation Profiling. Heatmap of unsupervised hierarchical cluster analysis of DNA methylation data. Green indicates lower methylation β-value while red stands for higher β-value.

Among the 343 hypomethylated CpG sites that were associated with CNS relapse, these affected a total of 211 genes. Over-Representation Analysis (ORA) using GO Biological Process (GOBP) terms highlighted an association of pathways associated with enhanced cell migration and locomotion, among others (Figure 51). These findings suggest that

lymphoma cells with CNS tropism at diagnosis have an inherent and differential epigenomic profile that could be related to an enhanced ability to migrate.

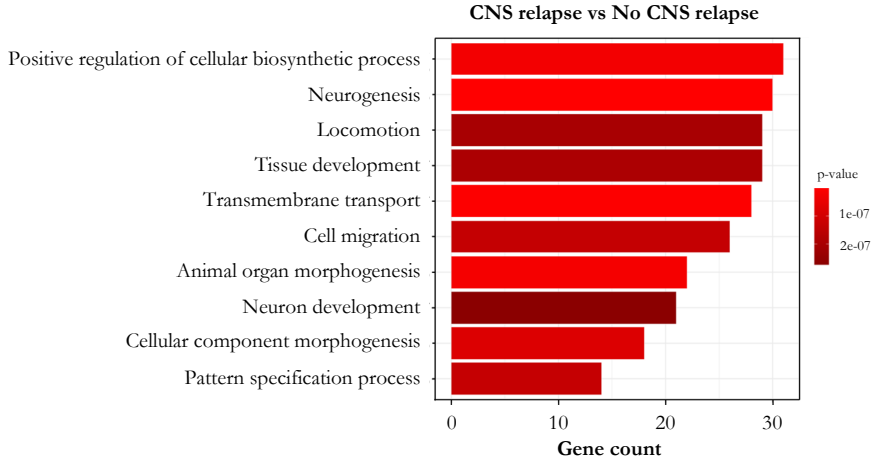

Figure 51 | Over-Representation Analysis (ORA) of the 211 genes affected by differential methylation. Identification of pathways that are associated with the subset of genes, using Gene Ontology Biological Process (GOBP) terms. Bars represent gene count and colour range indicate p-value ≤ 0.05.

We then analyzed the correlation between differentially methylated CpG sites and differentially expressed genes in the CNS-relapsed group. Results revealed a strong relationship between methylation levels and transcriptome expression. We identified several CpG sites with statistically significant associations ($p<0.05$) and notable correlation coefficients (R values) for multiple genes (Table 2).

These findings highlight the complex epigenetic landscape of CNS tropism of DLBCL and suggests further investigation.

CpG	Gene	R	P-value
cg11117364	AMOTL1	-0,622	8,6E-05
cg08032476	RAB34	-0,56155	0,00055
cg00124375	DDAH2	-0,49517	0,00291
cg24293126	SLC2A5	-0,47593	0,00444
cg23628232	AMOTL1	-0,46256	0,00588
cg19425773	VOPP1	-0,45833	0,00641
cg17091706	GTF2H3	-0,43386	0,01036
cg20703579	N4BP3	-0,41527	0,0146
cg18951982	C18orf54	-0,38645	0,02397
cg13392687	AMOTL1	-0,38476	0,02465
cg25036073	EIF5	-0,37895	0,02709
cg10293426	ROBO1	-0,37822	0,02742
cg07006935	VOPP1	-0,3674	0,03255
cg05830220	KLHDC4	-0,36363	0,03452
cg02032559	INO80C	-0,34357	0,04666
cg18877506	PDPN	-0,34256	0,04734
cg21379099	MECOM	-0,34033	0,0489
cg09764150	ESR2	0,36984	0,03133
cg04499254	HHAT	0,37392	0,02937
cg14173587	ABCA2	0,40743	0,01677
cg24583250	GMDS	0,44541	0,00829
cg11790196	FOXN3	0,52535	0,00142

Table 2 | Correlation between CpG site methylation and gene expression in CNS relapse. The table shows CpG site identifiers, associated genes, p-values, and correlation coefficients (R). Negative R values indicate inverse relationships between methylation and expression, while positive values suggest direct relationships.

6. Discussion

In the present doctoral thesis, the role of macrophages and T cells in the pathogenesis of primary CNS lymphoma and their responses to immunotherapies were investigated. In addition, novel macrophage-targeted therapies and the bioengineering of bispecific antibodies were explored, particularly for tumors with MHC I loss. Lastly, a multiomic approach was employed to comprehensively characterize the immune, genomic, transcriptomic, and epigenomic landscapes of DLBCL with CNS tropism at diagnosis, to better predict CNS relapse.

6.1. Interactions between macrophages and T cells in primary CNS lymphoma

Biopsy sampling is the primary diagnostic procedure for patients with CNS lymphoma. With that, only a small residual sample is typically left for research purposes, which significantly limits the ability to comprehensively study and characterize the complexity of the tumor microenvironment of CNS lymphoma tumors. As a result, robust animal models are essential to simulate primary CNS lymphoma and study the immune dynamics within the tumor. These models allow us to explore how the TME functions in a controlled environment and identify which therapies may be most effective in treating the disease.

Previous research has demonstrated significant infiltration of T cells and macrophages in the brains of CNS lymphoma patients. These and other *in vivo* studies have revealed high expression of immune checkpoint molecules, such as PD-1, SIRPα, and LILRB1, in infiltrating macrophages. Additionally, T cells display significant activity but also exhibit an exhaustion phenotype[141]. However, the precise interplay and contributions of macrophages and T cells in relation to immune evasion by PCNSL lymphoma remain largely unexplored.

To address this, we developed a syngeneic mouse model of PCNSL to investigate immune evasion and the dynamic interactions between malignant cells, macrophages, and T cells within the tumor microenvironment. We depleted microglia and systemic macrophages using a CSF-1R inhibitor and clodronate liposomes, while simultaneously impairing antitumoral T cell responses in the brain by downregulating MHC I in tumoral cells.

Our findings highlighted that microglia and infiltrating macrophages play a crucial role in both the pathogenesis of primary CNS lymphoma. The depletion of both resulted in accelerated early tumor growth, showing a 10-fold increase by day 7, compared to tumors in a fully immunocompetent TME. This indicates that tissue-resident and early infiltrating macrophages play an important role delaying the rapid establishment of the tumor and not supporting its progression in the initial stages.

Interestingly, previous research using a similar syngeneic mouse model of PCNSL demonstrated robust T cell infiltration starting on day 9 post-tumor induction, with $CD4^+$ T cells infiltrating first, followed by $CD8^+$ T cells[142]. We hypothesize macrophages control the initial tumoral growth and T cells mediate a more robust antitumoral response at a later stage. In our study, we detected infiltrating T cells in the tumor microenvironment 12 days after tumor inoculation, with similar levels observed in both immunocompetent and macrophage-depleted mice. These findings suggest that the tumor is likely responsible for releasing chemoattractants to promote T cell infiltration, and concurrently, disruptions in the blood-brain barrier may facilitate easier T cell entry into the brain.

Overall, a highly coordinated immune response occurs in the brain against lymphoma cells.

6.2. MHC I Deficiency and Macrophage Dependence in PCNSL Tumor Aggressiveness and Therapy Response

The absence of MHC I on tumor cells resulted in a more aggressive disease, as infiltrating T cells were unable to mount a cytotoxic response through the antigen presenting machinery. In contrast, WT tumors exhibited clearer signs of regression, where T cells could effectively recognize and target malignant cells.

Our results also demonstrated that both macrophages and T cells are necessary for a full anti-tumor response to PD-1 blockade. Blocking functions of either cell type resulted in only a partial response. This suggests that PD-L1 expression on tumor cells not only blocks T cell activity but also inhibits action of $PD\text{-}1^+$ macrophages in PCNSL. In macrophage-depleted mice, PD-1 blockade remained effective against MHC I-positive

tumors, indicating that infiltrating T cells drive the treatment response. However, this effect was not observed in MHC I-negative tumors, reaffirming that these tumors can only be controlled by macrophages. Neither anti-PD-1 nor anti-CD47 immunotherapy alone, or in combination, were sufficient to diminish the aggressiveness of MHC I KO PCNSL. However, some partial response was observed, which highlights the importance of macrophages in responding to these therapies. This suggests that when appropriately stimulated, macrophages can act as potent immune effector cells against MHC I KO PCNSL cells.

6.3. Target identification to enhance macrophage-mediated activity against MHC I-deficient lymphoma cells

It is well-established that PCNSL patients with downregulation of HLA molecules often experience poorer prognosis, lower progression-free survival, and reduced response to conventional treatments[196].

For the first time, we have demonstrated that primary CNS lymphomas presenting MHC I downregulation respond only to macrophage-mediated therapies. Furthermore, our findings indicate that new therapeutic targets, beyond those already studied, are needed to enhance full macrophage function and cytotoxicity against MHC I-deficient CNS lymphoma. To address this challenge, we conducted a comprehensive screening of hundreds of potential targets to identify those that could amplify macrophage action against lymphoma cells exhibiting MHC I loss.

Monoclonal antibody therapies are among the most successful therapies for B-cell lymphomas[197], and these work in part by activating innate immune cell effector functions including macrophage ADCP. This function can be further enhanced by Fc engineering strategies or by blockade of the CD47/SIRPα macrophage immune checkpoint[191,198]. Here, we describe a rational strategy to identify targets of opsonization and antibodies that stimulate macrophage-mediated cytotoxicity of lymphoma cells. Our screens highlighted the importance of MHC molecules in protecting lymphoma cells from macrophage attack and identified additional checkpoint molecules, such as CD85j

(LILRB1) and CD24, that could be targeted for therapeutic purposes in primary CNS lymphoma and other B-cell lymphomas presenting MHC I downregulation.

Interestingly, we also identified a number of cell surface targets that were highly expressed on B-cell lymphoma, yet their corresponding antibodies did not stimulate ADCP. These antigens may nonetheless be valuable targets for other therapeutic modalities, such as antibody-drug conjugates, CAR-T cell therapies, or bispecific T-cell engaging therapies.

6.4. Comprehensive profiling and development of bispecific antibodies to enhance macrophage-mediated cytotoxicity in B-cell lymphomas

A limitation of our screens is that they do not sample every possible antigen and every possible antibody that binds to the lymphoma cell surface. However, we provide the first comprehensive surfaceome profiling of B-cell lymphoma that is paired to functional anti-lymphoma responses by macrophages. From our efforts, we have identified consistent principles for macrophage-mediated cytotoxicity across mouse and human studies. Thus, the targets and hits we identified are true positives that were validated by confirmatory studies *in vitro*. Furthermore, the results of our screening efforts and combinatorial studies successfully guided and informed the development of a compendium of highly active bispecific antibodies.

Our rapid production and functional evaluation of bsAbs allowed us to create and discover bispecifics that maximally activate macrophage-mediated cytotoxicity of lymphoma cells while minimizing binding to red blood cells. These properties can enhance the therapeutic index for targeting B-cell lymphoma by increasing specificity to the tumor microenvironment. Importantly, bispecifics with the most favorable properties could not be predicted based on their intended targets alone; instead they were identified best by integration across multiple biochemical and functional studies. Thus, this strategy for rapid engineering and evaluation of bispecifics offers opportunities to advance the field of bsAb development.

6.5. Targeting both CD38 and CD47 is a promising approach to enhance macrophage-mediated anti-lymphoma responses

Among the most effective bsAbs that we generated was a WTa2d1xCD38 bispecific antibody. This agent exhibited minimal red blood cell binding while robustly stimulating anti-lymphoma responses *in vitro* and *in vivo*.

CD38 plays a pivotal role in orchestrating cell-mediated immune-modulatory functions and facilitating pro-tumoral interactions within the complex tumor microenvironment. It suppresses T cell activity through multiple mechanisms, including the production of adenosine, an immunosuppressive molecule, and by affecting cellular metabolism[199]. It is a well-established therapeutic target in multiple myeloma and is also expressed in B-cell lymphomas, while being downregulated in resting normal B cells[200]. In DLBCL, abnormal CD38 expression correlates with increased cellular proliferation, disease progression, and immune evasion by suppressing $CD8^+$ T cell function[201]. High CD38 expression has also been identified in PCNSL[141] and recognized as a significant prognostic marker in DLBCL[202], with studies showing that elevated levels are strongly linked to poor clinical outcomes. Additionally, other research has demonstrated that inhibiting the PD-1/PD-L1 pathway can lead to CD38 overexpression in some solid tumors, suppressing T-cell activity, and that daratumumab and nivolumab in combination show synergistic anti-tumoral effects[199]. This suggests that disrupting CD38-mediated pathways have the potential to simultaneously enhance anti-tumor immune responses and disrupt the supportive tumor microenvironment, offering a dual mechanism of action.

Since macrophages also express CD38, it is possible that the WTa2d1xCD38 bispecific is acting by multiple functions: (i) opsonizing cancer cells, (ii) blocking the CD47/SIRPα macrophage immune checkpoint, (iii) inhibiting CD38-mediated immunosuppression, and (iv) cross-linking macrophages and cancer cells to enhance immune effector functions (Figure 52).

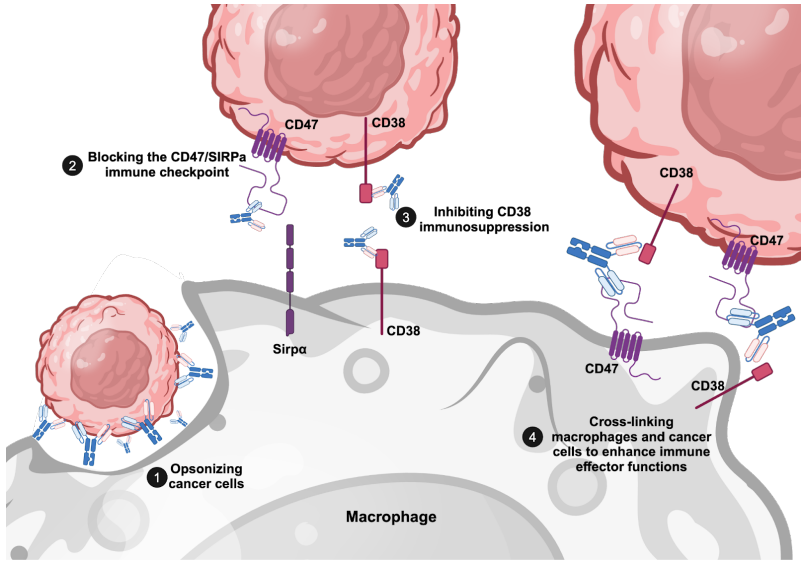

Figure 52 | Putative mechanisms of action for the WTa2d1xCD38 bispecific antibody.
Representation of the biological functions performed by the bsAb to enhance macrophage-mediated destruction of B-cell lymphoma cells. The WTa2d1xCD38 bispecific can act as an opsonin and engage Fc receptors on macrophages (1). It can also block immunosuppressive pathways on both the cancer and macrophage cell surface (2 and 3). Additionally, it can enhance the biophysical interactions of macrophages and B-cell lymphoma cells, bringing their cell membranes in close proximity to promote phagocytosis (4). Together, these functions maximally activate macrophage-mediated cytotoxicity of aggressive B-cell lymphoma cells. Image created using Biorender.com

Indeed, FcγR-blocking experiments showed that while FcγRs are important for the bsAb function, this effect was variable based on the receptor and the cell line, suggesting that the antibody may act through mechanisms in addition to opsonization. Since WTa2d1xCD38 exhibits minimal red blood cell binding, it may be an ideal agent to target macrophage-mediated killing of lymphoma cells while offering a maximal therapeutic window.

6.6. Harnessing macrophages as alternative effectors in R/R B-cell lymphomas

Macrophage-directed therapies, which have been less explored despite the high infiltration of macrophages and their anti-tumoral potential, also show promise for aggressive B-cell NHL that are resistant to conventional therapies. While DLBCL is considered potentially curable, approximately 30-40% of patients experience relapse after first line treatment with R-CHOP[203]. Although T-cell based treatments like CD19 CAR-T or immune checkpoint inhibitors are currently approved for R/R patients, they may not be optimal for all cases due to loss of antigen expression in malignant B cells, such as CD19 or CD20, poor T cell infiltration, T cell exhaustion and/or genetic alterations like MHC I loss that impede T cell-mediated responses[204]. In this study, we propose macrophages as potent immune effector cells and suggest macrophage-mediated therapies as a promising approach for R/R patients who have demonstrated resistance to T-cell therapies.

Research on Burkitt lymphoma has demonstrated that CD38 closely associates with CD19 in malignant B cells and engages with the IgM-BCR upon activation, forming a complex that promotes B cell activation, proliferation, survival, and potentially contributing to treatment resistance[205]. Targeting CD38 with monoclonal antibodies, such as daratumumab, disrupts the connection between IgM and CD19, leading to impaired proliferation and reduced survival of lymphoma cells[205].

However, although daratumumab has demonstrated anti-tumor activity in preclinical DLBCL models[206], it has shown limited single-agent activity in clinical trials for patients with R/R B-cell NHL, with only 8% of patients achieving a response[198]. Our studies suggest that the CD47/SIRPα macrophage immune checkpoint may be a significant barrier that prevents daratumumab from engaging macrophages as immune effector cells. The WTa2d1xCD38 bispecific antibody exhibits superior efficacy compared to daratumumab or magrolimab alone, and even surpasses the gold standard therapy, rituximab. This enhanced potency suggests that the WTa2d1xCD38 bsAb could offer a more effective treatment option for R/R B-cell lymphoma patients, bypassing resistance to conventional therapies.

Finally, our research also highlights that a bispecific format targeting more than one antigen is effective in targeting antigens that promote lymphoma progression as well as those that help evade immune recognition and attack. Other potential candidates that we identified in our screening appear to be promising treatments for further investigation in this context.

6.7. Identification of predictive factors for CNS infiltration in DLBCL

In aggressive DLBCL, refractory disease is common, and CNS involvement as a site of relapse remains a serious and often fatal outcome. Extensive research has been done to characterize secondary CNS lymphoma, with a primary focus on defining the genomic and transcriptomic profiles of malignant cells at relapse site[207,208]; however, a key aspect that needs further exploration is the identification of features that confer the ability to lymphoma cells to infiltrate the brain before the actual occurrence. It is important to understand that once these cells establish themselves in the brain, they may undergo changes influenced by the microenvironment, particularly within the complex brain microenvironment. Identification of such features could help to better identify patients that will likely relapse in the CNS as well as to uncover specific pathogenetic mechanisms for CNS tropism that could potentially be targeted to avoid CNS infiltration in the prophylaxis setting. To address this challenge, we performed a retrospective analysis of diagnostic samples from patients with known CNS relapse outcomes, comparing them to diagnostic samples from patients who experienced systemic relapse or remained relapse-free.

From our cohort, only 2 out of 11 patients who experienced brain relapse were initially classified as high-risk of CNS involvement at time of diagnosis, emphasizing the need to refine tools to identify patients at high risk of CNS relapse, like the CNS-IPI score. Moreover, more than half of patients in this group received CNS prophylaxis and still experienced a CNS relapse, questioning the efficacy of prophylactic treatment. However, it is important to highlight that all the high-risk patients categorized in the No Relapse group received prophylaxis and none of them encountered CNS relapse. This means

DLBCL tumors may exhibit intrinsic differential factors at diagnosis that confer certain tumors a much more aggressive phenotype, making CNS prophylaxis insufficient to prevent CNS involvement in those cases. Identifying these specific factors becomes essential for predicting and anticipating relapse, leading to more effective treatment.

Herein, we have identified several immunological, (epi)genetic, and transcriptomic factors at diagnosis characteristic and unique for DLBCL tumors with CNS tropism. These features not only distinguish this subgroup from others but also helps predicting CNS involvement.

Previous research has indicated that the ABC subtype inherently carries a higher risk of CNS relapse compared to GCB, although this does not necessarily correlate with *MYC/BCL2/BCL6* translocations. However, other studies have suggested an increased predisposition to CNS involvement at diagnosis in double- or triple-hit DLBCLs[166,168]. Our study did not identify COO or these translocations as predictive factors for CNS recurrence at diagnosis.

Schmitz et al. and Chapuy et al. categorized DLBCL tumors into distinct molecular subtypes based on shared genetic features, which have implications for predicting outcomes after R-CHOP therapy[85,209]. Among the identified genetic subtypes, the MCD or C5 subtype, characterized by *MYD88*^{L265P} and *CD79B* mutations[84], is prevalent in primary and secondary CNS lymphomas. In our study, using the LymphGen algorithm[173] for subtype classification, we found that no subtype was predictive for CNS recurrence at the time of diagnosis. Regarding *MYD88*^{L265P} and *CD79B* mutations, Kersten et al. did not observe such alterations at the time of diagnosis for secondary CNS lymphoma[210]. In our study, among patients with CNS relapse, only one case exhibited a mutation in *CD79B*, whereas none showed alterations in *MYD88*. This supports the hypothesis that these mutations may be crucial for tumor initiation in immune-privileged sites but not necessarily required for lymphoma cell homing to the CNS. Interestingly, PIM1 aberrant somatic hypermutation is specifically associated with CNS tropism at diagnosis. Zolyniak et al. demonstrated that PIM1-mutant DLBCL cells exhibit gene expression profiles associated with increased migratory potential and a propensity to spread to extranodal sites compared to non-mutant cells[211]. This suggests that mutations in PIM1 could be a potential factor for predicting DLBCL migration to the CNS at diagnosis. Notably, PIM1

is mutated in over 50% of primary CNS DLBCL samples, emphasizing its significance in this context. This high mutation frequency further supports the notion that PIM1 mutations may play a critical role in the pathogenesis and clinical behavior of DLBCL, particularly regarding its migration to the CNS[212].

It is important to consider that despite despite the clinical relevance of these findings, the limited number of samples in the CNS relapse group (n=7) restricts the robustness of the conclusions that can be drawn.

6.8. Increased expression of genes implicated in CNS entrance

In terms of gene expression, tumors with CNS tropism exhibited increased expression in genes that have been previously reported to be implicated in regulating B cell blood-brain barrier (BBB) penetrance in certain B-cell malignancies, such as *ITGA4*, *BTLA*, *CCR6* and *IL7R*. Previous research demonstrated elevated B and T Lymphocyte Attenuator (BTLA) expression at both the initial diagnosis and relapse stages in patients with aggressive B cell lymphoma[213]. Further validation in a spontaneous CNS metastasis murine model demonstrated higher BTLA expression in DLBCL cells that homed to the CNS compared to those infiltrating the spleen[214]. Chemokine receptor 6 (CCR6) is essential for blood:CSF barrier transit of leukocytes[215]; recent *in vivo* studies in pre-B acute lymphoblastic leukemia revealed higher CCR6 expression in cells that infiltrated the brain upon intravenous injection, in contrast to other anatomical sites[216]. Also, Interleukin 7 Receptor (IL7R) has demonstrated to be associated with disease recurrence and CNS involvement in some types of leukemia; high expression of this gene at diagnosis predicts CNS relapse risk and IL7R blocking antibody reduces CNS leukemic infiltration in pre-clinical models[217,218]. Among these hits, the *ITGA4* gene was the only one found to be upregulated in CNS-relapsed patients when compared to all other cohorts together. This gene encodes the α4 integrin subunit (CD49d) of Very Late Antigen 4 (VLA4); which is the best characterized molecule affecting B cell trafficking into the CNS[219]. Interaction between VLA4 on B cells and its endothelial ligand VCAM-1 is crucial for the migration of these cells across the blood-brain barrier. It is widely studied that expression of this

integrin on activated B cells in autoimmune encephalomyelitis and multiple sclerosis is required for cells to cross brain endothelial cells[220]. In fact, Natalizumab (an anti-α4 integrin monoclonal antibody) is used in clinical practice for multiple sclerosis to prevent the entry and accumulation of B cells in the brain[221,222] (Figure 53).

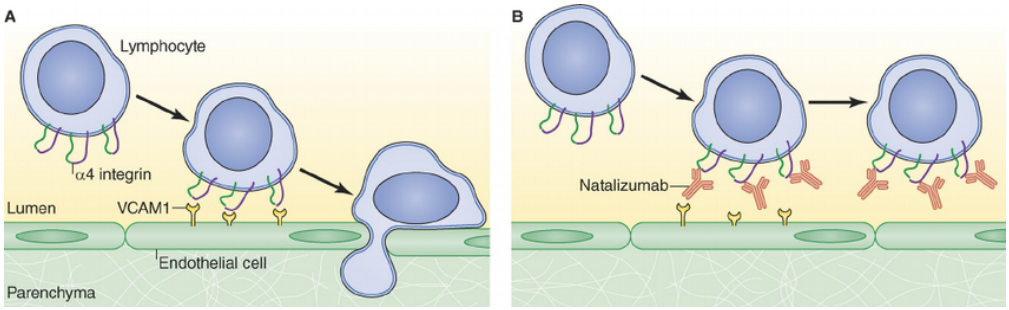

Figure 53 | Natalizumab blocks lymphocyte entry into the CNS.
A, α4 integrin binds to vascular cell adhesion molecule 1 (VCAM1) on inflamed brain endothelium. This interaction gives lymphocytes access to the central nervous system (CNS). **B**, Natalizumab binds to α4 integrin and blocks binding of lymphocytes to VCAM on inflamed brain endothelium, thereby preventing lymphocyte entry into the CNS. From Steinman L. J. Cell Biol. 2012

These findings could advance our understanding of the biological advantages that allow lymphoma cells to migrate into the CNS. Targeting VLA4 could be a promising therapeutic approach at diagnosis to prevent migration of malignant B cells to the brain in patients with DLBCL.

Herein, we have demonstrated that DLBCL cells at diagnosis already own specific genomic, transcriptomic and epigenomic hallmarks that could confer them a more aggressive phenotype and a higher capacity to infiltrate the CNS. However, the small sample size precludes the development of a multiomic score that could be further validated in external cohorts. Additional research in the field will help the scientific community to better delineate (epi)genetic and transcriptomic characteristics of DLBCL at diagnosis that can help us improve the accuracy of identification of patients at high risk of CNS relapse.

7. Conclusion

1. Macrophages and T cells are essential for controlling tumor growth and mediating a full anti-tumor response to PD-1 blockade in primary CNS lymphoma. Depletion of macrophages accelerated tumor progression, highlighting the important role of macrophages in the early control of tumor growth.

2. MHC I-negative PCNSL tumors exhibit a highly aggressive phenotype and rely solely on macrophages for control, as shown by the diminished response in immunocompetent mice and the complete lack of response in macrophage-depleted mice, compared to wild-type CNS lymphoma. Blockade of PD-1-PD-L1 and/or CD47-SIRPα pathways are insufficient to activate a robust macrophage-mediated anti-tumor response in this tumoral setting, highlighting the need for new macrophage-targeted therapies to combat MHC I-negative lymphoma.

3. Several novel antigens were identified as promising targets in both mouse and human systems, such as CD24, CD40, LILRB1, CD71 or CD38. Blocking them individually or in combination enhances macrophage activity against lymphoma cells *in vitro*, and this effect is particularly more potent against MHC I-negative cells. With these results, we developed a rapid platform to generate and evaluate bispecific antibodies, revealing new therapeutic strategies that effectively stimulate macrophage-mediated cytotoxicity against lymphoma cells *in vitro*.

4. Among the bispecific antibodies tested, WTa2d1xCD38, which is composed of a low-affinity SIRPα decoy protein and an anti-CD38 binding arm, has emerged as an optimal therapeutic candidate. It demonstrates potent macrophage-mediated cytotoxicity against lymphoma cells with minimal red blood cell binding, showing significant efficacy in both *in vitro* and *in vivo* models of aggressive B-cell lymphoma. This macrophage-mediated therapy could be applied to CNS lymphomas with MHC I downregulation as well as to R/R B-cell lymphoma patients who are unresponsive to T-cell therapies.

5. DLBCL tumors at diagnosis already possess distinct genomic, transcriptomic, and epigenetic features that are associated with CNS tropism. Specifically, these tumors show upregulation of genes related to cell migration and proliferation, including *ITGA4*, *CCR6*, *BTLA*, and *IL7R*, along with activation of growth pathways like E2F and MYC signaling. CpG hypomethylation in migration-related genes further supports their invasive potential. These findings highlight key molecular markers that may improve risk assessment and suggest new therapeutic targets, such as *ITGA4*, to prevent CNS infiltration.

8. Future research opportunities

The future research lines of this work would be the following:

1. Improving bispecific antibody production and characterization

The development of bispecific antibodies presents several experimental challenges. The production process can lead to undesirable outcomes such as truncated or non-functional isoforms. Future research should focus on optimizing the production of bispecific antibodies, ensuring consistency in quality and efficacy. This will involve enhancing the expression and purification protocols to minimize the formation of isoforms that lack the desired functional properties. Additionally, thorough *in vitro* and *in vivo* characterization of these antibodies will be critical to identify the most promising candidates. *In vivo* studies should continue with relevant models, focusing on CNS lymphoma to compare wild-type and MHC-I knockout settings.

2. Study other promising bispecific antibodies

Particular attention should be given to bispecific antibodies with LILRB1 or CD24 binding arms, as these targets hold potential for modulating immune responses against tumors. Following the production and purification of these candidates, preclinical testing will be essential to evaluate their efficacy.

3. Challenges in assessing immune interactions

One significant limitation in current bispecific antibody research is the reliance on immunocompromised mice models (e.g., NSG mice) due to the human-specific nature of the constructs. While this allows for the study of macrophage-mediated responses, the inability to evaluate interactions with T cells, NK cells, and other components of the immune system restricts the full understanding of the anti-tumor immune response. Future research should focus on developing humanized immune system models or adapting the constructs for use in immunocompetent models, which would allow for a more comprehensive evaluation of bispecific antibody efficacy.

4. Expanding Multiomic Analysis for Predicting CNS Involvement

The next logical step in this project is to perform a multiomic analysis to identify biomarkers that can more accurately predict CNS involvement outcomes. This approach offers the potential to reveal multi-dimensional data, providing a deeper understanding of disease progression and treatment response. Additionally, the integration of these biomarkers could enable the development of a predictive model at diagnosis, helping to stratify patients based on their risk of CNS involvement. However, a major limitation of this approach is the large number of variables and the relatively small sample size currently available. To address this:

- Future research should focus on increasing the number of samples, potentially through collaborations with other research groups or biobanks to build a larger cohort.
- Performing paired sample analysis, where samples are taken at both diagnosis and relapse, will be crucial for determining whether the biomarkers identified at diagnosis are maintained over time.

Summary of Key Future Directions:

- Optimizing the production and functional characterization of bispecific antibodies to minimize non-desirable isoforms and enhance efficacy.
- Prioritizing other bispecifics, like the ones with LILRB1 or CD24 binding arms for further study.
- Expanding *in vitro* and *in vivo* studies to include interactions with macrophages, T cells, and NK cells, and improving in vivo models to allow comprehensive immune response evaluation.
- Performing multiomic analyses with increased sample sizes, including paired diagnostic and relapse samples, to identify consistent biomarkers for CNS involvement

9. Bibliography

1. Doulatov S, Notta F, Laurenti E, Dick JE. Hematopoiesis: A Human Perspective. *Cell Stem Cell*. 2012;10(2):120–136.
2. Anthony BA, Link DC. Regulation of hematopoietic stem cells by bone marrow stromal cells. *Trends in Immunology*. 2014;35(1):32–37.
3. Morrison SJ, Scadden DT. The bone marrow niche for haematopoietic stem cells. *Nature*. 2014;505(7483):327–334.
4. Orkin SH, Zon LI. Hematopoiesis: An Evolving Paradigm for Stem Cell Biology. *Cell*. 2008;132(4):631–644.
5. Machlus KR, Italiano JE. The incredible journey: From megakaryocyte development to platelet formation. *Journal of Cell Biology*. 2013;201(6):785–796.
6. Cowland JB, Borregaard N. Granulopoiesis and granules of human neutrophils. *Immunological Reviews*. 2016;273(1):11–28.
7. Weiskopf K, Schnorr PJ, Pang WW, et al. Myeloid Cell Origins, Differentiation, and Clinical Implications. *Microbiol Spectr*. 2016;4(5):4.5.21.
8. Ginhoux F, Jung S. Monocytes and macrophages: developmental pathways and tissue homeostasis. *Nat Rev Immunol*. 2014;14(6):392–404.
9. Janeway CA, Medzhitov R. Innate Immune Recognition. *Annu. Rev. Immunol.* 2002;20(1):197–216.
10. Vivier E, Tomasello E, Baratin M, Walzer T, Ugolini S. Functions of natural killer cells. *Nat Immunol*. 2008;9(5):503–510.
11. Mesin L, Ersching J, Victora GD. Germinal Center B Cell Dynamics. *Immunity*. 2016;45(3):471–482.
12. Mandel EM, Grosschedl R. Transcription control of early B cell differentiation. *Current Opinion in Immunology*. 2010;22(2):161–167.
13. Chen JW, Schickel J-N, Tsakiris N, et al. Positive and negative selection shape the human naive B cell repertoire. *Journal of Clinical Investigation*. 2022;132(2):e150985.
14. Victora GD, Nussenzweig MC. Germinal Centers. *Annu. Rev. Immunol.* 2022;40(1):413–442.
15. Chi X, Li Y, Qiu X. V(D)J recombination, somatic hypermutation and class switch recombination of immunoglobulins: mechanism and regulation. *Immunology*. 2020;160(3):233–247.
16. Van Der Poel CE, Bajic G, Macaulay CW, et al. Follicular Dendritic Cells Modulate Germinal Center B Cell Diversity through FcγRIIB. *Cell Reports*. 2019;29(9):2745-2755.e4.
17. Calado DP, Sasaki Y, Godinho SA, et al. The cell-cycle regulator c-Myc is essential for the formation and maintenance of germinal centers. *Nat Immunol*. 2012;13(11):1092–1100.
18. Wen Y, Jing Y, Yang L, et al. The regulators of BCR signaling during B cell activation. *Blood Science*. 2019;1(2):119–129.
19. Dong Y, Pi X, Bartels-Burgahn F, et al. Structural principles of B cell antigen receptor assembly. *Nature*. 2022;612(7938):156–161.
20. Qiu Y, Chen T, Hu R, et al. Next frontier in tumor immunotherapy: macrophage-mediated immune evasion. *Biomark Res*. 2021;9(1):72.

21. Murray PJ, Allen JE, Biswas SK, et al. Macrophage Activation and Polarization: Nomenclature and Experimental Guidelines. *Immunity*. 2014;41(1):14–20.
22. Virág L, Jaén RI, Regdon Z, Boscá L, Prieto P. Self-defense of macrophages against oxidative injury: Fighting for their own survival. *Redox Biology*. 2019;26:101261.
23. Anderson NR, Minutolo NG, Gill S, Klichinsky M. Macrophage-Based Approaches for Cancer Immunotherapy. *Cancer Research*. 2021;81(5):1201–1208.
24. Vannella KM, Wynn TA. Mechanisms of Organ Injury and Repair by Macrophages. *Annu. Rev. Physiol.* 2017;79(1):593–617.
25. Zhang M, Hutter G, Kahn SA, et al. Anti-CD47 Treatment Stimulates Phagocytosis of Glioblastoma by M1 and M2 Polarized Macrophages and Promotes M1 Polarized Macrophages In Vivo. *PLoS ONE*. 2016;11(4):e0153550.
26. Noy R, Pollard JW. Tumor-Associated Macrophages: From Mechanisms to Therapy. *Immunity*. 2014;41(1):49–61.
27. Colonna M, Butovsky O. Microglia Function in the Central Nervous System During Health and Neurodegeneration. *Annu. Rev. Immunol.* 2017;35(1):441–468.
28. Junker F, Gordon J, Qureshi O. Fc Gamma Receptors and Their Role in Antigen Uptake, Presentation, and T Cell Activation. *Front. Immunol.* 2020;11:1393.
29. Anania JC, Chenoweth AM, Wines BD, Hogarth PM. The Human FcγRII (CD32) Family of Leukocyte FcR in Health and Disease. *Front. Immunol.* 2019;10:464.
30. Yeap WH, Wong KL, Shimasaki N, et al. CD16 is indispensable for antibody-dependent cellular cytotoxicity by human monocytes. *Sci Rep*. 2016;6(1):34310.
31. Zahavi D, AlDeghaither D, O'Connell A, Weiner LM. Enhancing antibody-dependent cell-mediated cytotoxicity: a strategy for improving antibody-based immunotherapy. *Antibody Therapeutics*. 2018;1(1):7–12.
32. Hanahan D, Weinberg RA. Hallmarks of Cancer: The Next Generation. *Cell*. 2011;144(5):646–674.
33. Martínez-Jiménez F, Priestley P, Shale C, et al. Genetic immune escape landscape in primary and metastatic cancer. *Nat Genet*. 2023;55(5):820–831.
34. Ghorani E, Swanton C, Quezada SA. Cancer cell-intrinsic mechanisms driving acquired immune tolerance. *Immunity*. 2023;56(10):2270–2295.
35. Dhatchinamoorthy K, Colbert JD, Rock KL. Cancer Immune Evasion Through Loss of MHC Class I Antigen Presentation. *Front. Immunol.* 2021;12:636568.
36. Rusakiewicz S, Semeraro M, Sarabi M, et al. Immune Infiltrates Are Prognostic Factors in Localized Gastrointestinal Stromal Tumors. *Cancer Research*. 2013;73(12):3499–3510.
37. Ryschich E, Nötzel T, Hinz U, et al. Control of T-Cell–Mediated Immune Response by HLA Class I in Human Pancreatic Carcinoma. *Clinical Cancer Research*. 2005;11(2):498–504.
38. Pardoll DM. The blockade of immune checkpoints in cancer immunotherapy. *Nat Rev Cancer*. 2012;12(4):252–264.

39. Parvez A, Choudhary F, Mudgal P, et al. PD-1 and PD-L1: architects of immune symphony and immunotherapy breakthroughs in cancer treatment. *Front. Immunol.* 2023;14:1296341.
40. Jiang Y, Chen M, Nie H, Yuan Y. PD-1 and PD-L1 in cancer immunotherapy: clinical implications and future considerations. *Human Vaccines & Immunotherapeutics*. 2019;15(5):1111–1122.
41. Jiang Y, Li Y, Zhu B. T-cell exhaustion in the tumor microenvironment. *Cell Death Dis*. 2015;6(6):e1792–e1792.
42. He X, Xu C. PD-1: A Driver or Passenger of T Cell Exhaustion? *Molecular Cell*. 2020;77(5):930–931.
43. Ribas A, Wolchok JD. Cancer immunotherapy using checkpoint blockade. *Science*. 2018;359(6382):1350–1355.
44. Gordon SR, Maute RL, Dulken BW, et al. PD-1 expression by tumour-associated macrophages inhibits phagocytosis and tumour immunity. *Nature*. 2017;545(7655):495–499.
45. Fenalti G, Villanueva N, Griffith M, et al. Structure of the human marker of self 5-transmembrane receptor CD47. *Nat Commun*. 2021;12(1):5218.
46. Zhang W, Huang Q, Xiao W, et al. Advances in Anti-Tumor Treatments Targeting the CD47/SIRPα Axis. *Front. Immunol.* 2020;11:18.
47. Huang J, Liu F, Li C, et al. Role of CD47 in tumor immunity: a potential target for combination therapy. *Sci Rep*. 2022;12(1):9803.
48. Constantinides M, Fayd'herbe De Maudave A, Potier-Cartereau M, et al. Direct Cell Death Induced by CD20 Monoclonal Antibodies on B Cell Lymphoma Cells Revealed by New Protocols of Analysis. *Cancers*. 2023;15(4):1109.
49. Van Wagoner CM, Rivera-Escalera F, Jaimes-Delgadillo NC, et al. Antibody-mediated phagocytosis in cancer immunotherapy. *Immunological Reviews*. 2023;319(1):128–141.
50. Grillo-Lopez A, White C, Dallaire B, et al. Rituximab The First Monoclonal Antibody Approved for the Treatment of Lymphoma. *CPB*. 2000;1(1):1–9.
51. Marhelava K, Pilch Z, Bajor M, Graczyk-Jarzynka A, Zagozdzon R. Targeting Negative and Positive Immune Checkpoints with Monoclonal Antibodies in Therapy of Cancer. *Cancers*. 2019;11(11):1756.
52. Hirano F, Kaneko K, Tamura H, et al. Blockade of B7-H1 and PD-1 by Monoclonal Antibodies Potentiates Cancer Therapeutic Immunity. *Cancer Research*. 2005;65(3):1089–1096.
53. Homet Moreno B, Zaretsky JM, Garcia-Diaz A, et al. Response to Programmed Cell Death-1 Blockade in a Murine Melanoma Syngeneic Model Requires Costimulation, CD4, and CD8 T Cells. *Cancer Immunology Research*. 2016;4(10):845–857.
54. Davids MS, Kim HT, Costello C, et al. A multicenter phase 1 study of nivolumab for relapsed hematologic malignancies after allogeneic transplantation. *Blood*. 2020;135(24):2182–2191.
55. Lesokhin AM, Ansell SM, Armand P, et al. Nivolumab in Patients With Relapsed or Refractory Hematologic Malignancy: Preliminary Results of a Phase Ib Study. *JCO*. 2016;34(23):2698–2704.

56. Weiskopf K, Weissman IL. Macrophages are critical effectors of antibody therapies for cancer. *mAbs*. 2015;7(2):303–310.
57. Weiskopf K. Cancer immunotherapy targeting the CD47/SIRPα axis. *European Journal of Cancer*. 2017;76:100–109.
58. Weiskopf K, Jahchan NS, Schnorr PJ, et al. CD47-blocking immunotherapies stimulate macrophage-mediated destruction of small-cell lung cancer. *Journal of Clinical Investigation*. 2016;126(7):2610–2620.
59. Maute R, Xu J, Weissman IL. CD47–SIRPα-targeted therapeutics: status and prospects. *Immuno-Oncology and Technology*. 2022;13:100070.
60. Chen J, Johnson L, McKenna K, et al. MDS-482 Impact Of Magrolimab in Combination With Azacitidine on Red Blood Cells (RBCs) in Patients With Higher-Risk Myelodysplastic Syndromes (HR MDS). *Clinical Lymphoma Myeloma and Leukemia*. 2022;22:S317–S318.
61. Tumeh PC, Harview CL, Yearley JH, et al. PD-1 blockade induces responses by inhibiting adaptive immune resistance. *Nature*. 2014;515(7528):568–571.
62. Van Duijn A, Van Der Burg SH, Scheeren FA. CD47/SIRPα axis: bridging innate and adaptive immunity. *J Immunother Cancer*. 2022;10(7):e004589.
63. Barkal AA, Weiskopf K, Kao KS, et al. Engagement of MHC class I by the inhibitory receptor LILRB1 suppresses macrophages and is a target of cancer immunotherapy. *Nat Immunol*. 2018;19(1):76–84.
64. Ansell SM, Bröckelmann PJ, Von Keudell G, et al. Nivolumab for relapsed/refractory classical Hodgkin lymphoma: 5-year survival from the pivotal phase 2 CheckMate 205 study. *Blood Advances*. 2023;7(20):6266–6274.
65. Reinke S, Bröckelmann PJ, Iaccarino I, et al. Tumor and microenvironment response but no cytotoxic T-cell activation in classic Hodgkin lymphoma treated with anti-PD1. *Blood*. 2020;136(25):2851–2863.
66. Steidl C, Farinha P, Gascoyne RD. Macrophages predict treatment outcome in Hodgkin's lymphoma. *Haematologica*. 2011;96(2):186–189.
67. Kamper P, Bendix K, Hamilton-Dutoit S, et al. Tumor-infiltrating macrophages correlate with adverse prognosis and Epstein-Barr virus status in classical Hodgkin's lymphoma. *Haematologica*. 2011;96(2):269–276.
68. Singh R, Shaik S, Negi B, et al. Non-Hodgkin's lymphoma: A review. *J Family Med Prim Care*. 2020;9(4):1834.
69. Küppers R. Mechanisms of B-cell lymphoma pathogenesis. *Nat Rev Cancer*. 2005;5(4):251–262.
70. Thandra KC, Barsouk A, Saginala K, et al. Epidemiology of Non-Hodgkin's Lymphoma. *Medical Sciences*. 2021;9(1):5.
71. Alaggio R, Amador C, Anagnostopoulos I, et al. The 5th edition of the World Health Organization Classification of Haematolymphoid Tumours: Lymphoid Neoplasms. *Leukemia*. 2022;36(7):1720–1748.
72. Grimm KE, O'Malley DP. Aggressive B cell lymphomas in the 2017 revised WHO classification of tumors of hematopoietic and lymphoid tissues. *Annals of Diagnostic Pathology*. 2019;38:6–10.
73. Basso K. Biology of Germinal Center B Cells Relating to Lymphomagenesis. *HemaSphere*. 2021;5(6):e582.

74. Pasqualucci L. The germinal center in the pathogenesis of B cell lymphomas. *Hematological Oncology*. 2023;41(S1):62–69.
75. Basso K, Dalla-Favera R. Germinal centres and B cell lymphomagenesis. *Nat Rev Immunol*. 2015;15(3):172–184.
76. Xie Y, Pittaluga S, Jaffe ES. The Histological Classification of Diffuse Large B-cell Lymphomas. *Seminars in Hematology*. 2015;52(2):57–66.
77. Tavakkoli M, Barta SK. 2024 Update: Advances in the risk stratification and management of large B-cell lymphoma. *American J Hematol*. 2023;98(11):1791–1805.
78. Kanas G, Ge W, Quek RGW, et al. Epidemiology of diffuse large B-cell lymphoma (DLBCL) and follicular lymphoma (FL) in the United States and Western Europe: population-level projections for 2020–2025. *Leukemia & Lymphoma*. 2022;63(1):54–63.
79. Jelicic J, Juul-Jensen K, Bukumiric Z, et al. Prognostic indices in diffuse large B-cell lymphoma: a population-based comparison and validation study of multiple models. *Blood Cancer J.* 2023;13(1):157.
80. Crump M, Neelapu SS, Farooq U, et al. Outcomes in refractory diffuse large B-cell lymphoma: results from the international SCHOLAR-1 study. *Blood*. 2017;130(16):1800–1808.
81. Pasqualucci L, Dalla-Favera R. Genetics of diffuse large B-cell lymphoma. *Blood*. 2018;131(21):2307–2319.
82. Saito M, Novak U, Piovan E, et al. BCL6 suppression of BCL2 via Miz1 and its disruption in diffuse large B cell lymphoma. *Proc. Natl. Acad. Sci. U.S.A.* 2009;106(27):11294–11299.
83. Alizadeh AA, Eisen MB, Davis RE, et al. Distinct types of diffuse large B-cell lymphoma identified by gene expression profiling. *Nature*. 2000;403(6769):503–511.
84. Chapuy B, Stewart C, Dunford AJ, et al. Molecular subtypes of diffuse large B cell lymphoma are associated with distinct pathogenic mechanisms and outcomes. *Nat Med*. 2018;24(5):679–690.
85. Schmitz R, Wright GW, Huang DW, et al. Genetics and Pathogenesis of Diffuse Large B-Cell Lymphoma. *N Engl J Med*. 2018;378(15):1396–1407.
86. Ngo VN, Young RM, Schmitz R, et al. Oncogenically active MYD88 mutations in human lymphoma. *Nature*. 2011;470(7332):115–119.
87. Chapuy B, Roemer MGM, Stewart C, et al. Targetable genetic features of primary testicular and primary central nervous system lymphomas. *Blood*. 2016;127(7):869–881.
88. Ennishi D. The biology of the tumor microenvironment in DLBCL: Targeting the “don’t eat me” signal. *JCEH*. 2021;61(4):210–215.
89. Scott DW, Gascoyne RD. The tumour microenvironment in B cell lymphomas. *Nat Rev Cancer*. 2014;14(8):517–534.
90. Challa-Malladi M, Lieu YK, Califano O, et al. Combined Genetic Inactivation of β2-Microglobulin and CD58 Reveals Frequent Escape from Immune Recognition in Diffuse Large B Cell Lymphoma. *Cancer Cell*. 2011;20(6):728–740.

91. Huse K, Blaker Y, Wise JF, et al. Reduced Immune-Cell Infiltration in MHC Class I Negative DLBCL. *Blood*. 2023;142(Supplement 1):179–179.
92. Merdan S, Subramanian K, Ayer T, et al. Gene expression profiling-based risk prediction and profiles of immune infiltration in diffuse large B-cell lymphoma. *Blood Cancer J.* 2021;11(1):2.
93. Serna L, Azcoaga P, Brahmachary M, Caffarel MM, Braza MS. Diffuse large B-cell lymphoma microenvironment displays a predominant macrophage infiltrate marked by a strong inflammatory signature. *Front. Immunol.* 2023;14:1048567.
94. Kridel R, Steidl C, Gascoyne RD. Tumor-associated macrophages in diffuse large B-cell lymphoma. *Haematologica*. 2015;100(2):143–145.
95. Ciavarella S, Vegliante MC, Fabbri M, et al. Dissection of DLBCL microenvironment provides a gene expression-based predictor of survival applicable to formalin-fixed paraffin-embedded tissue. *Annals of Oncology*. 2018;29(12):2363–2370.
96. Li Y-L, Shi Z-H, Wang X, Gu K-S, Zhai Z-M. Tumor-associated macrophages predict prognosis in diffuse large B-cell lymphoma and correlation with peripheral absolute monocyte count. *BMC Cancer*. 2019;19(1):1049.
97. Cai Q, Liao H, Lin S, et al. High expression of tumor-infiltrating macrophages correlates with poor prognosis in patients with diffuse large B-cell lymphoma. *Med Oncol*. 2012;29(4):2317–2322.
98. Marinaccio C, Ingravallo G, Gaudio F, et al. Microvascular density, CD68 and tryptase expression in human Diffuse Large B-Cell Lymphoma. *Leukemia Research*. 2014;38(11):1374–1377.
99. Abrisqueta P. New Insights into First-Line Therapy in Diffuse Large B-Cell Lymphoma: Are We Improving Outcomes? *JCM*. 2024;13(7):1929.
100. Roschewski M, Staudt LM, Wilson WH. Diffuse large B-cell lymphoma—treatment approaches in the molecular era. *Nat Rev Clin Oncol*. 2014;11(1):12–23.
101. Riihijarvi S, Fiskvik I, Taskinen M, et al. Prognostic influence of macrophages in patients with diffuse large B-cell lymphoma: a correlative study from a Nordic phase II trial. *Haematologica*. 2015;100(2):238–245.
102. Melchardt T, Egle A, Greil R. How I treat diffuse large B-cell lymphoma. *ESMO Open*. 2023;8(1):100750.
103. Atallah-Yunes SA, Robertson MJ, Davé UP, Ghione P, Perna F. Novel Immune-Based treatments for Diffuse Large B-Cell Lymphoma: The Post-CAR T Cell Era. *Front. Immunol.* 2022;13:901365.
104. Yamauchi N, Maruyama D. Current development of chimeric antigen receptor T-cell therapy for diffuse large B-cell lymphoma and high-grade B-cell lymphoma. *European J of Haematology*. 2024;112(5):662–677.
105. Buatois V, Johnson Z, Salgado-Pires S, et al. Preclinical Development of a Bispecific Antibody that Safely and Effectively Targets CD19 and CD47 for the Treatment of B-Cell Lymphoma and Leukemia. *Molecular Cancer Therapeutics*. 2018;17(8):1739–1751.
106. Ribeiro ML, Normant E, Garau DR, et al. PS1310 THE NOVEL BISPECIFIC CD47-CD19 ANTIBODY TG-1801 POTENTIATES THE ACTIVITY OF

UBLITUXIMAB-UMBRALISIB (U2) DRUG COMBINATION IN PRECLINICAL MODELS OF B-NHL. *HemaSphere*. 2019;3(S1):598.
107. Rimsza LM. Loss of MHC class II gene and protein expression in diffuse large B-cell lymphoma is related to decreased tumor immunosurveillance and poor patient survival regardless of other prognostic factors: a follow-up study from the Leukemia and Lymphoma Molecular Profiling Project. *Blood*. 2004;103(11):4251–4258.
108. Song JY, Nwangwu M, He T-F, et al. Low T-cell proportion in the tumor microenvironment is associated with immune escape and poor survival in diffuse large B-cell lymphoma. *haematol*. 2023;108(8):2167–2177.
109. Cappell KM, Kochenderfer JN. Long-term outcomes following CAR T cell therapy: what we know so far. *Nat Rev Clin Oncol*. 2023;20(6):359–371.
110. Zhao J, Wei C, Wang S, et al. The intrinsic defects of T cells impact the efficacy of CAR-T therapy in patients with diffuse large B-cell lymphoma. *Blood Cancer J.* 2023;13(1):186.
111. Zeller T, Lutz S, Münnich IA, et al. Dual checkpoint blockade of CD47 and LILRB1 enhances CD20 antibody-dependent phagocytosis of lymphoma cells by macrophages. *Front. Immunol.* 2022;13:929339.
112. Advani R, Flinn I, Popplewell L, et al. CD47 Blockade by Hu5F9-G4 and Rituximab in Non-Hodgkin's Lymphoma. *N Engl J Med*. 2018;379(18):1711–1721.
113. Russ A, Hua AB, Montfort WR, et al. Blocking "don't eat me" signal of CD47-SIRPα in hematological malignancies, an in-depth review. *Blood Reviews*. 2018;32(6):480–489.
114. Chao MP, Alizadeh AA, Tang C, et al. Anti-CD47 Antibody Synergizes with Rituximab to Promote Phagocytosis and Eradicate Non-Hodgkin Lymphoma. *Cell*. 2010;142(5):699–713.
115. Haldorsen IS, Krossnes BK, Aarseth JH, et al. Increasing incidence and continued dismal outcome of primary central nervous system lymphoma in Norway 1989–2003: Time trends in a 15-year national survey. *Cancer*. 2007;110(8):1803–1814.
116. Mendez JS, Ostrom QT, Gittleman H, et al. The elderly left behind—changes in survival trends of primary central nervous system lymphoma over the past 4 decades. *Neuro-Oncology*. 2018;20(5):687–694.
117. Houillier C, Soussain C, Ghesquières H, et al. Management and outcome of primary CNS lymphoma in the modern era: An LOC network study. *Neurology*. 2020;94(10):.
118. Dandachi D, Ostrom QT, Chong I, et al. Primary central nervous system lymphoma in patients with and without HIV infection: a multicenter study and comparison with U.S national data. *Cancer Causes Control*. 2019;30(5):477–488.
119. Louis DN, Perry A, Wesseling P, et al. The 2021 WHO Classification of Tumors of the Central Nervous System: a summary. *Neuro-Oncology*. 2021;23(8):1231–1251.

120. Falini B, Martino G, Lazzi S. A comparison of the International Consensus and 5th World Health Organization classifications of mature B-cell lymphomas. *Leukemia*. 2023;37(1):18–34.
121. Campo E, Jaffe ES, Cook JR, et al. The International Consensus Classification of Mature Lymphoid Neoplasms: a report from the Clinical Advisory Committee. *Blood*. 2022;140(11):1229–1253.
122. Abrey LE, Ben-Porat L, Panageas KS, et al. Primary Central Nervous System Lymphoma: The Memorial Sloan-Kettering Cancer Center Prognostic Model. *JCO*. 2006;24(36):5711–5715.
123. Ferreri AJM, Blay J-Y, Reni M, et al. Prognostic Scoring System for Primary CNS Lymphomas: The International Extranodal Lymphoma Study Group Experience. *JCO*. 2003;21(2):266–272.
124. Bessell EM, Graus F, Lopez-Guillermo A, et al. Primary non-Hodgkin's lymphoma of the CNS treated with CHOD/BVAM or BVAM chemotherapy before radiotherapy: long-term survival and prognostic factors. *International Journal of Radiation Oncology*Biology*Physics*. 2004;59(2):501–508.
125. Zhou X, Niu X, Li J, et al. Risk Factors for Early Mortality in Patients with Primary Central Nervous System Lymphoma: A Large-Cohort Retrospective Study. *World Neurosurgery*. 2020;138:e905–e912.
126. Braggio E, Van Wier S, Ojha J, et al. Genome-Wide Analysis Uncovers Novel Recurrent Alterations in Primary Central Nervous System Lymphomas. *Clinical Cancer Research*. 2015;21(17):3986–3994.
127. Chen R, Zhou D, Wang L, Zhu L, Ye X. MYD88 ^{L265P} and CD79B double mutations type (MCD type) of diffuse large B-cell lymphoma: mechanism, clinical characteristics, and targeted therapy. *Therapeutic Advances in Hematology*. 2022;13:204062072110728.
128. Villa D, Tan KL, Steidl C, et al. Molecular features of a large cohort of primary central nervous system lymphoma using tissue microarray. *Blood Advances*. 2019;3(23):3953–3961.
129. Nosrati A, Monabati A, Sadeghipour A, et al. MYC, BCL2, and BCL6 rearrangements in primary central nervous system lymphoma of large B cell type. *Ann Hematol*. 2019;98(1):169–173.
130. Cobbers JMJL, Wolter M, Reifenberger J, et al. Frequent In activation of *CDKN2A* and Rare Mutation of *TP53* in PCNSL. *Brain Pathology*. 1998;8(2):263–276.
131. Montesinos-Rongen M, Küppers R, Schlüter D, et al. Primary Central Nervous System Lymphomas Are Derived from Germinal-Center B Cells and Show a Preferential Usage of the V4–34 Gene Segment. *The American Journal of Pathology*. 1999;155(6):2077–2086.
132. Schwindt H, Vater I, Kreuz M, et al. Chromosomal imbalances and partial uniparental disomies in primary central nervous system lymphoma. *Leukemia*. 2009;23(10):1875–1884.
133. Marcelis L, Antoranz A, Delsupehe A-M, et al. In-depth characterization of the tumor microenvironment in central nervous system lymphoma reveals

implications for immune-checkpoint therapy. *Cancer Immunol Immunother*. 2020;69(9):1751–1766.
134. Elpek KG, Lacelle C, Singh NP, Yolcu ES, Shirwan H. CD4+CD25+ T Regulatory Cells Dominate Multiple Immune Evasion Mechanisms in Early but Not Late Phases of Tumor Development in a B Cell Lymphoma Model. *The Journal of Immunology*. 2007;178(11):6840–6848.
135. Borst K, Dumas AA, Prinz M. Microglia: Immune and non-immune functions. *Immunity*. 2021;54(10):2194–2208.
136. Ponzoni M, Berger F, Chassagne-Clement C, et al. Reactive perivascular T-cell infiltrate predicts survival in primary central nervous system B-cell lymphomas. *Br J Haematol*. 2007;138(3):316–323.
137. Komohara Y, Horlad H, Ohnishi K, et al. M2 Macrophage/Microglial Cells Induce Activation of Stat3 in Primary Central Nervous System Lymphoma. *J Clin Exp Hematopathol*. 2011;51(2):93–99.
138. Four M, Cacheux V, Tempier A, et al. PD 1 and PDL 1 expression in primary central nervous system diffuse large B-cell lymphoma are frequent and expression of PD 1 predicts poor survival. *Hematological Oncology*. 2017;35(4):487–496.
139. Cho H, Kim SH, Kim S-J, et al. Programmed cell death 1 expression is associated with inferior survival in patients with primary central nervous system lymphoma. *Oncotarget*. 2017;8(50):87317–87328.
140. Kim S, Nam SJ, Park C, et al. High tumoral PD-L1 expression and low PD-1 $^{+}$ or CD8 $^{+}$ tumor-infiltrating lymphocytes are predictive of a poor prognosis in primary diffuse large B-cell lymphoma of the central nervous system. *OncoImmunology*. 2019;8(9):e1626653.
141. Heming M, Haessner S, Wolbert J, et al. Intratumor heterogeneity and T cell exhaustion in primary CNS lymphoma. *Genome Med*. 2022;14(1):109.
142. Donnou S, Galand C, Daussy C, et al. Immune adaptive microenvironment profiles in intracerebral and intrasplenic lymphomas share common characteristics. *Clinical and Experimental Immunology*. 2011;165(3):329–337.
143. Pollari M, Brück O, Pellinen T, et al. PD-L1 $^{+}$ tumor-associated macrophages and PD-1 $^{+}$ tumor-infiltrating lymphocytes predict survival in primary testicular lymphoma. *Haematologica*. 2018;103(11):1908–1914.
144. Programmed Cell Death Ligand 1 Expression in Primary Central Nervous System Lymphomas: A Clinicopathological Study. *AR*. 2017;37(10):.
145. Gao H-X, Fraser E, Merlini M, et al. Regulation of CNS Lymphoma Progression By the Myeloid Microenvironment. *Blood*. 2021;138(Supplement 1):448–448.
146. Jiménez I, Carabia J, Bobillo S, et al. Repolarization of tumor infiltrating macrophages and increased survival in mouse primary CNS lymphomas after XPO1 and BTK inhibition. *J Neurooncol*. 2020;149(1):13–25.
147. Baraniskin A, Schroers R. Liquid Biopsy and Other Non-Invasive Diagnostic Measures in PCNSL. *Cancers*. 2021;13(11):2665.
148. Grommes C, DeAngelis LM. Primary CNS Lymphoma. *JCO*. 2017;35(21):2410–2418.

149. Bairey O, Shargian-Alon L, Siegal T. Consolidation Treatment for Primary Central Nervous System Lymphoma: Which Modality for Whom? *Acta Haematol*. 2021;144(4):389–402.
150. Nayak L, Hedvat C, Rosenblum MK, Abrey LE, DeAngelis LM. Late relapse in primary central nervous system lymphoma: clonal persistence. *Neuro-Oncology*. 2011;13(5):525–529.
151. Kaulen LD, Baehring JM. Treatment Options for Recurrent Primary CNS Lymphoma. *Curr. Treat. Options in Oncol.* 2022;23(11):1548–1565.
152. Ferreri AJM, Cwynarski K, Pulczynski E, et al. Chemoimmunotherapy with methotrexate, cytarabine, thiotepa, and rituximab (MATRix regimen) in patients with primary CNS lymphoma: results of the first randomisation of the International Extranodal Lymphoma Study Group-32 (IELSG32) phase 2 trial. *The Lancet Haematology*. 2016;3(5):e217–e227.
153. Bromberg JEC, Issa S, Bakunina K, et al. Rituximab in patients with primary CNS lymphoma (HOVON 105/ALLG NHL 24): a randomised, open-label, phase 3 intergroup study. *The Lancet Oncology*. 2019;20(2):216–228.
154. Ferreri AJM, Cwynarski K, Pulczynski E, et al. Long-term efficacy, safety and neurotolerability of MATRix regimen followed by autologous transplant in primary CNS lymphoma: 7-year results of the IELSG32 randomized trial. *Leukemia*. 2022;36(7):1870–1878.
155. Qiu Y, Li Z, Pouzoulet F, et al. Immune checkpoint inhibition by anti-PDCD1 (anti-PD1) monoclonal antibody has significant therapeutic activity against central nervous system lymphoma in an immunocompetent preclinical model. *Br J Haematol*. 2018;183(4):674–678.
156. Nayak L, Iwamoto FM, LaCasce A, et al. PD-1 blockade with nivolumab in relapsed/refractory primary central nervous system and testicular lymphoma. *Blood*. 2017;129(23):3071–3073.
157. Furuse M, Nonoguchi N, Omura N, et al. Immunotherapy of Nivolumab with Dendritic Cell Vaccination Is Effective against Intractable Recurrent Primary Central Nervous System Lymphoma: A Case Report. *Neurol. Med. Chir.(Tokyo)*. 2017;57(4):191–197.
158. Bobillo S, Khwaja J, Ferreri AJM, Cwynarski K. Prevention and management of secondary central nervous system lymphoma. *haematol*. 2022;108(3):673–689.
159. Boehme V, Schmitz N, Zeynalova S, Loeffler M, Pfreundschuh M. CNS events in elderly patients with aggressive lymphoma treated with modern chemotherapy (CHOP-14) with or without rituximab: an analysis of patients treated in the RICOVER-60 trial of the German High-Grade Non-Hodgkin Lymphoma Study Group (DSHNHL). *Blood*. 2009;113(17):3896–3902.
160. Kridel R, Dietrich P-Y. Prevention of CNS relapse in diffuse large B-cell lymphoma. *The Lancet Oncology*. 2011;12(13):1258–1266.
161. Eyre TA, Djebbari F, Kirkwood AA, Collins GP. Efficacy of central nervous system prophylaxis with stand-alone intrathecal chemotherapy in diffuse large B-cell lymphoma patients treated with anthracycline-based chemotherapy in the rituximab era: a systematic review. *Haematologica*. 2020;105(7):1914–1924.

162. Gleeson M, Counsell N, Cunningham D, et al. Central nervous system relapse of diffuse large B-cell lymphoma in the rituximab era: results of the UK NCRI R-CHOP-14 versus 21 trial. *Annals of Oncology*. 2017;28(10):2511–2516.
169. Chua BJG, Low CE, Yau CE, et al. Recent updates on central nervous system prophylaxis in patients with high-risk diffuse large B-cell lymphoma. *Exp Hematol Oncol*. 2024;13(1):1.
170. Savage KJ. Secondary CNS relapse in diffuse large B-cell lymphoma: defining high-risk patients and optimization of prophylaxis strategies. *Hematology*. 2017;2017(1):578–586.
171. Bobillo S, Joffe E, Sermer D, et al. Prophylaxis with intrathecal or high-dose methotrexate in diffuse large B-cell lymphoma and high risk of CNS relapse. *Blood Cancer J.* 2021;11(6):113.
172. Rőszer T. Understanding the Mysterious M2 Macrophage through Activation Markers and Effector Mechanisms. *Mediators of Inflammation*. 2015;2015(1):816460.
173. Wright GW, Huang DW, Phelan JD, et al. A Probabilistic Classification Tool for Genetic Subtypes of Diffuse Large B Cell Lymphoma with Therapeutic Implications. *Cancer Cell*. 2020;37(4):551-568.e14.
174. Dobin A, Davis CA, Schlesinger F, et al. STAR: ultrafast universal RNA-seq aligner. *Bioinformatics*. 2013;29(1):15–21.
175. Li B, Dewey CN. RSEM: accurate transcript quantification from RNA-Seq data with or without a reference genome. *BMC Bioinformatics*. 2011;12(1):323.
176. Law CW, Chen Y, Shi W, Smyth GK. voom: precision weights unlock linear model analysis tools for RNA-seq read counts. *Genome Biol*. 2014;15(2):R29.
177. Tilford CA, Siemers NO. Gene Set Enrichment Analysis. *Protein Networks and Pathway Analysis*. 2009;563:99–121.
178. Steen CB, Liu CL, Alizadeh AA, Newman AM. Profiling Cell Type Abundance and Expression in Bulk Tissues with CIBERSORTx. *Stem Cell Transcriptional Networks*. 2020;2117:135–157.
179. Chen N, Dennis S, Danaher P, et al. Analytical Validation of the nCounter®-based Lymphoma Subtyping Test (LST) for Cell-of-Origin (COO) Identification in Formalin-Fixed Paraffin-Embedded (FFPE) Diffuse Large B-Cell Lymphoma (DLBCL) Specimens. *Blood*. 2016;128(22):2933–2933.
180. Cesano A. nCounter® PanCancer Immune Profiling Panel (NanoString Technologies, Inc., Seattle, WA). *j. immunotherapy cancer*. 2015;3(1):42.
181. Scott DW, Wright GW, Williams PM, et al. Determining cell-of-origin subtypes of diffuse large B-cell lymphoma using gene expression in formalin-fixed paraffin-embedded tissue. *Blood*. 2014;123(8):1214–1217.
182. Bindea G, Mlecnik B, Tosolini M, et al. Spatiotemporal Dynamics of Intratumoral Immune Cells Reveal the Immune Landscape in Human Cancer. *Immunity*. 2013;39(4):782–795.
183. Newman AM, Liu CL, Green MR, et al. Robust enumeration of cell subsets from tissue expression profiles. *Nat Methods*. 2015;12(5):453–457.

184. Whalley C, Payne K, Domingo E, et al. Ultra-Low DNA Input into Whole Genome Methylation Assays and Detection of Oncogenic Methylation and Copy Number Variants in Circulating Tumour DNA. *Epigenomes*. 2021;5(1):6.
185. Vaccaro K, Allen J, Whitfield TW, et al. Targeted therapies prime oncogene-driven lung cancers for macrophage-mediated destruction. *Journal of Clinical Investigation*. 2024;134(9):e169315.
186. Komohara Y, Ohnishi K, Kuratsu J, Takeya M. Possible involvement of the M2 anti-inflammatory macrophage phenotype in growth of human gliomas. *The Journal of Pathology*. 2008;216(1):15–24.
187. Fleetwood AJ, Lawrence T, Hamilton JA, Cook AD. Granulocyte-Macrophage Colony-Stimulating Factor (CSF) and Macrophage CSF-Dependent Macrophage Phenotypes Display Differences in Cytokine Profiles and Transcription Factor Activities: Implications for CSF Blockade in Inflammation. *The Journal of Immunology*. 2007;178(8):5245–5252.
188. Zaretsky JM, Garcia-Diaz A, Shin DS, et al. Mutations Associated with Acquired Resistance to PD-1 Blockade in Melanoma. *N Engl J Med*. 2016;375(9):819–829.
189. Cornel AM, Mimpen IL, Nierkens S. MHC Class I Downregulation in Cancer: Underlying Mechanisms and Potential Targets for Cancer Immunotherapy. *Cancers*. 2020;12(7):1760.
190. Ridgway JBB, Presta LG, Carter P. 'Knobs-into-holes' engineering of antibody C_H3 domains for heavy chain heterodimerization. *Protein Eng Des Sel*. 1996;9(7):617–621.
191. Weiskopf K, Ring AM, Ho CCM, et al. Engineered SIRPα Variants as Immunotherapeutic Adjuvants to Anticancer Antibodies. *Science*. 2013;341(6141):88–91.
192. Sikic BI, Lakhani N, Patnaik A, et al. First-in-Human, First-in-Class Phase I Trial of the Anti-CD47 Antibody Hu5F9-G4 in Patients With Advanced Cancers. *JCO*. 2019;37(12):946–953.
193. Ito M, Hiramatsu H, Kobayashi K, et al. NOD/SCID/γcnull mouse: an excellent recipient mouse model for engraftment of human cells. *Blood*. 2002;100(9):3175–3182.
194. Pasqualucci L, Neumeister P, Goossens T, et al. Hypermutation of multiple proto-oncogenes in B-cell diffuse large-cell lymphomas. *Nature*. 2001;412(6844):341–346.
195. Dobashi A. Molecular Pathogenesis of Diffuse Large B-Cell Lymphoma. *J Clin Exp Hematop*. 2016;56(2):71–78.
196. Ma L, Gong Q. Recent advances and challenges in primary central nervous system lymphoma: a narrative review. *Transl Cancer Res*. 2023;12(5):1335–1352.
197. Bello C, Sotomayor EM. Monoclonal Antibodies for B-Cell Lymphomas: Rituximab and Beyond. *Hematology*. 2007;2007(1):233–242.
198. Salles G, Gopal AK, Minnema MC, et al. Phase 2 Study of Daratumumab in Relapsed/Refractory Mantle-Cell Lymphoma, Diffuse Large B-Cell

Lymphoma, and Follicular Lymphoma. *Clinical Lymphoma Myeloma and Leukemia*. 2019;19(5):275–284.
199. Calabretta E, Carlo-Stella C. The Many Facets of CD38 in Lymphoma: From Tumor–Microenvironment Cell Interactions to Acquired Resistance to Immunotherapy. *Cells*. 2020;9(4):802.
200. Romero-Ramírez H, Morales-Guadarrama MT, Pelayo R, López-Santiago R, Santos-Argumedo L. CD38 expression in early B-cell precursors contributes to extracellular signal-regulated kinase-mediated apoptosis. *Immunology*. 2015;144(2):271–281.
201. Morandi F, Morandi B, Horenstein AL, et al. A non-canonical adenosinergic pathway led by CD38 in human melanoma cells induces suppression of T cell proliferation. *Oncotarget*. 2015;6(28):25602–25618.
202. Wada F, Shimomura Y, Yabushita T, et al. CD38 expression is an important prognostic marker in diffuse large B-cell lymphoma. *Hematological Oncology*. 2021;39(4):483–489.
203. Lu T, Zhang J, Xu-Monette ZY, Young KH. The progress of novel strategies on immune-based therapy in relapsed or refractory diffuse large B-cell lymphoma. *Exp Hematol Oncol*. 2023;12(1):72.
204. Ong SY, Chen Y, Tan MSY, et al. Current perspectives on resistance to chimeric antigen receptor T-cell therapy and strategies to improve efficacy in B-cell lymphoma. *European J of Haematology*. 2024;112(2):144–152.
205. Kläsener K, Herrmann N, Håversen L, et al. Targeting CD38 with monoclonal antibodies disrupts key survival pathways in paediatric Burkitt's lymphoma malignant B cells. *Clin & Trans Imm*. 2024;13(10):e70011.
206. Vidal-Crespo A, Matas-Céspedes A, Rodriguez V, et al. Daratumumab displays in vitro and in vivo anti-tumor activity in models of B-cell non-Hodgkin lymphoma and improves responses to standard chemo-immunotherapy regimens. *Haematologica*. 2020;105(4):1032–1041.
207. Ollila TA, Kurt H, Waroich J, et al. Genomic subtypes may predict the risk of central nervous system recurrence in diffuse large B-cell lymphoma. *Blood*. 2021;137(8):1120–1124.
208. Magnes T, Wagner S, Thorner AR, et al. Clonal evolution in diffuse large B-cell lymphoma with central nervous system recurrence. *ESMO Open*. 2021;6(1):100012.
209. Wight J, Blombery P, Lickiss J, et al. Systemic diffuse large B-cell lymphoma involving the central nervous system have high rates of defective antigen presentation and immune surveillance. *haematol*. 2024;
210. Kraan W, Horlings HM, Van Keimpema M, et al. High prevalence of oncogenic MYD88 and CD79B mutations in diffuse large B-cell lymphomas presenting at immune-privileged sites. *Blood Cancer Journal*. 2013;3(9):e139–e139.
211. Kersten MJ, Kraan W, Doorduijn J, et al. Diffuse large B cell lymphomas relapsing in the CNS lack oncogenic MYD88 and CD79B mutations. *Blood Cancer Journal*. 2014;4(12):e266–e266.

212. Zhu Q, Wang J, Zhang W, et al. Whole-Genome/Exome Sequencing Uncovers Mutations and Copy Number Variations in Primary Diffuse Large B-Cell Lymphoma of the Central Nervous System. *Front. Genet.* 2022;13:878618.
213. Przemysław Juszczyński AZ. PIM1 Point Mutations Increase Migration of Diffuse Large B-Cell Lymphoma (DLBCL) Cells. *Blood*. 142 (Supplement 1):
214. Geng H, Chen Z, Anderson S, et al. Expression of B and T Lymphocyte Attenuator (BTLA) Correlates with CNS Metastasis and Adverse Prognosis in Activated B-Cell Lymphoma and Acute Lymphoblastic Leukemia. *Blood*. 2015;126(23):3900–3900.
215. Reboldi A, Coisne C, Baumjohann D, et al. C-C chemokine receptor 6–regulated entry of TH-17 cells into the CNS through the choroid plexus is required for the initiation of EAE. *Nat Immunol*. 2009;10(5):514–523.
216. Halsey C, Williams MT, Yousafzai Y, et al. Central Nervous System Involvement in a Xenograft Model of Pre-B Acute Lymphoblastic Leukaemia Is Associated with Dysfunctional CXCR4 Expression and Upregulation of the Neurotropic Chemokine Receptors CCR6 and CX3CR1,. *Blood*. 2011;118(21):3449–3449.
217. Alsadeq A, Lenk L, Vadakumchery A, et al. IL7R is associated with CNS infiltration and relapse in pediatric B-cell precursor acute lymphoblastic leukemia. *Blood*. 2018;132(15):1614–1617.
218. Almeida ARM, Neto JL, Cachucho A, et al. Interleukin-7 receptor α mutational activation can initiate precursor B-cell acute lymphoblastic leukemia. *Nat Commun*. 2021;12(1):7268.
219. Härzschel A, Zucchetto A, Gattei V, Hartmann TN. VLA-4 Expression and Activation in B Cell Malignancies: Functional and Clinical Aspects. *IJMS*. 2020;21(6):2206.
220. Lehmann-Horn K, Sagan SA, Winger RC, et al. CNS accumulation of regulatory B cells is VLA-4-dependent. *Neurol Neuroimmunol Neuroinflamm*. 2016;3(2):e212.
221. Bonig H, Wundes A, Chang K-H, Lucas S, Papayannopoulou T. Increased numbers of circulating hematopoietic stem/progenitor cells are chronically maintained in patients treated with the CD49d blocking antibody natalizumab. *Blood*. 2008;111(7):3439–3441.
222. Schwab N, Schneider-Hohendorf T, Wiendl H. Therapeutic uses of anti-α4-integrin (anti-VLA-4) antibodies in multiple sclerosis. *International Immunology*. 2015;27(1):47–53.

10. Appendix

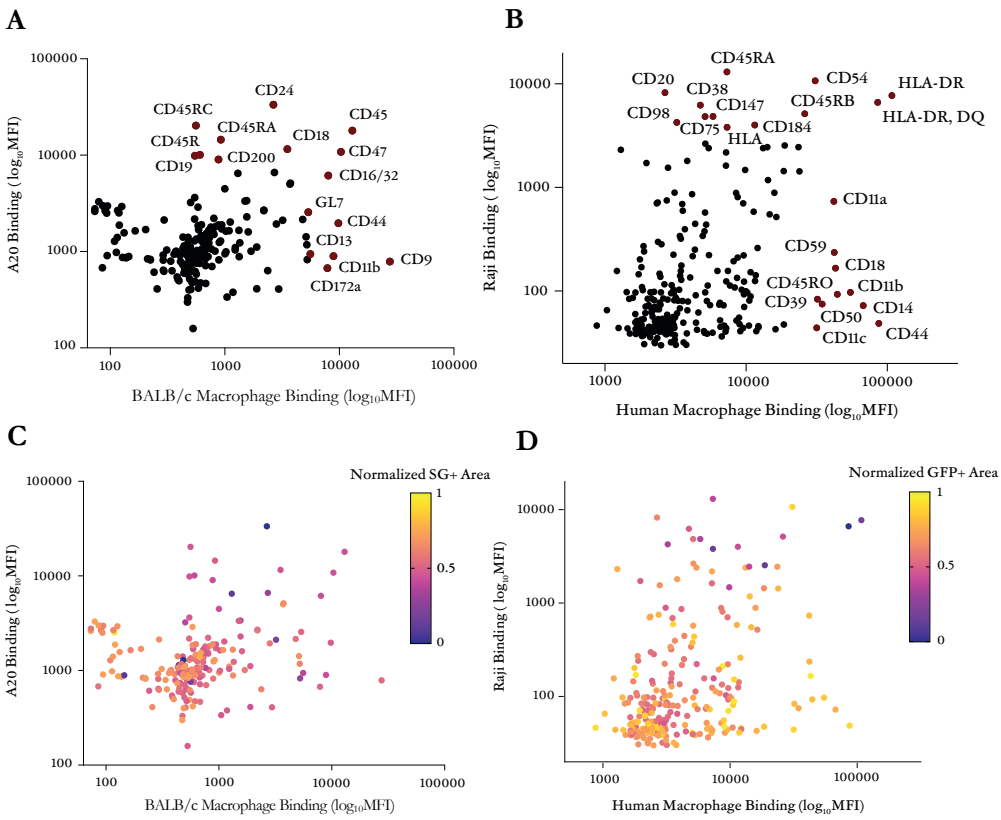

Appendix Figure 1 | Binding of antibodies from libraries to B-cell lymphoma cells and macrophages. A,B, Scatter plots depicting cell-based binding of each individual antibody from the murine antibody library binding to A20 lymphoma cells and BALB/c macrophages (**A**), and from the human antibody library to Raji lymphoma cells and primary human macrophages combined from n = 3 independent donors (**B**).. Mean fluorescence intensity (MFI) was assessed by flow cytometry. The target antigens highlighted exceeded the 95th percentile for binding to either cancer or macrophages cells. **C,D,** Multiple variable scatter plot depicting the relationship between the binding of the antibody library to lymphoma cells and/or macrophages and the functional anti-tumor effects of each antibody in co-culture with macrophages (color scale) in the murine (**C**) and human (**D**) systems. Color scale represents the cancer cell area at the last time point in co-culture assays, with blue indicating greater anti-lymphoma activity and yellow indicating lesser anti-lymphoma activity.

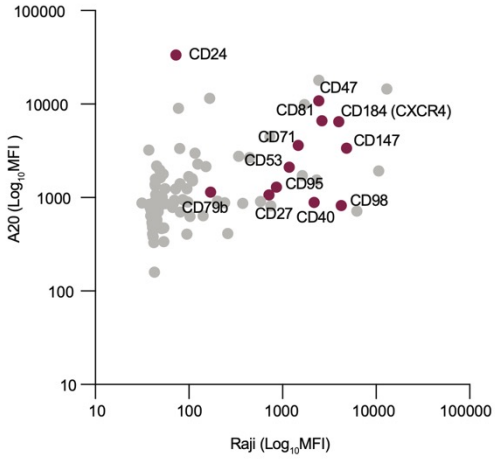

Appendix Figure 2 |A, Comparison of antigens and antibodies evaluated from libraries in the murine and human systems. Scatter plot depicting the relationship between binding of 92 shared targets in both human (Raji) and murine systems (A20). The highlighted antigens are the selected antibody hits that exceeded the 95th percentile of functional activity from the co-culture assays with macrophages and B-cell lymphomas as single agents. Binding (MFI) was determined by flow cytometry using Alexa 647-conjugated streptavidin (A20) or Alexa 647-conjugated anti-Ig antibodies (Raji) for detection.

ABL1	*BTK*	*CHD2*	*FAT1*	*HLA-C*	*JAK1*	*NF1*	*PPM1D*	*SF1*	*TLR2*
ACTB	*CALR*	*CHEK2*	*FAT4*	*HLA-DMA*	*JAK2*	*NFKBIA*	*PRDM1*	*SF3A1*	*TMEM30A*
ANKRD26	*CARD11*	*CIITA*	*FBXW7*	*HLA-DMB*	*JAK3*	*NFKBIE*	*PRKCB*	*SF3B1*	*TNFAIP3*
ARID1A	*CBL*	*CREBBP*	*FLT3*	*HRAS*	*KDM6A*	*NOTCH1*	*PRPF8*	*SGK1*	*TNFRSF10A*
ARID1B	*CBLB*	*CSF3R*	*FOXO1*	*ICAM1*	*KIT*	*NOTCH2*	*PTEN*	*SH2B3*	*TNFRSF14*
ARID2	*CCND1*	*CSNK1A1*	*FYN*	*ID3*	*KLF2*	*NPM1*	*PTPN1*	*SMARCA4*	*TP53*
ASXL1	*CCND3*	*CUX1*	*GATA1*	*IDH1*	*KLHL6*	*NRAS*	*PTPN11*	*SMC1A*	*TRAF2*
ATM	*CCR4*	*CXCR4*	*GATA2*	*IDH2*	*KMT2A*	*NSD2*	*PTPN6*	*SMC3*	*TRAF3*
B2M	*CD274*	*DDX3X*	*GNA13*	*IGLL5*	*KMT2C*	*P2RY8*	*PTPRD*	*SOCS1*	*U2AF1*
BCL10	*CD28*	*DDX41*	*GNAI2*	*IKBKB*	*KMT2D*	*PAX5*	*RAD21*	*SPEN*	*U2AF2*
BCL2	*CD58*	*DNMT3A*	*GNAS*	*IKZF1*	*KRAS*	*PDCD1LG2*	*RB1*	*SRSF2*	*UBE2A*
BLC6	*CD70*	*DTX1*	*GNB1*	*IKZF3*	*LCK*	*PHF6*	*REL*	*STAG1*	*UBR5*
BCL7A	*CD79A*	*EBF1*	*H1-2*	*IL4R*	*MAP2K1*	*PIK3CD*	*RHOA*	*STAG2*	*VAV1*
BCOR	*CD79B*	*EGR2*	*H1-4*	*INPP5D*	*MAP3K14*	*PIM1*	*RPS15*	*STAT3*	*WT1*
BCORL1	*CD80*	*EP300*	*H1-5*	*IRF2BP2*	*MED12*	*PIM2*	*RUNX1*	*STAT5B*	*XPO1*
BIRC3	*CD83*	*ETNK1*	*H2BC4*	*IRF4*	*MEF2B*	*PLCG1*	*S1PR2*	*STAT6*	*ZFP36L1*
BRAF	*CD86*	*ETV6*	*H3C2*	*IRF8*	*MPL*	*PLCG2*	*SAMHD1*	*TBL1XR1*	*ZMYM3*
BTG1	*CDKN2A*	*EZH2*	*HLA-A*	*ITGB2*	*MYC*	*POT1*	*SETBP1*	*TCF3*	*ZNF217*
BTG2	*CEBPA*	*FAS*	*HLA-B*	*ITPKB*	*MYD88*	*POU2F2*	*SETD2*	*TET2*	*ZRSR2*

Appendix Table 1 | Genes included in NGS panel.

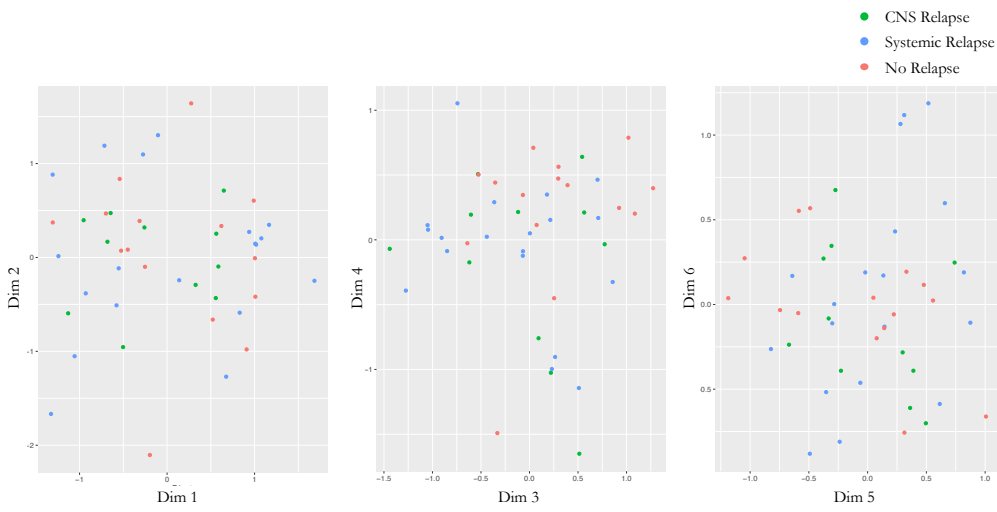

Appendix Figure 3 | Principal Component Analysis (PCA) Maps. The PCA maps illustrate dimensions 1 vs 2, 3 vs 4, and 5 vs 6. Each dot represents a sample, color-coded as follows: green for CNS Relapse, blue for Systemic Relapse, and red for No Relapse. No distinct clustering is observed among the different groups.

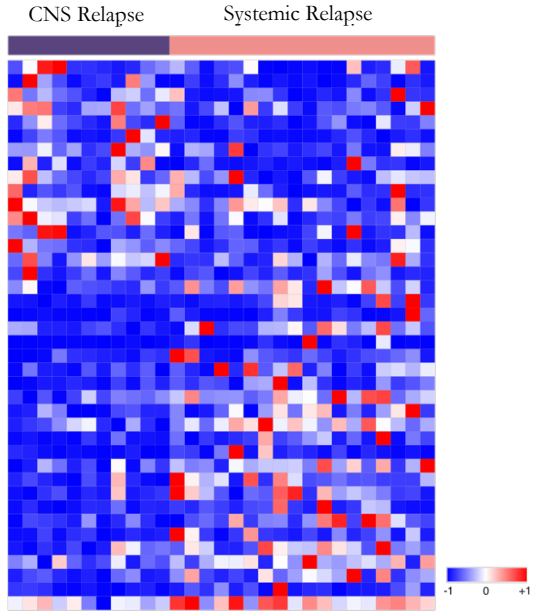

Appendix Figure 4 | RNAseq gene expression data. Heatmap representing normalized expression of selected genes with significant differential expression (Log2FC ≥ 1 and p-value ≤ 0.05) when comparing CNS Relapse vs. Systemic Relapse. Expression levels are indicated by a color gradient from red (high expression) to blue (low expression). Genes are arranged in descending order of expression within the CNS Relapse group.

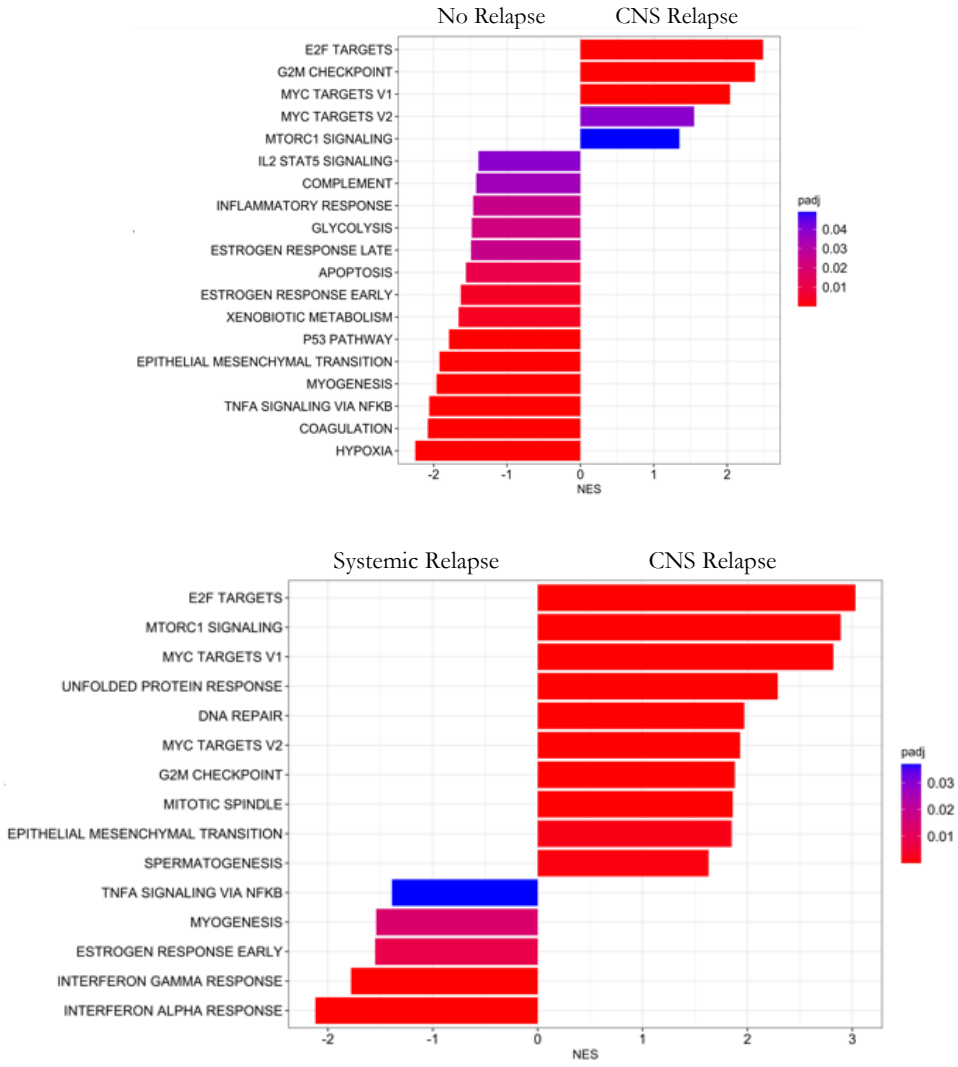

Appendix Figure 5 | Pathway enrichment analysis. A,B, GSEA analysis using MSigDB Hallmark database, comparing CNS Relapse vs. No Relapse (**A**) and CNS Relapse vs. Systemic Relapse (**B**); and using the GO terms (**c**) comparing CNS Relapse vs. No CNS Relapse. A positive Normalized Enrichment Score (NES) indicates enrichment in gene sets in the CNS Relapse group, while a negative NES indicates enrichment in the No Relapse group. The color range indicates significant Padj ≤ 0.05.

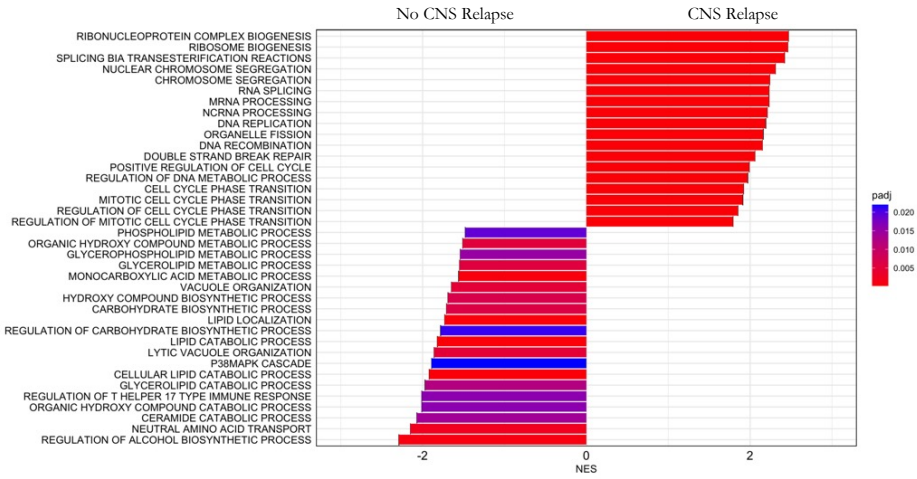

Appendix Figure 6 | Pathway enrichment analysis. GSEA analysis using the GO terms, comparing CNS Relapse vs. No CNS Relapse. A positive Normalized Enrichment Score (NES) indicates enrichment in gene sets in the CNS Relapse group, while a negative NES indicates enrichment in the No CNS Relapse group. The color range indicates significant Padj ≤ 0.05. GO = Gene Ontology

10.1. Scientific communications

10.1.1. Poster 1: Macrophages play a key role in controlling tumor growth and response to immunotherapy in primary central nervous system lymphoma

Reference: **Carlota Pages-Geli**, Daniel Medina, Cristina Hernandez, Patricia Fernandez, Gemma Pujadas, Francesc Bosch, Marta Crespo; Macrophages Play a Key Role in Controlling Tumor Growth and Response to Immunotherapy in Primary Central Nervous System Lymphoma. *Blood* 2023; 142 (Supplement 1): 1642. doi: https://doi.org/10.1182/blood-2023-180719

Blood 142 (2023) 1642–1643

The 65th ASH Annual Meeting Abstracts

POSTER ABSTRACTS

622.LYMPHOMAS: TRANSLATIONAL-NON-GENETIC

Macrophages Play a Key Role in Controlling Tumor Growth and Response to Immunotherapy in Primary Central Nervous System Lymphoma

Carlota Pages-Geli[1], *Daniel Medina, MSc,BSc*[2], *Cristina Hernandez*[1], *Patricia Fernandez*[1], *Gemma Pujadas, PhD*[2], *Francesc Bosch, MD PhD*[3,2], *Marta Crespo, PhD*[1]

[1] Experimental Hematology, Vall d'Hebron Institute of Oncology (VHIO), Barcelona, Spain
[2] Experimental Hematology, Vall d'Hebron Institute of Oncology (VHIO), Barcelona, Spain
[3] Hematology Department, Vall d'Hebron University Hospital, Barcelona, Spain

Introduction Primary Central Nervous System Lymphoma (PCNSL) represents 5% of extranodal lymphomas. Current treatments include high-dose chemotherapy in combination with an anti-CD20 antibody, and whole-brain radiation, both of which are limited by their toxicity. Although some advances have been achieved during the last few years, the prognosis of patients with CNS lymphoma is substantially worse than those with other type of lymphomas, with 5-year survival rates around 30%.
The highly aggressive nature of CNS lymphomas is in part due to the fact that the brain is an immunoprivileged organ; it presents very low levels of immunosurveillance, which contributes to inefficient immune responses against malignant cells. Of note, up to 70% of patients diagnosed with PCNSL also exhibit genetic alterations to avoid recognition by the immune system, like loss of MHC-I, that prevent presentation of tumor antigens, and amplifications in PD-L1, which increase the negative stimuli in cytotoxic T cells.
The PD-1/PD-L1 interaction has mainly been considered to be a checkpoint that regulates T cells. However, it has recently been found that tumor-associated macrophages can also express PD-1 and become activated to attack tumor cells when it is blocked. Moreover, macrophages have also been found to be inhibited by MHC-I expression on cancer cells. Thus, cancer cells that downregulate MHC-I to avoid T cell surveillance are particularly vulnerable to macrophages phagocytosis, especially when other macrophage immune checkpoints are blocked, such as CD47.
Against this background, we aimed to decipher the differential role of macrophages and T cells in the tumor growth and response to immunotherapy in primary CNS lymphoma.
Methods Luciferase-expressing A20 murine B-cell lymphoma cells were genetically modified to knock-out MHCI or MHCII by CRISPR-Cas9 and injected into the brain of immunocompetent (IC) or macrophage-depleted (MD) mice. Once tumours were stablished, mice were treated intravenously with seven injections, twice a week, of anti-PD1, anti-CD47 or the combination of both. We monitored mice for survival and tumoral growth. Additionally, brains were collected from mice treated with three injections for analysis of macrophages, B cells and T cells using flow cytometry and IHC.
Results In IC mice, all anti-PD1 treated mice showed significant differences in tumoral growth and survival compared to vehicle; however, MHCI- tumors had the lowest overall survival (Figure 1A). With anti-CD47 therapy, only MHCI- PCNSL mice had a significantly increased survival compared to vehicle. Combination was effective in all groups, but no drug synergy was seen. In MD mice, all tumors were more aggressive than in IC mice. With anti-PD1, MHCI+ PCNSL mice achieved a complete tumor regression and survived longer in comparison to vehicle. On the contrary, MHCI- PCNSL mice didn't respond to anti-PD1 therapy (Figure 1B). Of notice, MHCI+ PCNSL in both MD and IC models had a higher infiltration of active T cells when treated with anti-PD1. In MHCI- PCNSL, infiltrated T cells had less expression of activation markers in both models and macrophages were polarized to an M2 phenotype in IC mice.
Conclusions Our study revealed a remarkable response to anti-PD1 therapy in MHCI+ CNS lymphoma tumors, regardless of the presence of macrophages in the tumor microenvironment. This indicates that T cells would be primarily responsible for the observed tumour regression. However, targeting CD47 in MHCI+ PCNSL was found to be insufficient in restoring macrophage phagocytosis. Despite observing positive effects of anti-PD1 and anti-CD47 drugs in our MHCI- immunocompetent mouse model, MHCI downregulation still induces a very aggressive, lethal disease. This suggests that these tumors can only be controlled by macrophages, as supported by the lack of treatment response in a MD microenvironment.
Our findings highlight the critical role of macrophages in controlling the growth of lymphoma cells in the brain and their significance in the immunotherapy response for CNS lymphomas, particularly when MHCI expression is deficient. Blocking

PD1 exhibits superior efficacy when macrophages are present, indicating T cells are not the only player in this tumoral scenario. As a result, our study suggests that a promising approach for treating primary CNS lymphomas would involve targeting both T cells and macrophages.

10.1.2. Poster 2: Unbiased discovery of novel antibody therapies that stimulate macrophage-mediated destruction of B-cell lymphoma

Reference: Juliano Ribeiro, **Carlota Pages-Geli**, José Velarde, Anna Meglan, Jasmine Blandin, Kyle Vaccaro, Marta Crespo, Kipp Weiskopf; Abstract PO-038: Unbiased discovery of novel antibody therapies that stimulate macrophage-mediated destruction of B-cell lymphoma. *Blood Cancer Discov* 1 May 2024; 5 (3_Supplement): PO–038. https://doi.org/10.1158/2643-3249.LYMPHOMA24-PO-038

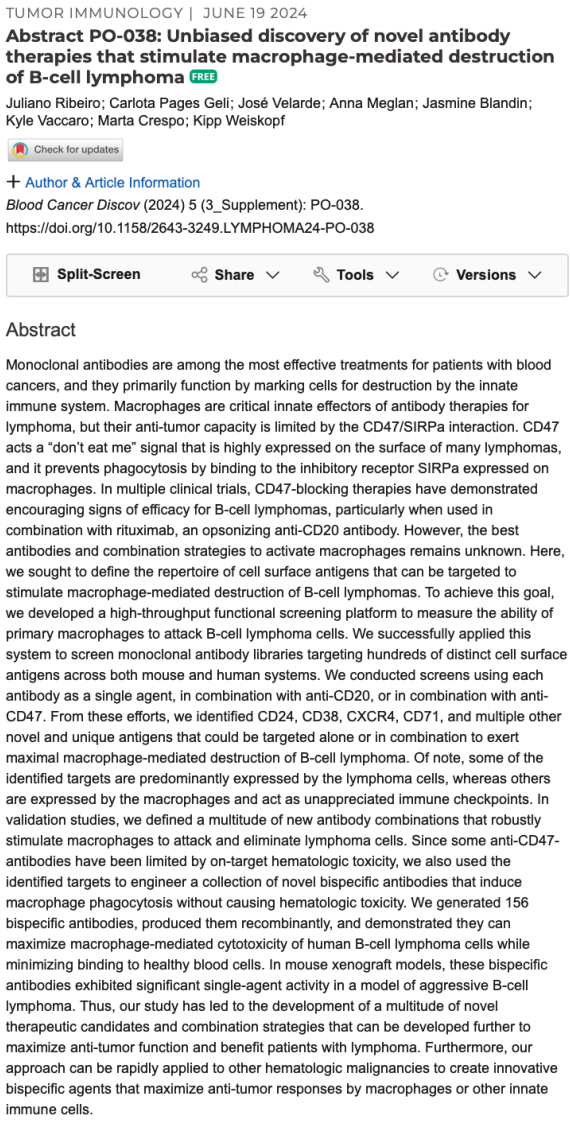

TUMOR IMMUNOLOGY | JUNE 19 2024

Abstract PO-038: Unbiased discovery of novel antibody therapies that stimulate macrophage-mediated destruction of B-cell lymphoma FREE

Juliano Ribeiro; Carlota Pages Geli; José Velarde; Anna Meglan; Jasmine Blandin; Kyle Vaccaro; Marta Crespo; Kipp Weiskopf

Check for updates

+ Author & Article Information

Blood Cancer Discov (2024) 5 (3_Supplement): PO-038.

https://doi.org/10.1158/2643-3249.LYMPHOMA24-PO-038

Split-Screen Share Tools Versions

Abstract

Monoclonal antibodies are among the most effective treatments for patients with blood cancers, and they primarily function by marking cells for destruction by the innate immune system. Macrophages are critical innate effectors of antibody therapies for lymphoma, but their anti-tumor capacity is limited by the CD47/SIRPa interaction. CD47 acts a “don’t eat me” signal that is highly expressed on the surface of many lymphomas, and it prevents phagocytosis by binding to the inhibitory receptor SIRPa expressed on macrophages. In multiple clinical trials, CD47-blocking therapies have demonstrated encouraging signs of efficacy for B-cell lymphomas, particularly when used in combination with rituximab, an opsonizing anti-CD20 antibody. However, the best antibodies and combination strategies to activate macrophages remains unknown. Here, we sought to define the repertoire of cell surface antigens that can be targeted to stimulate macrophage-mediated destruction of B-cell lymphomas. To achieve this goal, we developed a high-throughput functional screening platform to measure the ability of primary macrophages to attack B-cell lymphoma cells. We successfully applied this system to screen monoclonal antibody libraries targeting hundreds of distinct cell surface antigens across both mouse and human systems. We conducted screens using each antibody as a single agent, in combination with anti-CD20, or in combination with anti-CD47. From these efforts, we identified CD24, CD38, CXCR4, CD71, and multiple other novel and unique antigens that could be targeted alone or in combination to exert maximal macrophage-mediated destruction of B-cell lymphoma. Of note, some of the identified targets are predominantly expressed by the lymphoma cells, whereas others are expressed by the macrophages and act as unappreciated immune checkpoints. In validation studies, we defined a multitude of new antibody combinations that robustly stimulate macrophages to attack and eliminate lymphoma cells. Since some anti-CD47-antibodies have been limited by on-target hematologic toxicity, we also used the identified targets to engineer a collection of novel bispecific antibodies that induce macrophage phagocytosis without causing hematologic toxicity. We generated 156 bispecific antibodies, produced them recombinantly, and demonstrated they can maximize macrophage-mediated cytotoxicity of human B-cell lymphoma cells while minimizing binding to healthy blood cells. In mouse xenograft models, these bispecific antibodies exhibited significant single-agent activity in a model of aggressive B-cell lymphoma. Thus, our study has led to the development of a multitude of novel therapeutic candidates and combination strategies that can be developed further to maximize anti-tumor function and benefit patients with lymphoma. Furthermore, our approach can be rapidly applied to other hematologic malignancies to create innovative bispecific agents that maximize anti-tumor responses by macrophages or other innate immune cells.

10.1.3. Poster 3: Deciphering transcriptomic and (epi)genetic signatures of central nervous system infiltration in patients diagnosed with diffuse large B-cell lymphoma

Reference: Carlota Pages-Geli, Sabela Bobillo, Pau Abrisqueta, Josep Castellvi, Laura Palomo, Damiana Alvarez, Manel Esteller, Francesc Bosch, Marta Crespo; Deciphering Transcriptomic and (Epi)Genetic Signatures of Central Nervous System Infiltration in Patients Diagnosed with Diffuse Large B-Cell Lymphoma. *Blood* 2023; 142 (Supplement 1): 1618. doi: https://doi.org/10.1182/blood-2023-174653

ELSEVIER

Blood 142 (2023) 1618–1619

The 65th ASH Annual Meeting Abstracts

POSTER ABSTRACTS

621.LYMPHOMAS: TRANSLATIONAL-MOLECULAR AND GENETIC

Deciphering Transcriptomic and (Epi)Genetic Signatures of Central Nervous System Infiltration in Patients Diagnosed with Diffuse Large B-Cell Lymphoma

Carlota Pages-Geli[1], Sabela Bobillo, MD PhD[2], Pau Abrisqueta, MD PhD[2,1], Josep Castellvi, MD[3], Laura Palomo[1], Damiana Alvarez, PhD[4], Manel Esteller, MD PhD[4], Francesc Bosch, MD PhD[1,2], Marta Crespo, PhD[1]

[1] Experimental Hematology, Vall d'Hebron Institute of Oncology (VHIO), Barcelona, Spain
[2] Hematology Department, Vall d'Hebron University Hospital, Barcelona, Spain
[3] Department of Pathology, Vall d'Hebron University Hospital, Barcelona, Spain
[4] Cancer Epigenetics, Josep Carreras Leukaemia Research Institute, Badalona, Spain

Introduction Central Nervous System (CNS) involvement in Diffuse Large B Cell Lymphoma (DLBCL) is a rare complication with bad prognosis. The CNS Prognostic Index is employed to categorize patients at a high risk of CNS relapse; however, its effectiveness is not accurate. The discovery of precise biomarkers for predicting CNS involvement in DLBCL patients remains unmet. Our objective was to characterize the immune, transcriptomic, genomic and epigenomic hallmarks of systemic tumors at diagnosis of patients who later experienced relapse in the CNS. By exploring these biological profiles, we sought to gain valuable insights into the underlying mechanisms and potential biomarkers associated with CNS relapse in DLBCL.
Methods We conducted a retrospective study including 38 patients diagnosed with nodal DLBCL who experienced relapse within the first two years after diagnosis. Among these patients, 12 individuals relapsed specifically in the CNS, while 26 relapsed in systemic sites. As a control group, we included 21 patients who did not relapse. DNA and RNA were extracted from FFPE tumor samples collected at diagnosis. To evaluate immune cell infiltration, we utilized the nCounter PanCancer Immune Profiling Panel (Nanostring); cell-of-origin (COO) was determined using the Lymph2Cx assay. Transcriptomic profiles were generated by bulk RNA sequencing and mutational analysis was performed using a custom targeted NGS panel, which included the most frequently mutated genes observed in lymphoid neoplasms. Methylation profiles were obtained using the Illumina Infinium MethylationEPIC Array 850K.
Results Immune profiling analysis showed cell composition was not significantly different between groups; however, we observed distinct immune gene expression patterns at diagnosis in patients who experienced CNS relapse. Multiple genes were overexpressed in the CNS-relapsed group compared to non-relapsed group, which encompassed various functional categories including chemokine signaling such as *IL7R* (FC=2; P=0.05) and *CCR6* (FC=3.4; P=0.01); adhesion like *VCAM1* (FC=1.6; P=0.03) and *ITGA4* (FC=2.2; P=0.006); and immune regulation such as *CD1A* (FC=4.8; P=0.001), *LTB* (FC=3.3; P=0.009) and *BTLA* (FC=2.3; P=0.02) (Fig.1A). The *ITGA4* gene also presented higher expression levels in the CNS-relapsed group when compared to both systemic-relapsed and non-relapsed groups combined (FC=1.7; P=0.03). No significant differences were observed in the COO classification between groups. Whole-genome transcriptomic data revealed enrichment in gene sets associated with proliferation and survival in the CNS-relapsed group (Fig.1B). Analysis of genetic alterations indicated that patients with CNS relapse exhibited an increased mutation load and frequency in *PIM1*, *IGLL5*, and *KMT2D* genes. Finally, analysis of the CNS relapse-related epigenome showed 343 differentially hypomethylated CpG sites compared to both systemic and non-relapsed groups together, affecting a total of 211 genes. Pathway enrichment analysis of these genes revealed a link between CNS infiltration and cell migration and locomotion.
Conclusions Tumors from DLBCL patients that will relapse in the CNS present a higher chemokine, adhesion and proliferation signatures at diagnosis. Of notice, BTLA, CCR6 and IL7R proteins have been previously reported to be implicated in B cell entry into the CNS in B-cell malignancies. Interestingly, patients with CNS relapse demonstrated significant overexpression of the *ITGA4* gene, which encodes the integrin α4 subunit (CD49d) of the Very Late Antigen-4. Engagement between CD49d on B cells and its endothelial ligand VCAM-1 is required for migration of these cells across the blood-brain barrier. In fact, Natalizumab (anti-CD49d mAb) is administered in multiple sclerosis to impede entrance and accumulation of B cells in the brain. Initial experiments in mice have shown increased expression of CD49d in lymphoma B cells that have infiltrated the brain, compared to those in the spleen. Herein, we have demonstrated that DLBCL cells at diagnosis already own specific transcriptomic and (epi)genetic hallmarks that could confer a higher capacity to infiltrate the CNS. Validation of these findings in larger cohorts of patients could improve selection of patients with an increased risk of CNS involvement in need of prophylactic CNS-directed therapies at diagnosis.